博士論文

Liquefaction characteristics of dense sand specimens with pre-shear histories in torsional shear tests
（せん断履歴のある密な砂供試体のねじりせん断試験における液状化特性）

劉　偉晨

Department of Civil Engineering
University of Tokyo
Tokyo, Japan

Abstract

Due to cyclic loading during earthquakes, liquefaction occurs in saturated cohesionless soil because of the loss of effective stress. In the 1964 Niigata earthquake, in which huge damage was caused to buildings or structures, the liquefaction phenomenon firstly aroused the attention of soil mechanical scholars. From that time, a lot of study and research has been done on the topic of liquefaction by geotechnical researchers.

In the past, liquefaction was considered to happen easily on the saturated loose sandy ground where the excess pore water pressure is easier to accumulate during cyclic loadings. Thus, in the past few decades, the study of liquefaction was mainly focused on loose sands or medium dense ones. However, with the development of the society, evaluation of liquefaction resistance of saturated dense sands also becomes important especially during the construction of essential structures such as nuclear power plants, large-scale oil tanks, or earth-fill dams. Since this kind of critical structures asks for stable behavior even under large seismic motions, the aseismic design for them should be based on a high acceleration which may be dangerous even for dense sand foundations.

Regarding the study on liquefaction behavior of dense sands, pioneer researchers found very different performance for dense sand samples with similar relative density but obtained by different methods. For example, results of laboratory testing showed that sand specimens obtained by the frozen sampling method from in-situ had better liquefaction resistance than reconstituted specimens prepared in the laboratory. Pioneer researcher considered this phenomenon might be caused by the so called “ageing effect”. During long time period, cementation between sand grains or strain histories brought by earthquakes affected the strength of sands to some extent. For cohesionless sands, the influence of cementation is so negligible that the only possible way for an increase in liquefaction resistance seems to be strain histories.

Study on the influence of strain history or pre-shear history has been conducted for several decades particularly on loose sands or medium dense ones. It has been found that the pre-shear history especially small strain histories could induce significant

increase of liquefaction resistance. Therefore, in this study, different types of pre-shear histories were applied to sand specimens prepared by silica sand with the initial relative density of 80% to investigate their influence on liquefaction behavior of dense sands.

In this study, a strain-controlled type of torsional shear apparatus was employed to apply undrained cyclic loading on hollow cylindrical sand specimens. Silica sand with number 7 grading was used to prepare the specimens through the air-pluviation method. After fully saturation by the double vacuum method, sand specimens were consolidated under isotropic condition to the target effective stress before subjecting to cyclic pre-shear loadings in various condition. After the pre-shear, sand specimens were isotropically consolidated again and then subjected to liquefaction test until the double amplitude of shear strain of 7.5% was reached.

For comparison purpose, a series of repeated liquefaction tests with no pre-shear history was carried out. In this series, sand specimens were subjected to cyclic loading with constant double amplitude of shear stress after isotropic consolidation. Drainage and reconsolidation were conducted after 7.5% of double amplitude of shear strain was reached and then cyclic loading was applied again. Results of this series showed that liquefaction resistance increased with liquefaction stages and the liquefaction history in former stage can also be seen as a kind of pre-shear history for the next stage.

Tests with pre-shear history were carried out in 2 different series that distinguished by the drainage condition during pre-shear stages. Pre-shear under drained condition was conducted by controlling the double amplitude of shear strain to be constant with large cyclic numbers. By changing strain amplitude and cyclic numbers in different cases, it was found both parameters could influence the liquefaction resistance. In this series, repeated liquefaction tests were also carried out after the pre-shear and first stage of liquefaction test. It was found that the pre-shear can only affect the liquefaction stage immediately after it.

Another series of tests were conducted with pre-shear history under undrained condition. In this series, cyclic loading during the pre-shear stage was applied until the pore water pressure reached 50% of the initial effective stress. After reconsolidated to the same initial effective stress, this kind of pre-shear was applied several times before

the liquefaction test. Results of tests indicated that the number of pre-shear stages could affect the liquefaction resistance significantly. Meanwhile, the effect of pre-shear in different stages can be accumulated.

In order to study the mechanism of the pre-shear effect, further analysis was carried out by means of the dissipated energy concept. During cyclic loading, the dissipated energy can be calculated by integration of the stress-strain relationship. Pioneer researchers has modified this method by normalizing the shear stress by the mean effective stress in order to calculate the normalized dissipated energy. Pioneer studies found that the (normalized) dissipated energy could be distinguished into the positive impact and the negative one which had different effect on the liquefaction resistance. Study on loose sands or medium dense sands considered the phase transformation line as a virtual boundary between these two effects. Before phase transformation, all the dissipated energy is thought to be positive impact while after that, it turns in to negative ones. However, this boundary might be not reasonable for dense sands. In the case of dense sands, due to larger cyclic stress ratio, the phase transformation line is always passed in the first loading cycles. It means when using the phase transformation line as the boundary to distinguish the positive and negative impact, there will be only negative impact left which cannot explain the increase of liquefaction resistance after pre-shear.

Therefore in this study, a new method is considered to distinguish the positive and negative impact during liquefaction tests on dense sand specimens. In this new method, the phase transformation line is still used as a boundary to separate every loading cycle in to three parts. When shear stress is inside the range of two phase transformation lines, the dissipated energy is considered to be positive impact and the rest parts are considered to be negative impact. After calculating the total normalized energy and distinguish it into positive and negative impact, it was found that the positive impact influenced the liquefaction resistance much more significantly than the negative one. Meanwhile, there was a linear relationship between the log of liquefaction resistance (number of cycles to reach 7.5% double amplitude of shear strain) and the log of positive impact.

Further investigation was made by re-analyzing the data from Dr. Aoyagi on medium dense sands to verify the applicability of the new distinguish method. However,

although cases with same shear histories showed the correlation between liquefaction resistance and the “positive impact”, the relationships were not consistent in cases with different shear history. Then the “net impact” was introduced by considering the “negative impact” on medium dense sand. It was found that with consideration of the negative impact, the relationships between the “normalized net impact” and the liquefaction resistance became more consistent in cases with different histories. It was considered that the “negative impact” had different influence on liquefaction resistance in different density ranges.

The last part of this study is an application of the normalized dissipated energy in predicting the liquefaction resistance curve through a single test. Considering the decrease of effective stress due to the cyclic loading, several points on liquefaction resistance curve can be obtained from a single test. However, due to the influence of former cyclic loadings, the liquefaction resistance of latter points is not accurate. With modification applying the normalized dissipated energy, the liquefaction resistance curve estimated by a single test became better and partly consistent with the typical liquefaction resistance curve obtained by a series of tests. However, further studies are still necessary to improve the accuracy of the modification.

Acknowledgement

The author would like to express the deepest and most sincere gratitude to his supervisor, Prof. Junichi Koseki for his guidance and kind support in the past three years. Prof. Koseki has been patiently answered all kinds of questions and gave useful advises, comments, encouragements and positive inspirations numerous times.

The author also would like to express the deepest appreciation to thesis committee members, Prof. Reiko Kuwano, Assoc. Prof. Watabane, Prof. Tsutomu Namikawa and Assoc. Prof. Takashi Kitoya for the suggestions and advice during discussions and lab seminars.

Deepest gratitude is also expressed to Mr. Takeshi Sato for designing, creating, advices and fixing the apparatuses. The author is also very thankful to the Assistant Prof. Kyokawa for his support in the research room and laboratory. The author wishes to thank Dr. Zhao for his kind instruction in conducting the torsional shear test.

The author would like to thank Dr. Fangwei Yu, Dr. Hailong Wang, Dr. Wenli Lin, Dr. Jiren Xie, Dr. Yudai Aoyagi, Dr. Jaylord Tan Tian and Dr. Zain Maqsood for their help and supports. The author would like to thank Xianfeng Li, Yuichi Tomita, Tomoki Shiozawa, Hayato Hamaguchi, Satoshi, Jimbo, Yutaro Yamazaki, Elise Baboz, Brahian Hugo Roman Cabrera, Ahsan Md Kamrul, Kebba Trawally, Masum Shaikh, Zafar Avzalshoev, Hiroki Kawasaki, Misa Hiraga and Tokio Morimoto.

Special gratitude is supplied to Mr. Hiroki Sato and Misako Sato, for their kind support as the host family of the author.

Hearty thanks are also extended to my parents and my wife Yujie Cui, for their continual encouragement and inspiring.

Table of Contents

List of Tables

List of Figures

Chapter 1 Introduction

1.1 Background

1.1.1 Liquefaction phenomenon

Liquefaction is a phenomenon that occurs in saturated cohesionless soil because of the loss of effective stress due to cyclic loadings during earthquakes. In the 1964 Niigata Earthquake, in which huge damage was caused to buildings and structures, the liquefaction phenomenon was first time recognized and reported (Ishihara and Koga, 1981). Since then, a lot of liquefaction cases were spotted and reported during earthquakes all around the world: similar liquefaction occurred during 1964 Alaska Earthquake (McCulloch and Bonilla, 1970), 1999 Chi-Chi Earthquake (Yuan et al., 2004), 2011 East Japan Earthquake (Towhata et al., 2014), 2011 Christchurch Earthquake (Cubrinovski et al., 2012) and 2016 Kumamoto Earthquake (Kiyota et al., 2017).

During earthquakes, due to the seismic loading, excess pore water pressure is generated in saturated sandy ground and consequently decreases the effective stress of the soil and induces liquefaction. Due to the mechanism of liquefaction, it was considered in the past that liquefaction could happen easier in saturated loose sandy ground where the excess pore water pressure is easier to accumulate during cyclic loadings or even monotonic loadings. In the past, most liquefaction cases were spotted in young (mostly after Holocene-age, deposited within 10,000 years) sandy deposits with high saturation degree and poor drainage, such as sands or gravels.

After decades of studying on liquefaction phenomenon, researches considered that the liquefaction resistance of a cohesionless soil mostly depends on the relative density,

cyclic stress ratio (indicating the relative magnitude of cyclic loading), and soil particle structures.

1.1.2 Liquefaction on dense sand

In the past, researchers found that liquefaction tended to happen in loose sandy soil or young sandy deposits. Results of laboratory tests showed that to some extent, the liquefaction resistance of sand was related to the relative density. Thus, liquefaction was considered to happen easily in the saturated loose sandy ground where the excess pore water pressure is easier to accumulate during cyclic loadings.

However, with the development of the society, evaluation of liquefaction resistance of saturated dense sands also becomes important especially during the construction of essential structures such as nuclear power plants, large-scale oil tanks, or earth-fill dams (Tatsuoka, 1982). Since this kind of critical structures asks for stable behavior even under large seismic motions, the aseismic design for them should be based on a high acceleration which may be dangerous even for dense sand foundations.

Regarding the study on liquefaction behavior of dense sands, pioneer researchers found very different performance for dense sand samples with similar relative density but obtained by different methods. For example, Ishihara (1977) proposed a linear relationship between liquefaction resistance and the relative density of sand specimen as follows:

$$\left(\sigma_{dp}/2\sigma_c'\right)_{20} = 0.0042D_r \qquad (1\text{-}1)$$

In this equation, $\left(\sigma_{dp}/2\sigma_c'\right)_{20}$ is the stress ratio in cyclic undrained triaxial tests which induces liquefaction at the number of 20 cycles and D_r is the relative density of the sand specimen expressed in percentage. But later study by Silver, et al. (1980) found that on dense sand specimen, the liquefaction resistance was no longer proportional to the relative density.

Yoshimi (1983) found that liquefaction resistance represented by the in-situ SPT-N value was different from the results of laboratory tests on the so-called undisturbed sample obtained by the tube sampling method. He also noticed that the data by the in-situ freezing method seemed to be consistent with its field behavior, which indicated the existence of disturbance in tube sampling method. The in-situ freezing seemed to be one possible solve to evaluate the liquefaction strength of a soil layer by laboratory tests, but because of its high cost, researchers were still considering using reconstituted samples in laboratory to simulate and predict the liquefaction resistance.

Study by Tatsuoka (1986) on different sample preparation methods showed differences existing between different preparation methods. He found the differences in the effects of sample preparation methods were significant in both triaxial and torsional shear tests. This result indicated that not only the relative density, different soil particle structures formed during different sample preparing methods may also attribute to the differences in liquefaction resistance.

Study by Towhata (2013) after the 2011 East Japan Earthquake emphasized the effect of ageing on the liquefaction resistance of sandy ground. Considering the long time period, liquefaction resistance will increase while the soil becomes denser and harder. During the long time ageing, not only the increase of relative density, the cementation between sand grains and strain histories induced by earthquakes can also affect the liquefaction resistance of the current sand layers.

1.1.3 Effects of strain history on liquefaction resistance

As mentioned above, strain histories during long time ageing were considered as one possible reason that strengthened the liquefaction resistance. In the past, Finn et al. (1970) firstly proposed that the strain history could affect the liquefaction resistance with simple shear test. They conducted consecutive liquefaction tests with consolidation in between. With reconsolidation after the first liquefaction, there were

always increase in relative density which were thought to strengthen the sand for the next liquefaction. However, they found that the former liquefaction history with a large amplitude of shear strain reduced the liquefaction resistance when the next liquefaction took place.

Seed et al. (1977) found similar phenomenon later in shaking table model test. They found that small strain amplitude in former liquefaction induced negligible change in relative density, but the liquefaction resistance increased a lot in the next time. On the contrary, large shaking magnitude which induced large shear strain and increase in relative density, the liquefaction resistance decreased in the next time. From that time, researchers realized that it was no longer appropriate to judge and evaluate the liquefaction resistance only by the density.

Detailed work regarding the effect of pre-shear history was carried out by Ishihara and Okada (1978, 1982) with undrained cyclic triaxial compression tests. With the concept of "the line of phase transformation" proposed by Ishihara et al. (1975), they distinguished the strain or stress history into two groups: "large pre-shearing" and "small pre-shearing". Pre-shear history with an effective stress path crossed the line of phase transformation was considered as the large pre-shearing, which could induce decrease in liquefaction resistance in the next time. On the other hand, the one which did not pass the line of phase transformation was considered as the small pre-shearing, which could increase the liquefaction resistance.

Suzuki and Toki (1984), Oda et al. (2001) and Wichtmann et al. (2005) conducted further study on this topic following the trace of those pioneer researchers mentioned above. But similar to those pioneer works, these studies on the pre-shearing effect focused only on the second time liquefaction.

Wahyudi et al. (2016) and Aoyagi et al. (2016) furtherly studied the effect of pre-shear history in multiple repeated liquefaction stages using a stacked-ring shear apparatus.

Similar as the former studies, they found that liquefaction resistance was affected by the shear strain amplitude. However, with multiple stages of liquefaction tests, the effect of pre-shear history in the first stage seemed to disappear after the second stage of liquefaction. By conducting repeated liquefaction tests on triaxial apparatus, Teparaksa (2017) found similar results as reported by Wahyudi et al. (2016) and Aoyagi et al. (2016). It was considered that the pre-shear history could only affect the liquefaction stage immediately after the pre-shear and disappeared after the next liquefaction.

Studies mentioned or not mentioned above on the topic of pre-shearing effects were mainly focused on loose sand or medium dense sand specimens. Therefore, information about pre-shearing effects on dense sand is not sufficient to explain the ageing effect or to prepare reconstituted samples for predicting the liquefaction resistance of field ground.

1.1.4 Application of energy concept in study of liquefaction

From 1980s, geotechnical researchers started to apply energy concept on analyzing the results of cyclic loading tests. With the stress-strain relationship obtained in laboratory testing, the dissipated energy during cyclic loading can be calculated. Researchers tried a lot to find the relationship between dissipated energy and the change in physical parameters of soil. For example, by triaxial testing, Simcock et al. (1983) studied the relationship between dissipated energy and the building up of excess pore water pressure during undrained cyclic loadings. Towhata and Ishihara (1985) studied on similar topic using a hollow cylindrical torsional shear apparatus. Similar investigations were also carried out by Okada and Nemat-Nasser (1994), Kazama et al. (2000) and Kokusho and Mimori (2015). In these studies, researchers also found that the dissipated energy might related with the type of sand, relative density, and pre-shearing histories.

Recently, with a stacked-ring shear apparatus developed in the Institute of Industrial Science, the University of Tokyo, Wahyudi (2014) studied the repeated liquefaction behavior using the following energy equation:

$$\sum \Delta W = \int q d\varepsilon = \int \tau d\gamma \qquad (1\text{-}2)$$

Aoyagi et al. (2016) later modified the equation to calculate the dissipated energy normalized by the current mean effective stress as follows:

$$\sum \frac{\Delta W}{p'} = \int \frac{q}{p'} d\varepsilon = \int \frac{\tau}{p'} d\gamma \qquad (1\text{-}3)$$

Aoyagi (2018) also pointed out that normalized dissipated energy accumulated in different loading stages might have different effect on the liquefaction resistance. With the border of the line of phase transformation, he divided the normalized dissipated energy into “positive effect” and “negative effect”. He suggested that before the effective stress path reaching the line of phase transformation, contractive behavior shown by the specimen accumulated positive effect while the rest was negative.

Another application of the normalized dissipated energy was reported by Matsui (2019). A procedure to draw the liquefaction resistance curve by single triaxial test was proposed and modified using the normalized dissipated energy.

In liquefaction test with a constant cyclic stress ratio, several cyclic loading cycles are needed to induce liquefaction or to reach the target double amplitude of strain. After every cycle of loading, the effective stress will decrease due to the accumulation of excess pore water pressure. Therefore, it can be considered that starting from this cycle of loading, it is a new liquefaction test with a relatively lower initial effective stress but a larger cyclic stress ratio, and it takes another number of cycles to reach the target liquefaction condition or strain amplitude. Then with data starting from different cycles of loading, liquefaction resistance curve can be obtained.

However, during the liquefaction test, due to the change of sand particle structure induced by the cyclic loading, liquefaction resistance is changing from the start to the

end. Therefore, it is necessary to modify the liquefaction resistance curve considering its changing during the single liquefaction test. Considering that the change of liquefaction resistance during the test might be relating with the dissipated energy or normalized dissipated energy, it is expected to derive a general relationship them.

1.2 Objective of the study

Based on the background introduced and previous study, the main objectives of this study are summarized as follows:

1. To compare the liquefaction behavior of dense sand without /with different kinds of pre-shear histories.

As mentioned in the background, liquefaction behavior of dense sand has not been extensively studied in the past. Since pre-shear history was considered as one of the reason that strengthened the soil, by studying the effect of pre-shear history on dense sand in detail, a procedure or method to reconstitute sand specimen that has similar strength as the field ground is expected to be proposed.

2. To analyze the liquefaction behavior of dense sand using the energy concept.

By applying the energy equation and modified energy equation introduced above, analysis will be carried out to study the relationship between dissipated energy (or normalized one) and the pre-shear effect.

3. Further expanded study applying energy concept in predicting the liquefaction resistance of sand.

After figuring out the relationship between dissipated energy (or normalized one) and pre-shear effect, attempt will be made to predict liquefaction resistance of sand. As mentioned in the background, during the procedure of predicting the liquefaction resistance using a single liquefaction test, it is necessary to modify the curve with help of energy concept.

1.3 Organization of the thesis

The organization of this thesis is shown as follows:

Chapter 1	**Introduction** This chapter introduces the background and previous study, study objective and thesis organization.
Chapter 2	**Material and Apparatus** This chapter introduced tested material, testing apparatus and testing methodology. Calculation of stresses and strains in torsional shear test is also presented in this chapter.
Chapter 3	**Testing Procedures and Programs** This chapter introduces the testing procedures of torsional shear test and test programs of this study.
Chapter 4	**Results of Torsional Shear Tests** This chapter presents the test result of repeated liquefaction test on torsional shear apparatus.
Chapter 5	**Analysis of Pre-shear Effects Based on the Energy Concept** This chapter shows the analysis and discussions on pre-shear effects applying the energy concept.
Chapter 6	**Application of Energy Concept to Estimate Liquefaction Resistance Curve Based on Result from a Single Test** This chapter introduces the attempt to draw the liquefaction resistance curve with a single liquefaction test with the application of the normalized dissipated energy.
Chapter 7	**Conclusions and Recommendation for Future Works** This chapter summarizes the findings from the results of liquefaction tests and analysis followed. Possible future works are also proposed in this chapter.

1.4 References

AOYAGI, Y., WAHYUDI, S., KOSEKI, J., SATA, T. and MIYASHITA, Y., 2016. Behavior of multiple-liquefaction under small to large strain levels and its analysis based on dissipated energy. *JSCE Journal of Earthquake Engineering*, Vol. 72(4), pp. I_167-I_176 (in Japanese).

AOYAGI, Y., 2018. Analysis of multiple-liquefaction characteristics in torsional shear and stacked ring shear tests based on energy concept. *Ph.D. Thesis. Department of Civil Engineering, the University of Tokyo, Japan (in Japanese).*

CUBRINOVSKI, M., HENDERSON, D. and BRADLEY, B., 2012. Liquefaction impacts in residential areas in the 2010-2011 Christchurch earthquakes. *Civil and Natural Resources Engineering, University of Canterbury.*

FINN, W.D.L., BRANSBY, P.L. and PICKERING, D.J., 1970. Effect of strain history on liquefaction of sand. *Journal of Soil Mechanics & Foundations Div,* Vol. 96(SM6)

ISHIHARA, K., TATSUOKA, F. and YASUDA, S., 1975. Undrained deformation and liquefaction of sand under cyclic stresses. *Soils and Foundations*, Vol.15(1), pp. 29-44.

ISHIHARA, K., 1977. Simple method of analysis for liquefaction of sand deposits during earthquake. *Soils and Foundations,* Vol. 17(3), pp. 1-17.

ISHIHARA, K. and OKADA, S., 1978. Effects of stress history on cyclic behavior of sand. *Soils and Foundations,* Vol. 18(4), pp. 31-45.

ISHIHARA, K. and KOGA, Y., 1981. Case studies of liquefaction in the 1964 Niigata earthquake. *Soils and Foundations,* Vol. 21(3), pp. 35-52.

ISHIHARA, K. and OKADA, S., 1982. Effects of large preshearing on cyclic behavior of sand. *Soils and Foundations,* Vol. 22(3), pp. 109-125.

KAZAMA, M., YAMAGUCHI, A. and YANAGISAWA, E., 2000. Liquefaction resistance from a ductility viewpoint. *Soils and Foundations,* Vol. 40(6), pp. 47-60.

KIYOTA, T., IKEDA, T., KONAGAI, K. and SHIGA, M., 2017. Geotechnical damage caused by the 2016 Kumamoto Earthquake, Japan. *International Journal of Geoengineering Case Histories*, Vol. 4(2), pp. 78-95.

KOKUSHO, T. and MIMORI, Y., 2015. Liquefaction potential evaluations by energy-based method and stress-based method for various ground motions. *Soil Dynamics and Earthquake Engineering,* Vol. 75, pp. 130-146.

MCCULLOCH, D.S. and BONILLA, M.G., 1970. *Effects of the earthquake of March 27, 1964, on the Alaska Railroad. US Government Printing Office.*

ODA, M., KAWAMOTO, K., SUZUKI, K., FUJIMORI, H. and SATO, M., 2001. Microstructural interpretation on reliquefaction of saturated granular soils under cyclic loading. *Journal of Geotechnical and Geoenvironmental Engineering*, Vol. 127(5), 416-423.

SEED, H. B., MORI, K. and CHAN, C., 1977. Influence of seismic history on liquefaction of sands. *Journal of Geotechnical and Geoenvironmental Engineering,* Vol. 103 (Proc. Paper 11318 Proceeding).

SILVER, M. L., CHAN, C.K., LADD, R.S., LEE, K.L., TIEDEMANN, D.A., TOWNSEND, F.C., VALERA, J.E. and WILSON, J.H., 1976. Cyclic triaxial strength of standard test sand. *Journal of the GT Div., Proc. of ASCE*, Vol. 102(GT5), pp. 511-523.

SILVER, M. L., TATSUOKA, F., PHUKUNHAPHAN, A. and AVRAMIDIS, A. S., 1980. Cyclic undrained strength of sand by triaxial test and simple shear test. *Proc. of the 7th World Conf. on Earthquake Eng., Istanbul*, Vol. 3, pp. 281-288.

SUZUKI, T. and TOKI, S., 1984. Effects of preshearing on liquefaction characteristics of saturated sand subjected to cyclic loading. *Soils and Foundations,* Vol. 24(2), pp. 16-28.

TATSUOKA, F., IWASAKI, T., TOKIDA, K., YASUDA, S., HIROSE, M., IMAI, T. and KON-NO, M., 1978. A method for estimating undrained cyclic strength of sandy soils using standard penetration resistances. *Soils and Foundations,* Vol. 18(3), pp. 43-58.

TATSUOKA, F., MURAMUTSU, M., SASAKI, T., 1982. Cyclic undrained stress-strain behavior of dense sands by torsional simple shear test. *Soils and Foundations*, Vol. 22 (2), pp. 55-70.

TATSUOKA, F., OCHI, K., FUJII, S. and OKAMOT, M., 1986. Cyclic undrained triaxial and torsional shear strength of sands for different sample preparation methods. *Soils and Foundations,* Vol. 26(3), pp. 23-41.

TEPARAKSA, J. 2017. Comparison of sand behavior under repeated liquefaction in triaxial and shaking table tests. *Ph.D. Thesis. Department of Civil Engineering, the University of Tokyo, Japan.*

TOWHATA, I., MARUYAMA, S., KASUDA, K., KOSEKI, J., WAKAMATSU, K., KIKU, H., KIYOTA, T., YASUDA, S., TAGUCHI, Y., AOYAMA, S. and

HAYASHIDA, T., 2014. Liquefaction in the Kanto region during the 2011 off the pacific coast of Tohoku earthquake. *Soils and Foundations*, Vol. 54 (4), pp. 859-873.

WAHYUDI, S., 2014. Cyclic simple shear tests using stacked-rings on multiple liquefaction properties of sands. *Ph.D. Thesis. Department of Civil Engineering, the University of Tokyo, Japan.*

WAHYUDI, S., KOSEKI, J., SATO, T. and CHIARO, G., 2016. Multiple-liquefaction behavior of sand in cyclic simple stacked-ring shear tests. *International Journal of Geomechanics,* Vol. 16(5), pp. C4015001.

WICHTMANN, T., NIEMUNIS, A., TRIANTAFYLLIDIS, T. and POBLETE, M., 2005. Correlation of cyclic preloading with the liquefaction resistance. *Soil Dynamics and Earthquake Engineering,* Vol. 25(12), pp. 923-932.

YUAN, H., YANG, S.H., ANDRUS, R.D. and JUANG, C.H., 2004. Liquefaction-induced ground failure: a study of the Chi-Chi earthquake cases. *Engineering Geology,* Vol. 71(1), pp. 141-155.

Chapter 2 Materials and Apparatus

2.1 Introduction

In this chapter, the details of the materials and two types of hollow cylindrical torsional shear apparatus employed in this study will be introduced.

In order to study the effect of pre-shear history without the interference of cementation, silica sand with number 7 grading was used in this study. In this chapter, the details of this material will be introduced.

In this study, two different sizes of hollow cylindrical torsional shear apparatus were employed. Liquefaction test with long-term pre-shear histories took a very long time so that two devices were employed in order to finish more tests. Since these two apparatuses have different sizes of specimens, a series of liquefaction tests with the same relative density of specimens, confining conditions, and loading programs were carried out to compare their possible differences. The results will be introduced in the 4^{th} chapter.

2.2 Tested materials

In Japan, Toyoura sand is widely used in geotechnical testing as a Japanese standard sand (JGS, 2014). However, due to its high price (mainly because of the transportation cost), it is sometime substituted by the silica sand in model tests or in large scale elementary tests. Silica sand is an artificial sand produced by crashing rocks. By means of sieving, sand with different particle sizes can be made to satisfy different requirement of using. In this study, due to the relatively large size of specimen, silica sand with number 7 grading was used instead of Toyoura sand. Generally, the number 7 grading of silica sand has a similar grain size distribution as Toyoura sand and is widely used in liquefaction tests as well. Table 2-1 shows some basic properties of silica sand with number 7 grading along with those of Toyoura sand, and Figure 2-1 shows their accumulated grain size distributions.

Teparaksa (2017) showed the laser scanning picture (shown in Figure 2-2) of Silica sand with number 7 grading. He found that the shape of silica sand was more angular than the Toyoura sand. In the past, research has already shown that more narrowly graded and rounded sand are more susceptible to liquefaction (Poulos et al., 1985) which means the Silica sand with number 7 grading may have a little bit stronger liquefaction resistance than the Toyoura sand.

Table 2-1 Properties of silica sand with number seven grading and Toyoura sand

Properties	**Silica Sand with number 7 grading**	**Toyoura Sand**
Specific gravity	2.640	2.656
Maximum Void Ratio	1.211	0.992
Minimum Void Ratio	0.700	0.632
Mean Particle Diameter, D_{50} (mm)	0.200	0.190

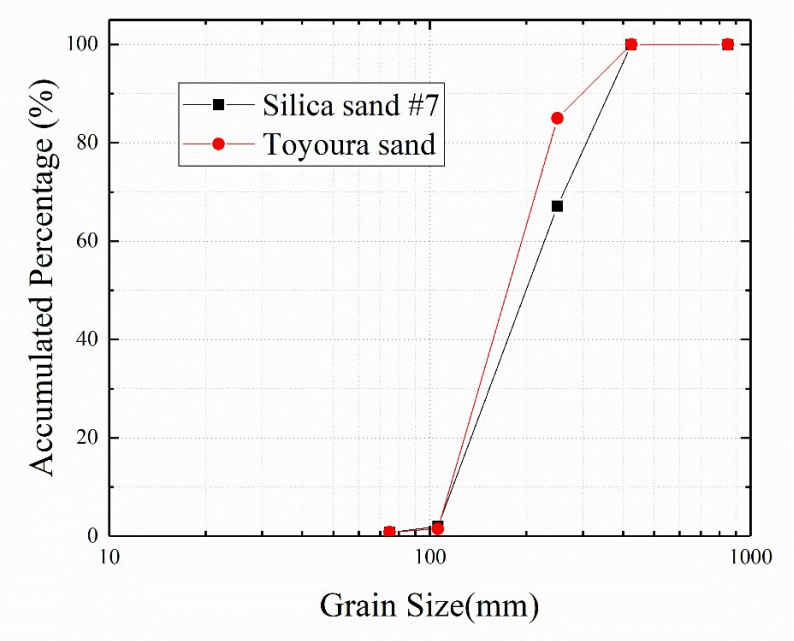

Figure 2-1 Grain size distribution of Silica sand with number 7 grading and Toyoura sand

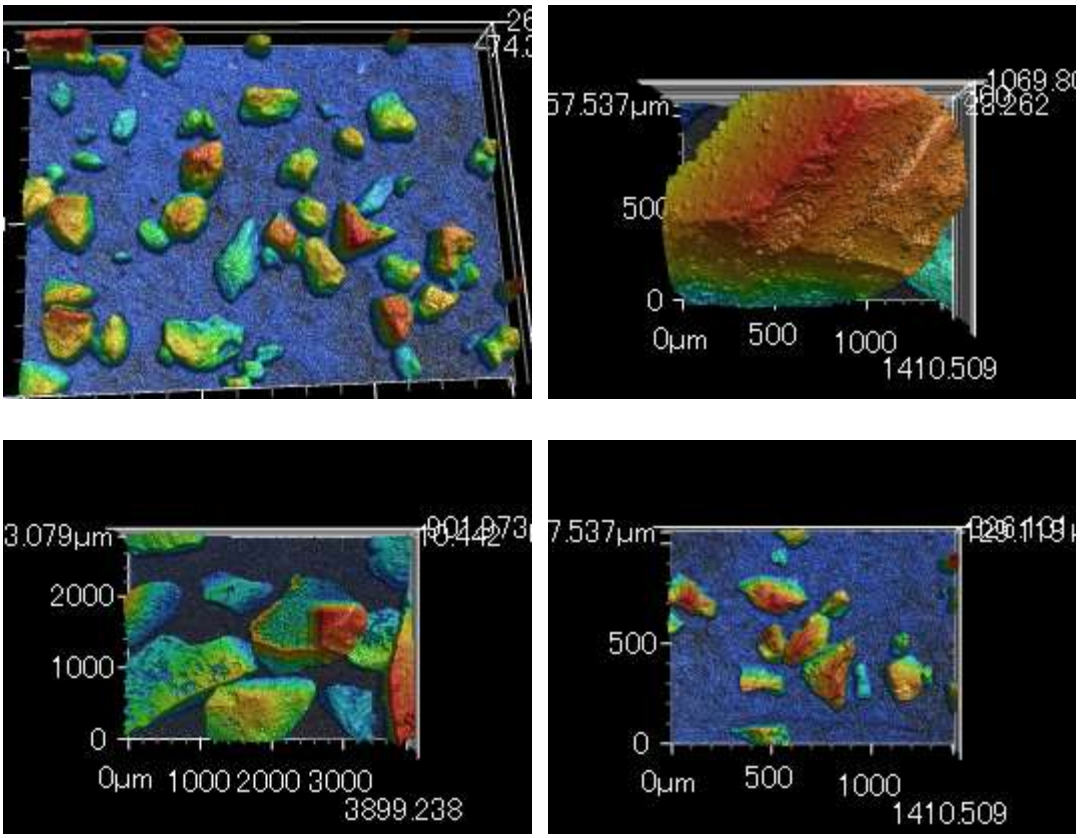

Figure 2-2 Laser photos of Silica sand with number 7 grading (Teparaksa, 2017)

2.3 Test apparatus and monitoring devices

In this study, two different sizes of hollow cylindrical torsional shear apparatus were employed. In this part, the details of these apparatus and monitoring devices will be introduced.

2.3.1 Mid-scale torsional shear apparatus

In this study, a mid-scale torsional shear apparatus developed at Institute of Industrial Science, the University of Tokyo was employed. The photo and schematic figure of this apparatus are shown in Figures 2-3, 2-4 and 2-5 (Zhao, 2017). This apparatus is capable for various specimen sizes with the height ranging from 200 to 300 mm, outer diameter ranging from 100 to 200 mm and inner diameter ranging from 60 mm to 160 mm. In this study, a hollow cylindrical specimen with 120 mm inner diameter, 200 mm outer diameter and 300 mm height was selected.

As shown in Figures 2-4 and 2-5, this apparatus mainly consists of two parts: cell body and loading systems. In the body part, a pressure cell produced by acrylic resin was applied to cover the sand specimen during confined conditions. A two-component load cell was installed between the loading shaft and top cap on specimen to measure the vertical load and torque. The external displacement transducer and potentiometer were set up to measure the vertical displacement and the rotation angle. For measuring the difference of pore water pressure and cell pressure which indicates the effective confining pressure, a high capacity differential pressure transducer was employed. For precise measurement of volume change (drainage amount of water), an electronic balance sealed in a chamber was employed.

The loading system shown in Figure 2-5 contains the vertical and torsional loading systems. The vertical loading capacity is 15 kN and the torsional one is 0.3 kN·m. Both

loading systems contain an AC servo motor, gear systems and electronic magnetic clutches. During working condition, the servo motor keeps moving in one direction and by controlling the clutch via voltage signal, loadings with different directions can be applied through gear systems to the loading shaft. In the torsional loading system, the loading shaft is connected to two metal belts. When the horizontal shaft moves with the rotation of motor, these two steel belts can transmit this horizontal loading into torque to the vertical loading shaft through a round metal plate. In addition, the vertical and torsional loading systems can work together without interference. The mutually independent feedback systems (monitoring devices) make it possible for the computer to control the vertical and torsional loading systems independently.

Generally, triaxial or torsional test apparatuses with this kind of loading system are considered as strain-controlled. Since the loading speed can be controlled by the motor via computer voltage output signals, constant loading speed can be appied. In addition, feedbacks from monitoring devices (displacement transducer, potentiometer and load cell) make it possible to stop the loading or change the loading direction after reaching the target strain amplitude or stress amplitude.

Load cell

Koseki et al. (2005) introduced a bronze load cell fixed between the vertical loading shaft and the top cap of specimen which can measure both vertical deviator loads and torque without mutual interference. The capacity of the load cell on this mid-scale torsional shear apparatus is 15 kN in vertical and 0.3 kN·m in torque. With the application of the amplifier and a 16 channels A/D signal converting system, the micro voltage signal generated from the strain gauge installed on the load cell will be transmitted and recorded by the computer.

External displacement transducer

In order to measure the vertical displacement of the specimen, an external displacement transducer was installed as shown in Figure 2-6. The displacement transducer was fixed on the cell with its pin touching beneath a metal plate that connected with the loading shaft. The range of this external displacement transducer is 10 mm.

Potentiometer

Figure 2-7 shows the potentiometer used for measuring the corresponding rotation angle of loading shaft. After conversion, this potentiometer can detect a maximum shear strain of 38%.

Gap sensor

As shown in Figure 2-8, a pair of metal plates are installed on the top cap of the specimen together with a pair of touchless displacement transducers (gap sensors). This kind of displacement transducer can measure the displacement with very high precision and low fluctuation. This kind of characteristic makes it very suitable for measuring the shear strain in the early loading stages, which can be used for calculating the shear modulus. Since its range is limited in 2 mm, after the first cycle of cyclic loading, it must be removed away by a handle.

High capacity differential pressure transducer (HCDPT)

In this apparatus, a high capacity differential pressure transducer is employed to measure the difference between pore water pressure and cell pressure. This difference is considered as the effective confining pressure during isotropic condition. As shown in Figure 2-4, the double sides of the transducer are connected with the specimen and cell.

Electronic Balance

Drainage from the specimen is measured by a high sensitivity electronic balance (AND FX-500i) in order to calculate the volume change of the specimen. With a precision of 0.001 g, this balance can measure the volume change more precisely than other methods (Fauzi and Koseki, 2014). The load cell of the balance is separated from the machine and sealed in a chamber that connected with the specimen by the drainage tube. This design makes the measurement possible with the application of backpressure to the specimen as shown in Figure 2-4.

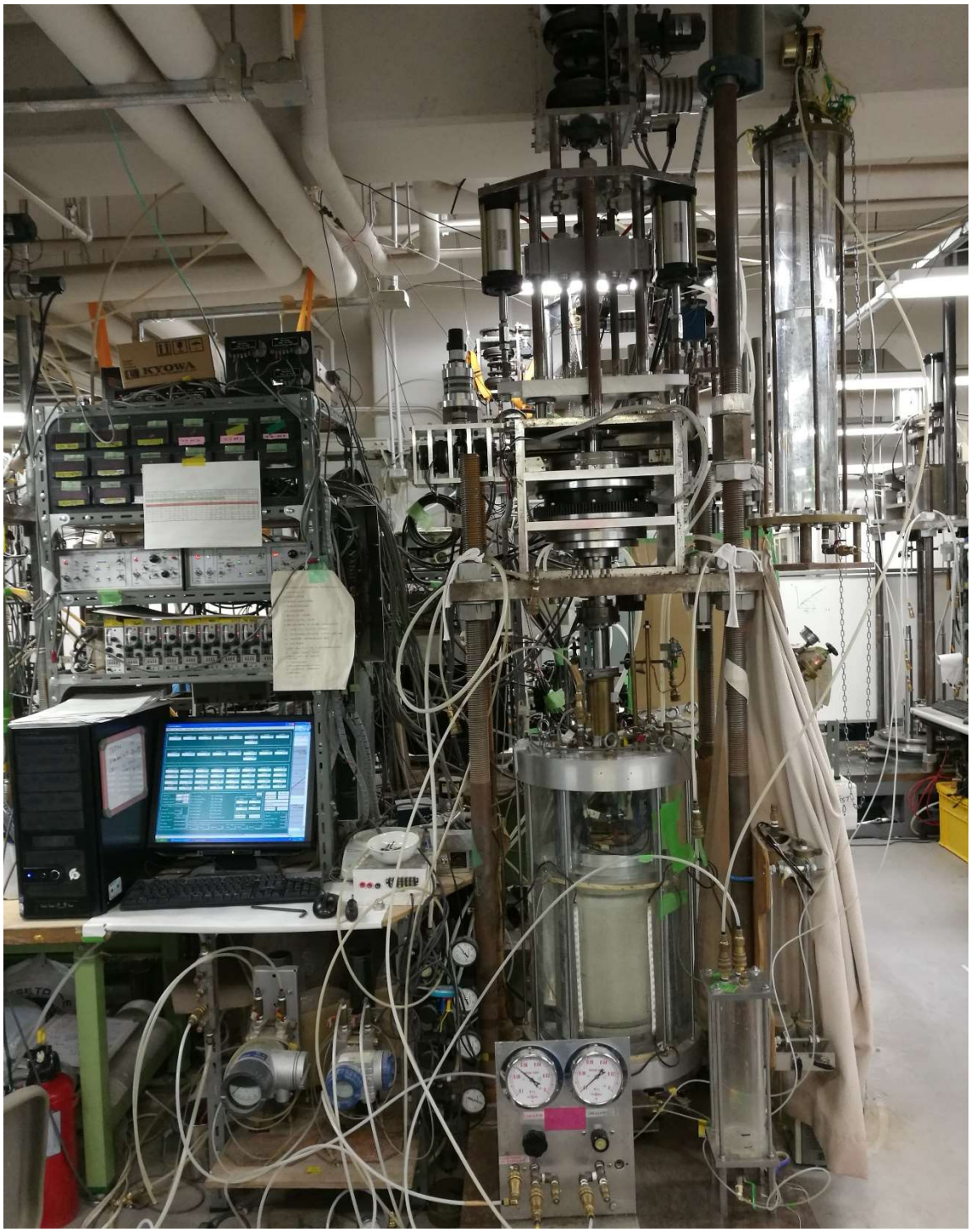

Figure 2-3 Photo of the mid-scale torsional shear apparatus

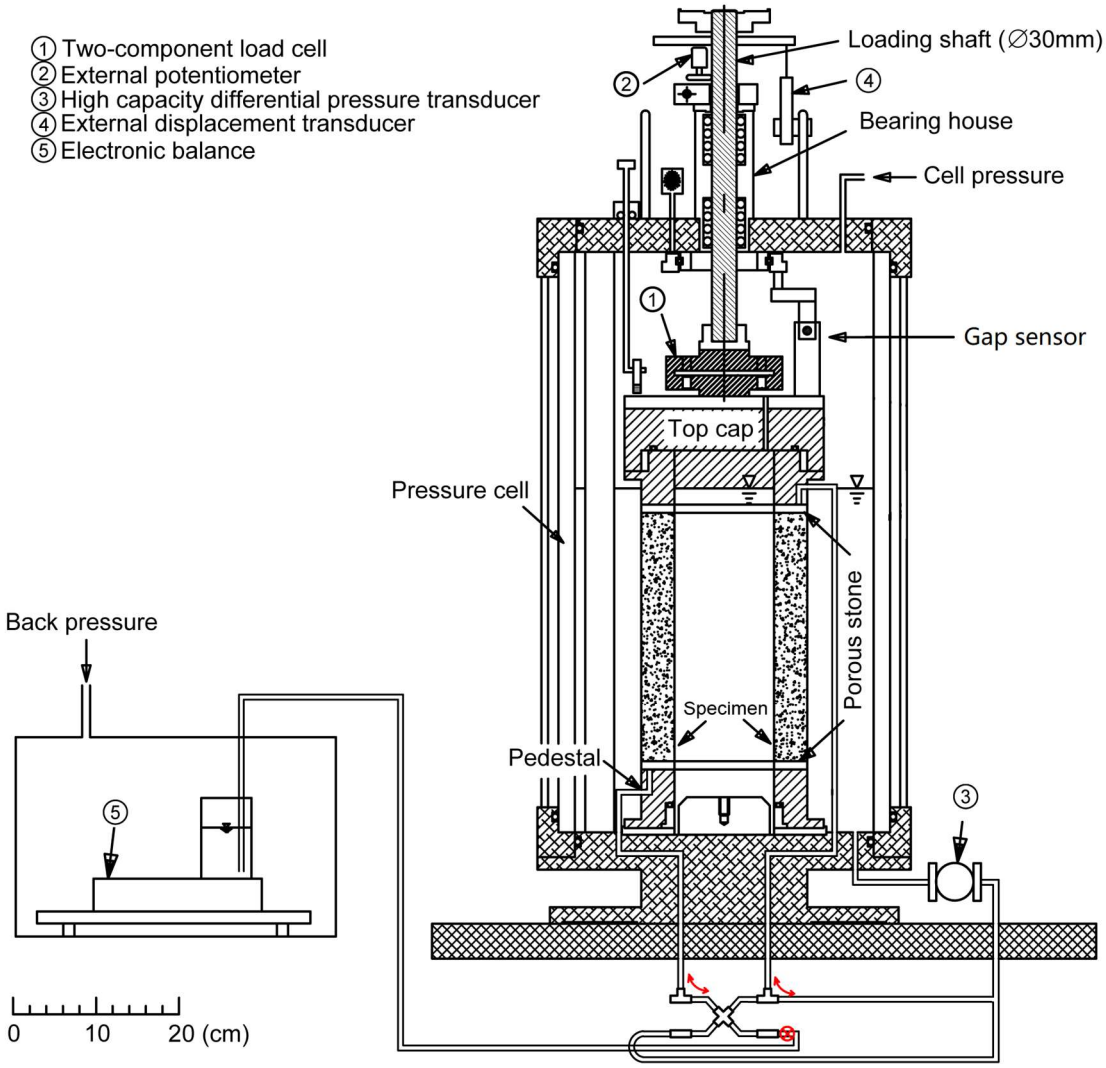

Figure 2-4 Schematic figure of the mid-scale torsional shear apparatus (body part) (Zhao, 2017)

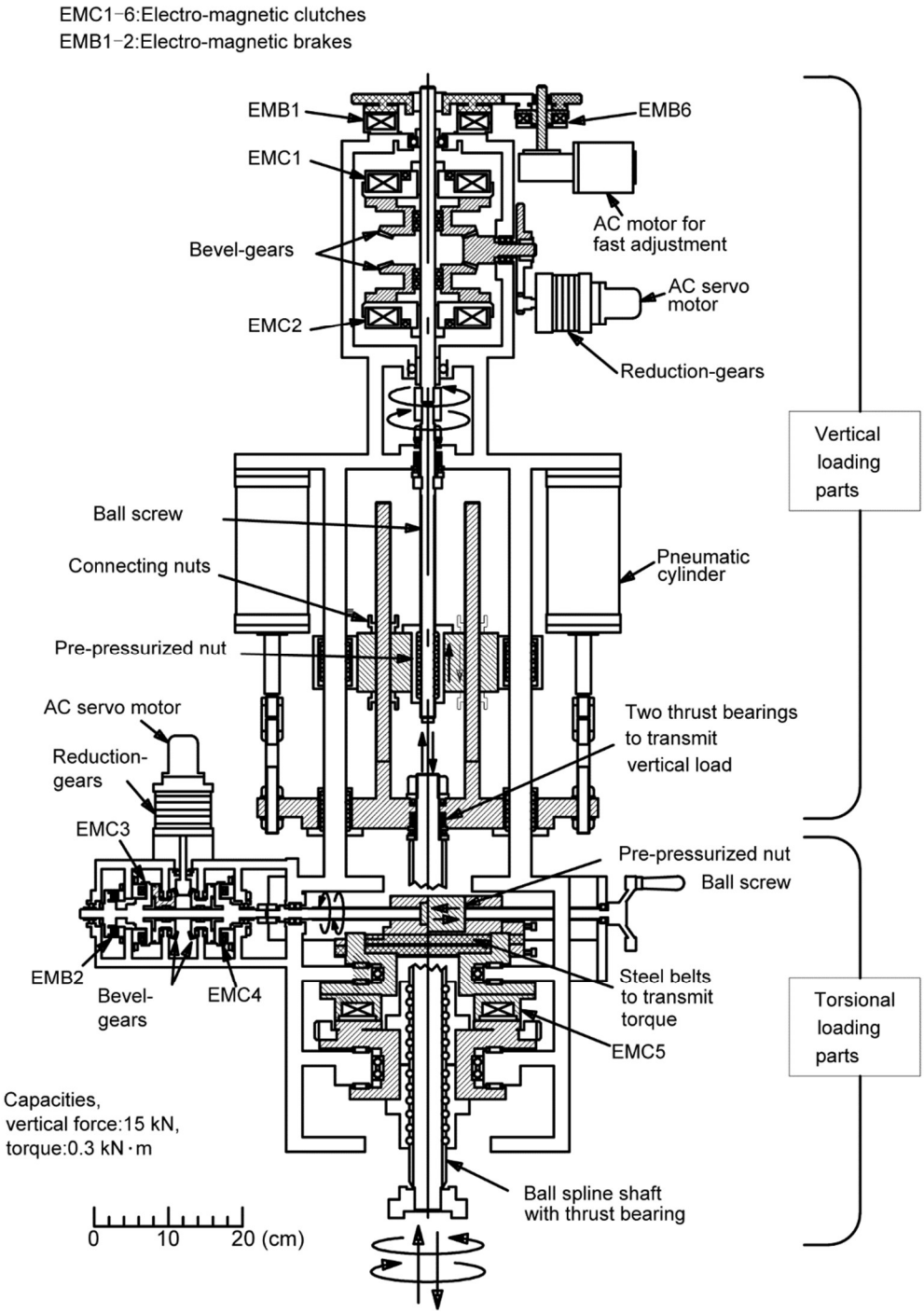

Figure 2-5 Schematic figure of the mid-scale torsional shear apparatus (loading system) (Zhao, 2017)

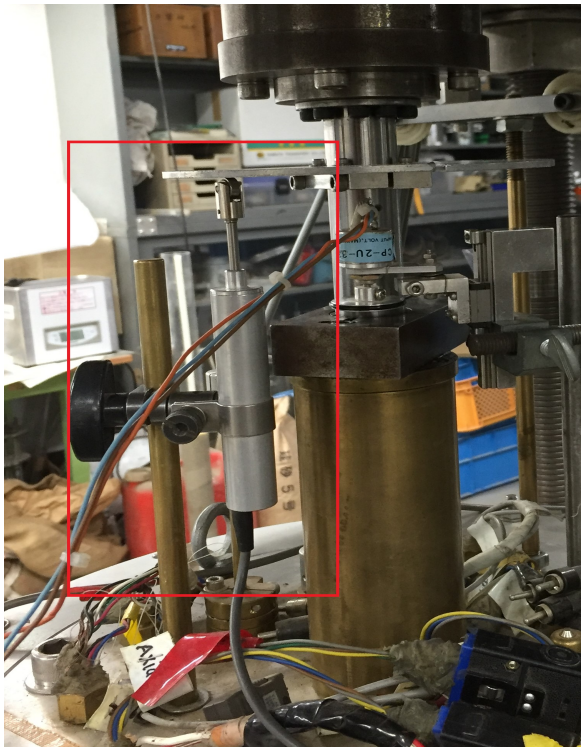

Figure 2-6 External displacement transducer

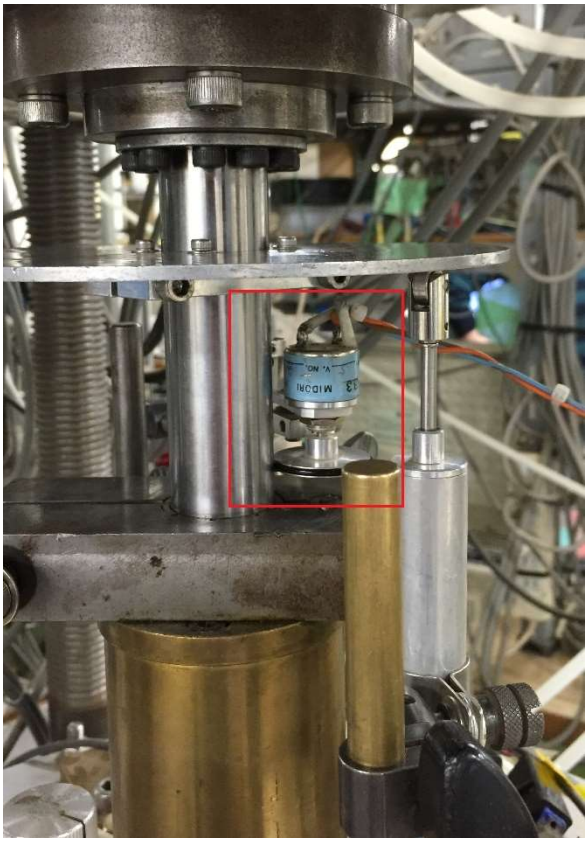

Figure 2-7 Potentiometer for measuring rotation angle

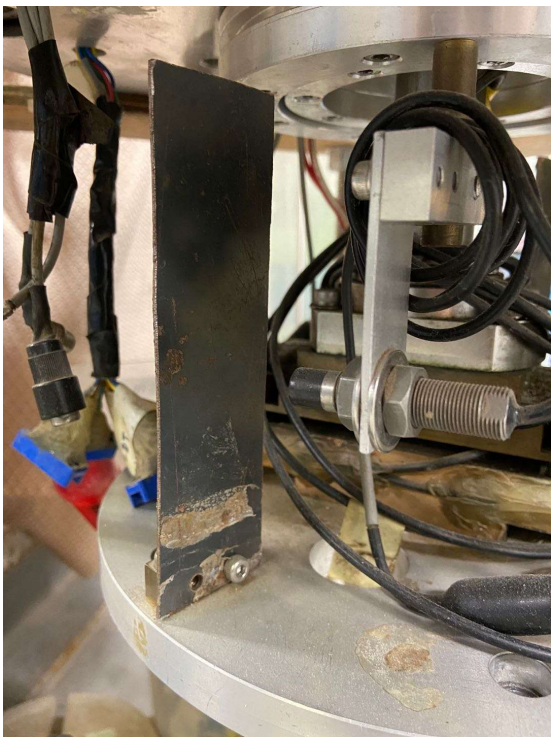

Figure 2-8 Gap sensor

2.3.2 Small-scale torsional shear apparatus

Considering the long time period for one liquefaction test with pre-shear history and repeated stages, a small-scale torsional shear apparatus was also employed in this study. This apparatus is capable for a hollow cylindrical specimen with the inner diameter of 60 mm, outer diameter of 100 mm, and 200 mm in height. It has similar loading systems as the mid-scale one (Sato et al., 1991) but with different motors (Oriental speed control motors are used in this apparatus). By receiving voltage signal from the computer, the magnetic clutch can change the loading direction. Instead of a pair of metal belts, a pair of metal chains are used to connect the horizontal and the vertical loading shafts. With same working mechanism, the movement of horizontal loading shaft can induce rotation of the vertical one through this converting system.

Load cell

A two component load cell with the capacity of 5000 N in vertical load and 50 N·m in torque is installed in this apparatus.

External displacement transducer

Same type of external displacement transducer with a range of 10 mm is employed as introduced in the mid-scale apparatus for measuring the vertical displacement of the specimen.

Potentiometer

Potentiometer is used in this apparatus for measuring the rotation angle of the loading shaft which can be converted into shear strain of the specimen.

Pore water pressure gauge

In this torsional apparatus, a pair of pore water pressure gauge are employed to measure the pore water pressure in the specimen and cell pressure independently. Two pore water pressure gauges are connected with specimen and cell subjectively. Effective confining pressure can be calculated with the recording data from these two gauges.

Low capacity differential pressure transducer (LCDPT)

The low capacity differential pressure transducer (LCDPT) are employed in this apparatus to measure the drainage from specimen. A double cell burette is connected to the two sides of the transducer and its inner cell is connected with the specimen with the drainage pipe. While keeping the water head of the outer cell, the differential pressure transducer can measure the change of water head in the inner cell. With calibration in advance, this change in water head pressure can be converted into volume change of the specimen.

2.4 Calculation of stresses and strains in torsional shear tests

The hollow cylindrical specimen can be considered as infinite long specimen at circumferential direction. But due to this cylindrical shape, shear stress is not uniform in the cross section of the specimen. It is assumed that the distribution of stress along radial direction is linear when the shear strain is small enough, and the sand will act as a plastic material after exceeding a large shear strain. In most cases, the sand stays in the status between elastic and plastic.

In this part, the calculation and definitions of various stresses and strains of torsional shear tests will be introduced. Analysis and discussions on the torsional shear test results will be based on these parameters.

2.4.1 General soil mechanical parameters

In this part, basic soil mechanical parameters used in later discussions will be briefly introduced.

Soil void ratio (e):

$$e = \frac{V_V}{V_S} = \frac{V - V_S}{V_S} \qquad (2\text{-}1)$$

where the V, V_V and V_S represent the total volume of soil, volume of void and volume of solid, respectively.

Soil relative density (D_r):

$$D_r = \frac{(e_{max} - e)}{(e_{max} - e_{\min})} \times 100\% \qquad (2\text{-}2)$$

where e_{max} and e_{min} are the maximum and minimum void ratio of the soil.

Degree of saturation (S_r):

$$S_r = \frac{V_W}{V_S} \times 100\% \qquad (2\text{-}3)$$

where V_W and V_S represent the volume of water and volume of solid of the soil.

In liquefaction test, the degree of saturation was reported to affect the result significantly. Therefore, as a more sensitive parameter, B value is much more widely used to check the saturation degree of soil specimens. Figure 2-9 shows the relationship between B value and the degree of saturation of Toyoura sand with the relative density of 60% (Yoshimi et al., 1989). The equation for calculating B value is as follows:

$$B = \frac{\Delta u}{\Delta \sigma_3} \quad (2\text{-}4)$$

where Δu is the increment of pore water pressure of specimen and $\Delta \sigma_3$ is the increment of minor total principle stress (in isotropic undrained condition).

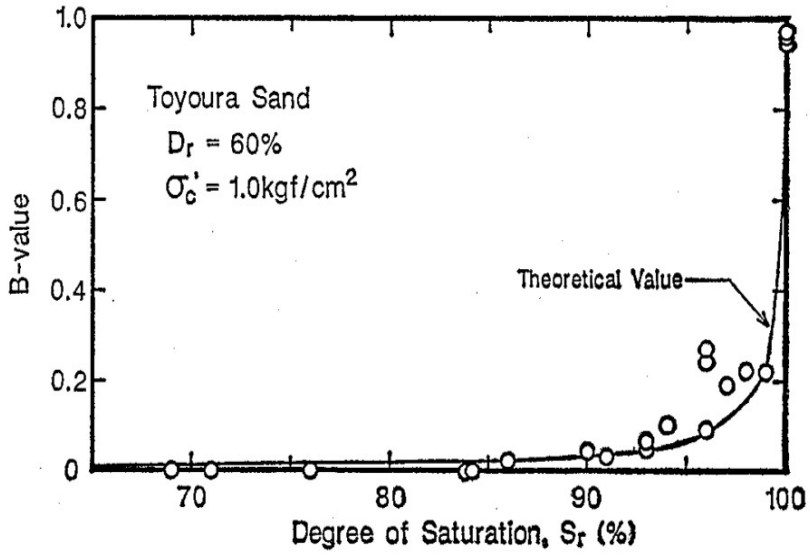

Figure 2-9 Relationship between degree of saturation and B-value (Yoshimi et al., 1989)

2.4.2 Stresses and strains in hollow cylindrical torsional shear test

In this part, various stresses and strains in hollow cylindrical torsional shear test will be introduced. Generally, Figure 2-10 shows the model of a hollow cylindrical specimen and various stresses and strains in the small element A. With the two types of hollow cylindrical torsional shear apparatuses, these 4 stresses can be controlled independently. In this study, the inner cell and outer cell are always connected so that the inner cell pressure (P_i) and outer cell pressure (P_o) are always equal to each other. These stresses

are named as radial stress (σ_r), circumferential stress (σ_θ), axial stress (σ_z) and shear stress ($\tau_{z\theta}$) correspond with radial strain (ε_r), circumferential strain (ε_θ), axial strain (ε_z) and shear strain ($\gamma_{z\theta}$), respectively.

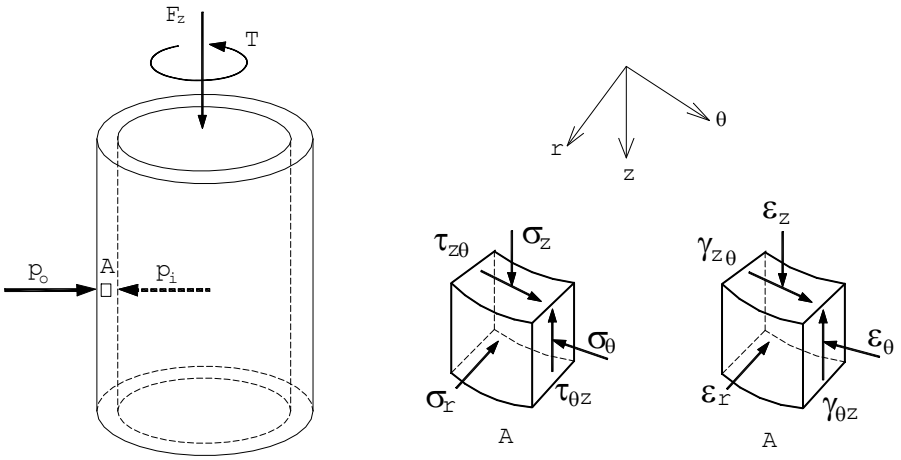

Figure 2-10 Stresses and strains in element A of a hollow cylindrical specimen

Computation for vertical stress

The average of vertical stress could be calculated by the following equation:

$$\overline{\sigma_z} = \frac{LC}{A} + \sigma_h + \sigma_{mem} \qquad (2\text{-}5)$$

where, LC is the deviator load measured by load cell, A is the cross section area of the specimen, σ_h is the horizontal stress that is equal to the cell pressure, and σ_{mem} is the correction stress induced by the membrane (Tatsuoka et al., 1986b).

Computation for radial circumferential stress

Timoshenko and Goodier (1970) proposed a solution for hollow cylinder specimen as a uniform material subjected to uniform inner cell pressure (P_i) and outer cell pressure (P_o). It is assumed that the stress distribution is symmetrical with respect to the vertical axis (z) of the hollow cylinder. It is also accumed that the stress components do not depend on the radial angle (θ) and are a function of radius (r) only. Therefore, shear

stress ($\tau_{r\theta}$) should be considered as 0 kPa. The equation of equilibrium in the radial direction yields is:

$$\frac{\partial \sigma_r}{\partial r} + \frac{\sigma_r - \sigma_\theta}{r} + \omega = 0 \qquad (2\text{-}6)$$

where ω is the body force. When ω is 0, equation (2-6) is satisfied by:

$$\sigma_r = \frac{B}{r^2} + 2C \qquad (2\text{-}7)$$

$$\sigma_\theta = -\frac{B}{r^2} + 2C \qquad (2\text{-}8)$$

where *B* and *C* are constants, which can be obtained by the following conditions:

$$\sigma_r|_{r=R_i} = p_i \qquad (2\text{-}9)$$

$$\sigma_r|_{r=R_o} = p_o \qquad (2\text{-}10)$$

where R_o and R_i are the outer and inner radii of the hollow cylindrical specimen, respectively.

By substituting equations (2-9) and (2-10) into equations (2-7) and (2-8):

$$\sigma_r = \frac{p_o R_o^{\,2} - p_i R_i^{\,2}}{R_o^{\,2} - R_i^{\,2}} - \frac{R_i^{\,2} R_o^{\,2} (P_o - P_i)}{R_o^{\,2} - R_i^{\,2}} \times \frac{1}{r^2} \qquad (2\text{-}11)$$

$$\sigma_\theta = \frac{p_o R_o^{\,2} - p_i R_i^{\,2}}{R_o^{\,2} - R_i^{\,2}} + \frac{R_i^{\,2} R_o^{\,2} (P_o - P_i)}{R_o^{\,2} - R_i^{\,2}} \times \frac{1}{r^2} \qquad (2\text{-}12)$$

Average stress components can be calculated without weighting and with weighting as follows (Ampadu, 1991):

Averaging without weighting:

$$\overline{\sigma_r} = \frac{\int_{R_i}^{R_o} \sigma_r dr}{\int_{R_i}^{R_o} dr} \quad , \quad \overline{\sigma_\theta} = \frac{\int_{R_i}^{R_o} \sigma_\theta dr}{\int_{R_i}^{R_o} dr} \qquad (2\text{-}13)$$

By substituting equation (2-11) and (2-12) into (2-13):

$$\overline{\sigma_r} = \frac{P_o R_o + P_i R_i}{R_o + R_i} \quad (2\text{-}14)$$

$$\overline{\sigma_\theta} = \frac{P_o R_o - P_i R_i}{R_o - R_i} \quad (2\text{-}15)$$

Averaging with weighting:

$$\int_{R_i}^{R_o} \sigma_r r dr = \int_{R_i}^{R_o} \overline{\sigma_r} r dr \quad (2\text{-}16)$$

$$\int_{R_i}^{R_o} \sigma_\theta r dr = \int_{R_i}^{R_o} \overline{\sigma_\theta} r dr \quad (2\text{-}17)$$

$$\overline{\sigma_r} = \frac{\int_{R_i}^{R_o} \sigma_r r dr}{\int_{R_i}^{R_o} r dr} \quad (2\text{-}18)$$

$$\overline{\sigma_\theta} = \frac{\int_{R_i}^{R_o} \sigma_\theta r dr}{\int_{R_i}^{R_o} r dr} \quad (2\text{-}19)$$

By substituting equation (2-11) and (2-12) into equation (2-18) and (2-19):

$$\overline{\sigma_r} = \frac{p_o R_o^{\,2} - p_i R_i^{\,2}}{R_o^{\,2} - R_i^{\,2}} - \frac{2R_i^{\,2} R_o^{\,2} (P_o - P_i)}{(R_o^{\,2} - R_i^{\,2})^2} \times \ln\left(\frac{R_o}{R_i}\right) \quad (2\text{-}20)$$

$$\overline{\sigma_\theta} = \frac{p_o R_o^{\,2} - p_i R_i^{\,2}}{R_o^{\,2} - R_i^{\,2}} + \frac{2R_i^{\,2} R_o^{\,2} (P_o - P_i)}{(R_o^{\,2} - R_i^{\,2})^2} \times \ln\left(\frac{R_o}{R_i}\right) \quad (2\text{-}21)$$

In this study, since the outer and inner cell pressures are equal to each other ($P_i = P_o$), it can be obtained from equations (2-20) and (2-21) that $\overline{\sigma_r} = \overline{\sigma_\theta} = P_o = P_i$.

Computation for shear stress

When the specimen is rotated by an angle $d\theta$, the rotation displacements of a sand particle on the radial direction will be $rd\theta$. Thus, the shear stress applied on the soil element is not uniform along the radial direction (with different distance to the center). The soil element may be considered to have an elastic stage under a small shear strain,

and then becomes elastic-plastic and eventually into the plastic stage. The toque that is applied to the specimen can be calculated as:

$$T = \int_{R_i}^{R_o} \int_0^{2\pi} \tau_{z\theta} r^2 d\theta dr = 2\pi \int_{R_i}^{R_o} \tau_{z\theta} r^2 dr \qquad (2\text{-}23)$$

If the material stays in a perfectly elastic stage in which $\tau_{z\theta}^{e} = kr$:

$$T = \int_{R_i}^{R_o} \int_0^{2\pi} \tau_{z\theta}^{e} r^2 d\theta dr = 2\pi k \int_{R_i}^{R_o} r^3 dr = \frac{\pi}{2}(R_o^4 - R_i^4)k \qquad (2\text{-}24)$$

Then the average shear stress along the radial direction is:

$$\overline{\tau_{z\theta}^{e}} = k \times \frac{R_o + R_i}{2} = \frac{T}{\pi(R_o^2 + R_i^2)(R_o - R_i)} \qquad (2\text{-}25)$$

$$k = \frac{2T}{\pi(R_o^4 - R_i^4)} \qquad (2\text{-}26)$$

On the other hand when the material is in a perfectly plastic stage where $\tau_{z\theta}^{p} = const$:

$$T = \int_{R_i}^{R_o} \int_0^{2\pi} \tau_{z\theta}^{p} r^2 d\theta dr = 2\pi \tau_{z\theta}^{p} \int_{R_i}^{R_o} r^2 dr = \frac{2\pi}{3}(R_o^3 - R_i^3) \times \tau_{z\theta}^{p} \qquad (2\text{-}27)$$

Then the average shear stress along the radial direction is:

$$\tau_{z\theta}^{p} = \overline{\tau_{z\theta}^{p}} = \frac{3T}{2\pi(R_o^3 - R_i^3)} \qquad (2\text{-}28)$$

In this study, the shear stress calculated as an average from equation (2-25) and equation (2-28) as shown below.

$$\overline{\tau_{z\theta}} = \frac{\overline{\tau_{z\theta}^{e}} + \overline{\tau_{z\theta}^{p}}}{2} = \frac{1}{2}\left[\frac{T}{\pi(R_o^2 + R_i^2)(R_o - R_i)} + \frac{3T}{2\pi(R_o^3 - R_i^3)}\right] \qquad (2\text{-}29)$$

In addition, since the membrane affected the torque, the torque should be corrected as:

$$T = T_{LC} - T_{mem} \qquad (2\text{-}30)$$

where T_{LC} is the torque detected by the load cell and T_{mem} is the membrane force (inner and outer membrane).

The membrane force can be calculated by the following equations:

$$T_{mem} = \frac{2}{3}\pi \times t_m \times E_m \times \frac{\theta}{H} \times (R_o^3 + R_i^3) \qquad (2\text{-}31)$$

where:

t_m: the thickness of membrane.

E_m: the elasticity modulus of membrane.

θ: the rotation angle detected by potentiometer.

H: the height of specimen.

Computation for principle stresses

Based on the four stresses components of element A shown in Figure 2-10, the principal stress of the corresponding element can be calculated and plotted in the Mohr's circle as shown in Figure 2-11.

$$\sigma_1 = \frac{\sigma_z + \sigma_\theta}{2} + \sqrt{(\frac{\sigma_z - \sigma_\theta}{2})^2 + \tau_{z\theta}^2} \qquad (2\text{-}32)$$

$$\sigma_2 = \sigma_r \qquad (2\text{-}33)$$

$$\sigma_3 = \frac{\sigma_z + \sigma_\theta}{2} - \sqrt{(\frac{\sigma_z - \sigma_\theta}{2})^2 + \tau_{z\theta}^2} \qquad (2\text{-}34)$$

The angle α, between the direction of maximum principal stress and vertical direction, could be calculated by:

$$tan\, 2\,\alpha = \frac{2\tau_{z\theta}}{\sigma_z - \sigma_\theta} \qquad (2\text{-}35)$$

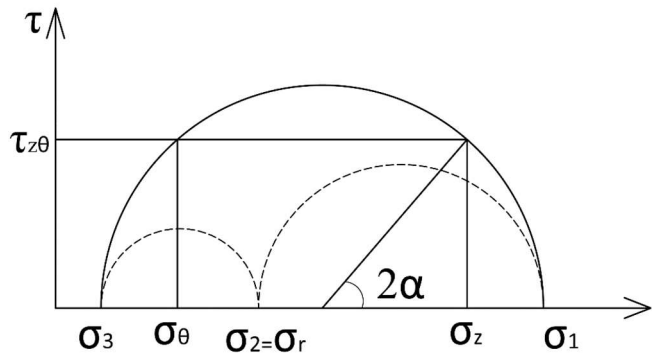

Figure 2-11 The stress statuses in hollow cylindrical torsional shear test

Computation for strains

Corresponding to the four stresses in element A, four strain components as shown in Figure 2-10, are named as axial strain (ε_z), radial strain (ε_r), circumferential strain (ε_θ) and shear strain ($\gamma_{z\theta}$).

As shown in Figure 2-12, the radial strain and circumferential strain are computed as:

$$\varepsilon_r = -\frac{u(r+dr)-u(r)}{dr} = -\frac{du}{dr} \qquad (2\text{-}36)$$

$$\varepsilon_\theta = -\frac{(r+u)d\theta - rd\theta}{rd\theta} = -\frac{u}{r} \qquad (2\text{-}37)$$

where:

u: the deformation of a soil element in radial direction.

r: the distance to center of hollow specimen.

If there is a linear relationship between $u(r)$ and r then:

$$\overline{\varepsilon_r} = -\frac{u_o - u_i}{R_o - R_i} \qquad (2\text{-}38)$$

$$\overline{\varepsilon_\theta} = -\frac{2\pi\left(\frac{(R_o+u_o)+(R_i+u_i)}{2} - \frac{R_o+R_i}{2}\right)}{2\pi\left(\frac{R_o+R_i}{2}\right)} = -\frac{u_o+u_i}{R_o+R_i} \qquad (2\text{-}39)$$

in which u_o and u_i are the increments of inner and outer radii, respectively.

In addition, the vertical strain is defined above.

$$\overline{\varepsilon_z} = \frac{\Delta H}{H_o} \qquad (2\text{-}40)$$

where:

ΔH: the displacement of specimen measured by external displacement transducer.

H_o: the initial height of specimen before testing.

As for the shear strain, it is defined by the following equation,

$$\gamma = \frac{r\Delta\theta}{H} \qquad (2\text{-}41)$$

$$\overline{\gamma} = \frac{\int_{R_i}^{R_o}\int_0^{2\pi} r \times \frac{\Delta\theta}{H} r dr d\theta}{\int_{R_i}^{R_o}\int_0^{2\pi} r dr d\theta} = \frac{2\Delta\theta(R_o^3 - R_i^3)}{3H(R_o^2 - R_i^2)} \qquad (2\text{-}42)$$

where:

H: the height of specimen.

$\Delta\theta$: the rotation angle detected by the potentiometer.

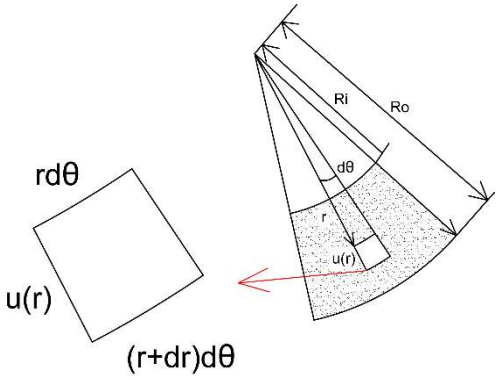

Figure 2-12 Radial and circumferential strains of a soil element

As for the volume strain, it is defined by:

$$\varepsilon_{vol} = \frac{\Delta V}{V_o} \qquad (2\text{-}43)$$

where ΔV is the volume change during consolidation measured by electronic balance, and V_o is the original volume of specimen.

Since the measurement of inner cylinder is very difficult and there may be non-uniform deformation along the height and the boundary of the specimen, some assumptions are made to compute the deformed inner and outer diameters by:

$$D_o = D_{oo} \times \sqrt{\frac{(1-\varepsilon_{vol})}{(1-\varepsilon_z)}} \quad (2\text{-}44)$$

$$D_i = D_{io} \times \sqrt{\frac{(1-\varepsilon_{vol})}{(1-\varepsilon_z)}} \quad (2\text{-}45)$$

where:

D_o: the deformed outer diameter of specimen.

D_i: the deformed inner diameter of specimen.

D_{oo}: the original outer diameter of specimen.

D_{io}: the original inner diameter of specimen.

2.5 Reference

AMPADU, S. K., 1991. Undrained Behaviour of Kaolin in Torsional Simple Shear. *Ph. D. Thesis. Department of Civil Engineering, the University of Tokyo, Japan.*

FAUZI, U. J. and KOSEKI, J., 2014. Local deformation properties of segregated sand specimen in hollow cylindrical torsional shear tests. *Bulletin of ERS, Institute of Industrial Science, University of Tokyo,* Vol. 47, pp. 27-36.

KOSEKI, J., YOSHIDA, T. and SATO, T., 2005. Liquefaction properties of Toyoura sand in cyclic torsional shear tests under low confining stress. *Soils and Foundations,* Vol. 45(5), pp. 103-113.

JGS., 2014. Laboratory testing standards of geomaterials. *The Japanese Geotechnical Society.*

POULOS, S.J., CASTRO, G. and FRANCE, J.W., 1985. Liquefaction evaluation procedure. *Journal of Geotechnical Engineering,* Vol. 111(6), pp. 772-792.

SATO, T., AMPADU, S. K., SAMUEL, I. K., MUKABI, J. N., TATSUOKA, F., 1991. The development of a strain controlled micro cyclic loading apparatus. *26th JGS Presentation* (In Japanese).

TATSUOKA, F., SONODA, S., HARA, K., FUKUSHIMA, S. and PRADHAN, T., 1986. Failure and deformation of sand in torsional shear. *Soils and Foundations,* Vol. 26(4), pp. 79-97.

TEPARAKSA, J., 2017. Comparison of sand behavior under repeated liquefaction in triaxial and shaking table tests. *Ph.D. Thesis. Department of Civil Engineering, the University of Tokyo, Japan.*

TIMOSHENKO, S. and GOODIER, J., 1970. Theory of Elasticity. *Auckland, McGraw-Hill, New York.*

YOSHIMI, Y., TANAKA, K. and TOKIMATSU, K., 1989. Liquefaction resistance of a partially saturated sand. *Soils and Foundations,* Vol. 29(3), pp. 157-162.

ZHAO, C., 2017. Direct and indirect local deformation measurements of sand specimen in undrained cyclic triaxial and torsional shear tests. *Ph. D. Thesis. Department of Civil Engineering, the University of Tokyo, Japan.*

Chapter 3 Testing Procedures and Programs

3.1 Introduction

In this chapter, the testing procedures during hollow cylindrical torsional shear tests and test programs will be introduced.

Since the basic principles of the two different apparatuses are similar, only the testing procedures of the mid-scale torsional shear test will be introduced.

3.2 Testing procedures of the mid-scale torsional shear test

This part consists of the preparation method of hollow cylindrical sand specimen on the mid-scale torsional shear apparatus and testing procedures.

3.2.1 Procedures of hollow cylindrical sand specimen preparation

In this study, in order to minimize the disturbance, sand specimens were all prepared just before the tests using the air-pluviation method. By dropping air-dried sand particles from a given height through a funnel, sand specimen with uniform relative density can be prepared easily. By changing the opening size of the funnel or the dropping height, specimens with different relative densities can be prepared (Vaid and Negussey, 1984).

Pre-works before specimen preparation

Before preparing the specimen, several pre-works should be done as follows.

1. Prepare the inner and outer membranes for the specimen.

In this study, rubber membranes were used to hold and seal the specimens during tests. Because of the hollow geometry, both outer and inner membranes are necessary. Considering the height of specimen, inner ring, top cap and space for rubber bands, the inner and outer membranes are prepared with heights of 500 mm and 370 mm, respectively. Then use the horizontal line to mark 35 mm high space for each side on the outer membrane for rubber band.

2. Calibrate the height opening size of funnel of air-pluviation.

This step is important in determining the relative density of sand specimen especially for different specimen sizes. In this study, the opening size and dropping height applied on the mid-scale torsional apparatus cannot be directly applied on the small-scale one

because the section of the small specimen mold cannot receive the sand perfectly. Therefore, narrower opening and a corresponding height were applied to reach similar relative density in the small-scale apparatus.

3. Dry the test sand.

The weight of sand used in preparation is important in calculating the relative density. Therefore, it is important to make sure there is no water in the sand before specimen preparation.

4. Clean up equipment and tools

For better precision, all equipment and tools used in the test should be cleaned up by a wipe or the air pressure gun. The water left in the water hose must be removed by the air gun since it may cause damage to the pressure gauge or affect the saturation progress later.

Specimen preparation

After all pre-works completed, sand specimen is prepared as follows.

1. Assemble the inner membrane and molds.

After cleaning up all equipment, apply some vacuum grease to the outer surface of the metal pedestal ring. Then attach the inner membrane out of the ring touching the surface with grease. Since the outer diameter of this metal ring is larger than the diameter of inner membrane, it is important to adjust the membrane to make sure it is uniformly stretched in the circumference. If it is not uniformly stretched, wrinkles will appear after specimen preparation on the membrane.

Then use the hollow metal pedestal (with porous stone fixed on) to fix the ring on the chassis of the apparatus. During this step, the rubber membrane should be carefully put

through the middle of the pedestal since slight touches with metal parts can induce fatal damage to the membrane.

After fixing the pedestal, set up four pieces of metal inner molds to help the inner membrane stand. In order to prevent the inner membrane from falling down, use a rubber band to fix it at the top of the molds. Then after checking the position of the inner molds (should be perfectly set up at the center of the apparatus) by measuring the distance between the molds and four pillars, use the long screw rod to fix the molds.

2. Set up the outer membrane and molds.

After applying vacuum grease on the outer side of pedestal, attach the outer membrane to the pedestal. Similar as the procedure in setting the inner membrane, make sure the outer membrane is set up uniformly and the edge of porous stone perfectly matches the line drawn on the membrane. Then use a rubber band to fix at the reserved 35 mm wide space. During this step, use a nylon thread to adjust the rubber band. Finally, put the black rubber O-ring above the rubber band and grease it. Be careful that the rubber O-ring should be positioned under the porous stone and not overlapped with the rubber band, or leakage will occur in later procedures.

Then install the two pieces of outer metal molds to cover the outer membrane. The rubber band and black rubber O-ring installed before should be carefully position into the groove at the bottom of the molds. In addition, when fixing together the two pieces of molds using a metal screw belt, make sure the membrane is not clamped in between.

After fixing the outer molds, put the outer membrane outward from the top of the molds and use a rubber band to fix. Also make sure there is no wrinkles appear on the membrane. Then apply -20 kPa negative pressure through the molds to tension the membrane.

3. Drop sand particles using the air-pluviation method through a funnel.

After setting up the membranes and molds, sand will be drop into the molds through a funnel with a long metal nozzle. A little weight is attached to the nozzle using a nylon thread to prompt the relative height between the nozzle opening and sand specimen surface. While dropping the sand, use a plastic bag or corrugated box to catch the sand scattered out of the molds. In order to keep the uniformity of relative density, the little weight hanging from the nozzle should always touches the surface of the specimen by moving upward the funnel.

4. Install the top cap.

After air-pluviation, flatten the surface of the specimen using a plastic ruler and gather the redundant sand in the plastic bag to calculate the absolute weight of sand used for the specimen. Before installing the top cap onto the specimen, grease the circumference of the outside same as the pedestal and put the rubber band on it in advance. Then set the pulley on one of the pillars to counterbalance the weight of the top cap. After appropriately counterbalanced the top cap, move it down to the surface of the specimen carefully and fix it to the pillars with a pair of special holders. Then fix the inner and outer membranes to the top cap with rubber bands carefully. After confirming that the top cap is firmly fixed by the holders, remove the counterweight and the pulley.

5. Apply effective stress and remove the metal molds

Connect the input hose of the vacuum pressure gauge to the vacuum pump. Then connect the two sides of specimen (from the top cap and the pedestal) together to the output joint of the vacuum pressure regulator through a water tank with a little water (around 1 cm water head). Then raise the vacuum pressure from 0 to -30 kPa gradually. During this procedure, air bubbles can be observed in the water tank because air in the specimen is being removed through the tank. After the pressure stabilized and no air

bubbles visible, remove the inner and outer molds carefully. Then measure the height and diameters of the specimen.

Inside cell monitoring devices set up

After completing the preparation of specimen, monitoring devices are set up as follows.

1. Install the load cell.

Install the upper frame with the loading rod and load cell onto the four pillars and fix with screws. Connect the cable of load cell and counterbalance the loading rod. Then adjust the amplifier to the calibrated value and clear the physical value of torque and vertical load in the controlling program. Carefully move the loading rod down and connect it with the top cap on specimen. During this step, the vertical stress and shear stress should be controlled to zero as closely as possible. After fixing the screws, add counterweight that equal to the weight of top cap and remove the top cap holders. Then connect the cables of gap sensors on the upper frame board and adjusting the position of gap sensors.

2. Install the gap sensor and cell.

After setting up the load cell and gap sensor, operations inside the cell are all finished. Before install the cell, lock the position of the loading rod tightly to avoid disturbance. Then remove the counterbalance and disconnect all cables on the upper frame board. For safety, it is very important to fix the cell soon after installing the cell with the crane. After fixing the cell, set up the counterweight and reconnect cables as what they used to be.

Connection of cell body and the loading system

After finishing the operations inside the cell and cell installation, the cell body and the loading system are connected as the following steps. Other sensors and monitoring devices are also installed.

1. Connect the loading rod to the loading system.

Connect the chassis of the apparatus with positive pressure source and raise it up slightly until the whole cell can be moved stably. Carefully move the cell into the loading system frame and lock it. Then manually move the loading shaft of the loading system down to touch with the loading shaft of the cell side and fix them together with four screws.

2. Install the external displacement transducer and potentiometer.

Attach the round metal plate to the loading shaft and install the external displacement transducer to it. And then install the potentiometer with its wheel touching on the loading shaft. It should be noticed that the external displacement transducer must be vertical, and the wheel of potentiometer should be horizontal. Finally, adjust their amplifiers and clear their value to 0 on the program.

After installing the sensors, turn on the motors of the loading system, unlock the loading shaft and apply the isotropic control program. After the deviator stress was controlled to 0, remove the counterweight piece by piece.

3.2.2 Saturation and consolidation

After specimen prepared as above, the specimen will be saturated and consolidated before the liquefaction test. The procedures are as follows.

Saturation using the double vacuum method

After isotropic control started, specimen is saturated as following steps.

1. Input the cell water and assemble the double vacuum system.

Input water to the pressure cell gradually until the specimen is fully emerged under the water level while keeping the cell pressure to 0. Then assemble the double vacuum system as shown in Figure 3-1. Then adjust the back pressure and cell pressure from -30 kPa and 0 to -98 kPa and -68 kPa with the vacuum pressure regulator. During this progress, the deviator stress should be always controlled to 0 by the vertical loading system. Then keep the condition for 10 hours.

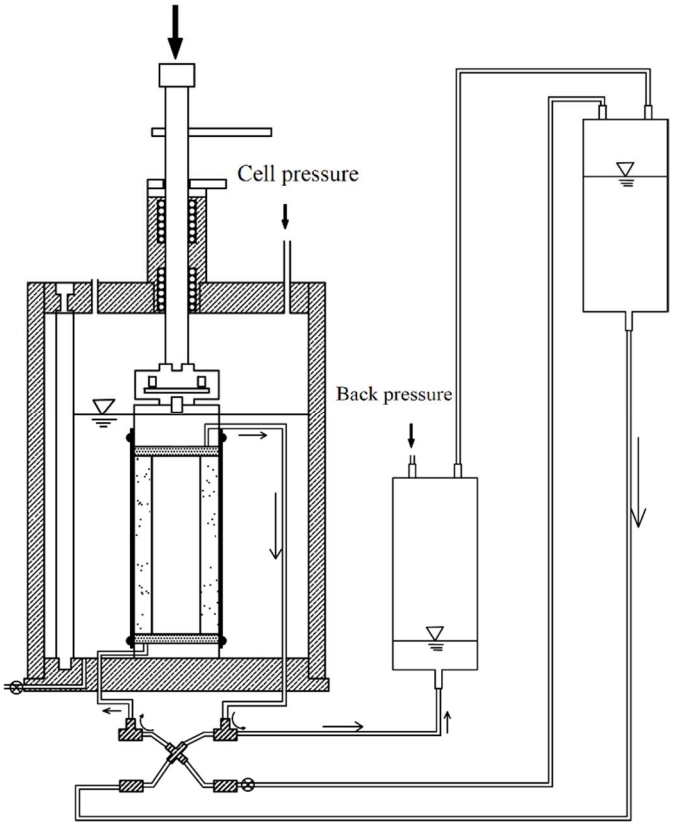

Figure 3-1 Connections of the double vacuum method (after Zhao, 2017)

2. Saturation and B-value checking.

After 10 hours under the double vacuum condition, open the valve to let water flow into the specimen. Before all the de-aired water flowing out from the higher water tank, adjust the back pressure and cell pressure from -98 kPa and -68 kPa to 0 and 30 kPa. Then assemble the connections of HCDTP and the chamber for drainage measurement.

With drainage being measured by the electronic balance, adjust the back pressure and cell pressure to 200 kPa and 230 kPa. Then close the drainage valve and record the cell pressure from the gauge and the effective stress from the computer. Then increase the cell pressure by 50 kPa under the undrained isotropic condition. After cell pressure becoming stable, record the two values again. Then reduce the cell pressure back to 230 kPa and record for the 3rd time. Calculate the B-value with these data and check whether it is larger than 0.96.

Isotropic consolidation

After saturation and B-value checking, the specimen will be subjected to a linear effective stress path to reach the target initial effective stress and then consolidated under isotropic condition. The procedures are as follows.

1. Linear effective stress path.

After saturation, open the drainage valve and increase the cell pressure gradually and linearly to 300 kPa while keeping the back pressure at 200 kPa.

2. Consolidation under isotropic condition.

After the target initial effective stress reached, consolidate the specimen under the isotropic condition for 1 hour.

3.2.3 Application of pre-shear history

For the cases without pre-shear histories, this part will be skipped during the test. And for those with pre-shear histories, the pre-shear history is applied as follows.

After isotropic consolidation, apply the pre-shear loading to the specimen. Details of different kinds of pre-shear histories will be introduced in the 4th chapter. After each stage of pre-shear loadings, reconsolidate the specimen as the same procedure introduced above for isotropic consolidation.

3.2.4 Undrained cyclic loading for liquefaction test

After isotropic consolidation or pre-shear loadings and reconsolidation, the specimen will be subjected to the undrained cyclic loadings as follows.

Undrained cyclic loading

After isotropic consolidation, close the drainage valve and lock the vertical displacement of the loading shaft. Then clear the volume change in the controlling program and start the cyclic loading program.

Reconsolidation and re-loading

After reaching the target double amplitude of shear strain, stop the controlling program. Then reduce the cell pressure to 230 kPa and open the drainage valve while controlling the deviator stress to 0. When the effective stress becomes stable, apply the linear effective stress path again as introduced above. Then repeat the step of isotropic consolidation and undrained cyclic loading again until all test stages finished.

3.3 Testing programs of this study

In this part, the details of testing programs of this study will be introduced. In order to investigate the liquefaction behavior of dense sand and the effects of pre-shear history, four series of liquefaction tests were conducted.

Test series A consisted of repeated liquefaction test on dense sand specimens with no pre-shear history before the first liquefaction stage. In this series, cyclic loadings with different cyclic stress ratios were applied to sand specimen with similar specimen relative density around 80% in different cases. In each case, the cyclic stress ratio was kept consistent from the first liquefaction stage to the last one.

Test series B consisted of four cases that had same testing condition as in series A but carried out by the small-scale torsional shear apparatus. This series of tests were carried out to check the feasibility of comparing different cases carried out by these two different apparatuses.

Test series C were carried out with drained pre-shear histories before the first stages of repeated liquefaction test. In this series, pre-shear history was applied with a constant double amplitude of shear strain with a large number of cycles. In different cases, different shear strain amplitudes and numbers of cycles were applied to investigate their effects. A special case with drained pre-shear was added at last to compare the effect of different drainage conditions during pre-shear. In this series, same CSR was used in all liquefaction test stages.

Test series D consisted of repeated liquefaction tests with undrained pre-shear histories. In this series, cyclic pre-shear history was applied under undrained condition to induce 0.5 excess pore water pressure ratio in each pre-shear stage. In different cases, different

numbers of pre-shear stages were applied to investigate its influence. Then several cases were carried out with the same pre-shear program but different CSR during liquefaction test stages to draw the complete liquefaction resistance curve and compare with that of no pre-shear ones.

3.4 References

VAID, Y. P. and NEGUSSEY, D., 1984. Relative density of pluviated sand samples. *Soils and Foundations*, Vol. 24(2), pp. 101-105.

ZHAO, C., 2017. Direct and indirect local deformation measurements of sand specimen in undrained cyclic triaxial and torsional shear test. *Ph.D. Thesis. Department of Civil Engineering, the University of Tokyo, Japan.*

Chapter 4 Results of Torsional Shear Tests

4.1 Introduction

In this chapter, the results of hollow cylindrical torsional shear tests will be introduced. As the testing programs introduced in chapter 3, liquefaction tests on dense sand specimens were carried out with different kinds of pre-shear histories in different series.

In this thesis, the liquefaction resistance is represented by the number of cyclic loadings to induce 7.5% double amplitude of shear strain since all liquefaction and repeated liquefaction stages in this study were stopped at the target double amplitude of shear strain of 7.5%. In addition, the relationship between cyclic stress ratio and the number of cycles to induce 7.5% double amplitude of shear strain is used to compare the liquefaction resistance.

4.2 Repeated liquefaction tests without pre-shear history

In this part, the results of repeated liquefaction tests on dense sand specimens will be shown and discussed. For comparison purposes, all the tests were carried out with specimens of similar initial relative densities, same loading speed, initial effective stress, and maximum double amplitude of shear strain. In order to draw the liquefaction resistance curve, different cases were carried out with various cyclic stress ratio (CSR). In addition, each case consists of multiple liquefaction stages with a consistent cyclic stress ratio from the first stage to the last one.

Since two torsional shear apparatuses with different specimen sizes were employed in this study, several cases with the same conditions were conducted by both apparatuses to make a comparison.

4.2.1 Liquefaction tests with the mid-scale torsional apparatus

The details of repeated liquefaction tests carried out with the mid-scale torsional shear apparatus labeled as series A are shown in Table 4-1. Except for case A-9, all these tests were started with the similar initial relative densities (after consolidation) around 78~81%. In addition, all liquefaction and repeated liquefaction tests in this part were conducted under the same initial effective stress of 100 kPa. Each case consisted of 3~6 repeated liquefaction stages.

Table 4-1 Test conditions of repeated liquefaction tests

Case ID	Initial relative density, D_{ri} (%)	Maximum double amplitude of shear strain, γ_{DAmax} (%)	Cyclic stress ratio, τ_{cyc}/σ_0'
A-1	79.0	7.5	1.20
A-2	79.0	7.5	1.00
A-3	79.1	7.5	0.90
A-4	79.2	7.5	0.60
A-5	79.2	7.5	0.30
A-6	78.7	7.5	0.25
A-7	79.3	7.5	0.20
A-8	79.2	7.5	0.17
A-9	86.5	7.5	1.00

In order to confirm the repeatability of the specimen preparation, relationships between the volumetric strain and vertical axial strain during isotropic consolidation are plotted as shown in Figure 4-1.

As an example and reference case for further discussion, case A-2 with the cyclic stress ratio of 1.00 is selected to show its analyzed data in this part. Figures 4-2 to 4-6 show some relationships and time histories from the first liquefaction stage to the last one. For each liquefaction stage, the effective stress path, relationship between shear stress and shear strain, time history of shear stress, time history of shear strain and time history excess pore water pressure ratio are shown from (a) to (e), respectively.

The effective stress paths in different stages generally show a similar trend in early loading stages. With such a high cyclic stress ratio, dense sand specimens show obvious positive dilatancy in the very early cyclic loading cycles.

In the first liquefaction stage, both excess pore water pressure and shear strain increased rapidly. It can be noticed that after the first loading cycle, the excess pore water pressure accumulated so fast that 80% of initial effective stress was lost. In addition, with such a high cyclic stress ratio, the effective stress path passed the line of phase transformation in the first loading cycle as well. As a result, with no more than two cycles of cyclic loading, 7.5% double amplitude of shear strain was reached and over 98% of initial effective stress was lost due to the accumulation of excess pore water pressure.

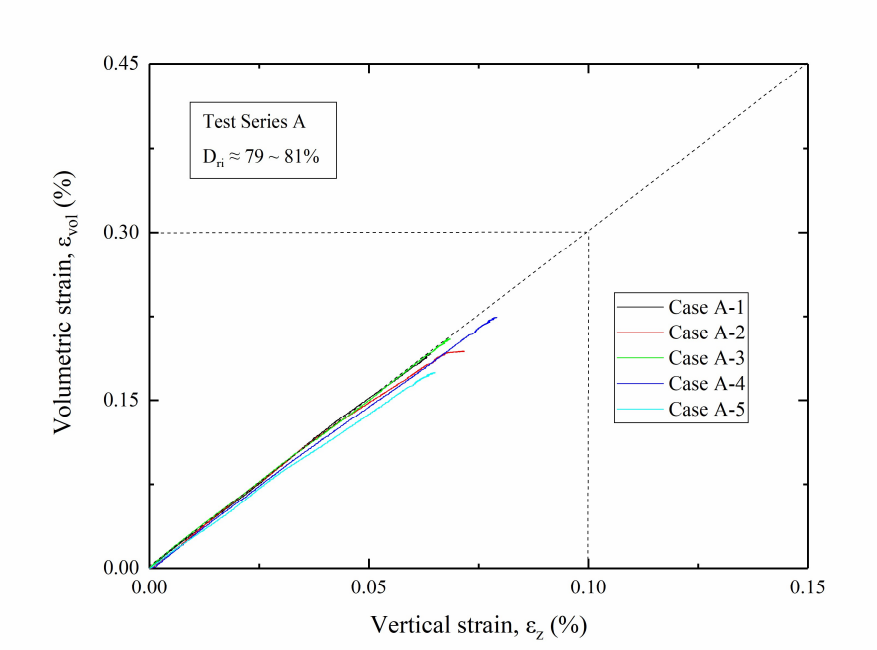

Figure 4-1 Relationship between volumetric strain and vertical strain during consolidation

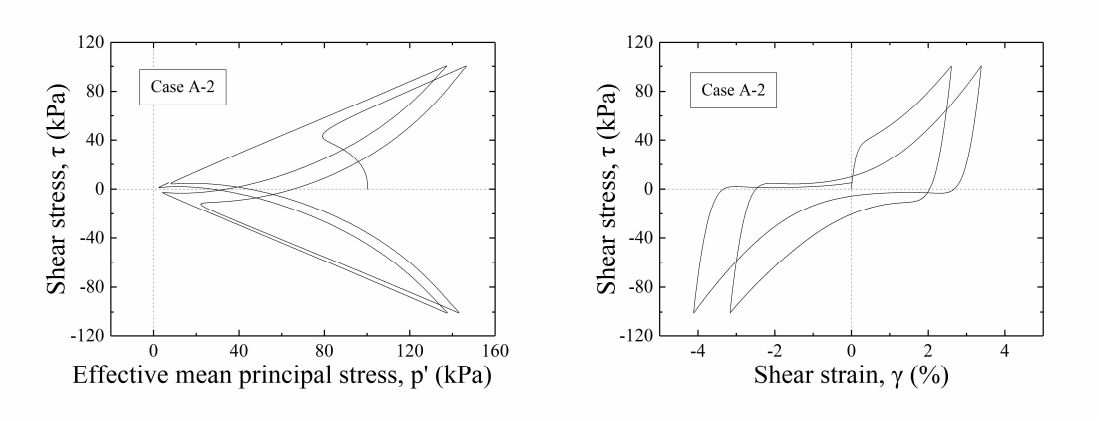

(a) Effective stress path (b) Stress-strain relationship

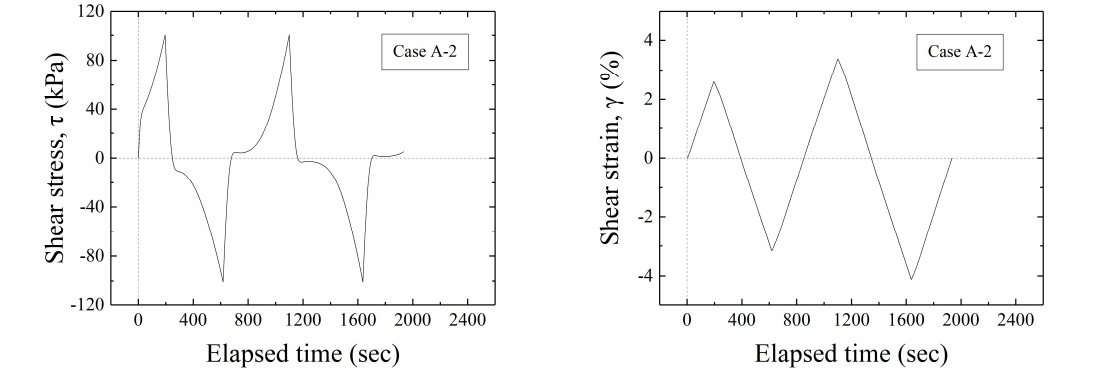

(c) Time history of shear stress (d) Time history of shear strain

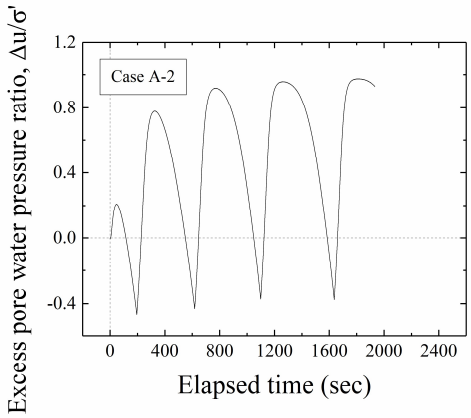

(e) Time history of excess pore water pressure ratio

Figure 4-2 Various relationships and time histories of case A-2 (1st stage)

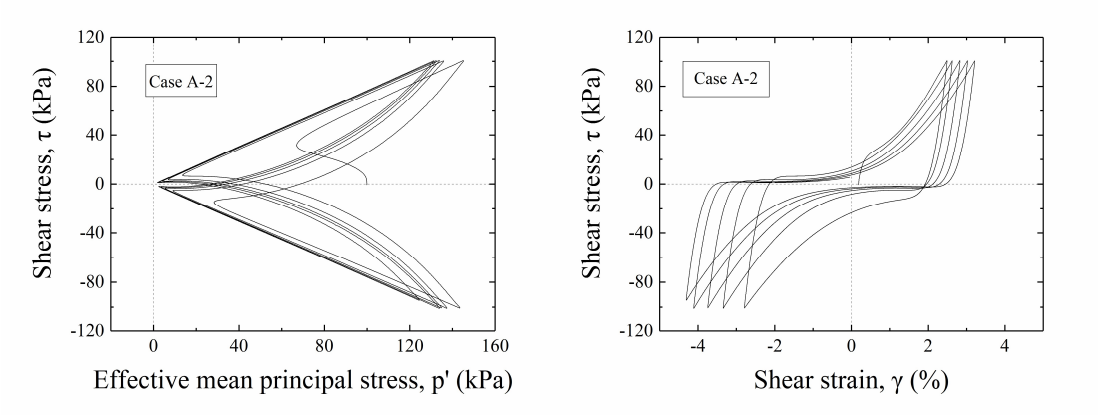

(a) Effective stress path

(b) Stress-strain relationship

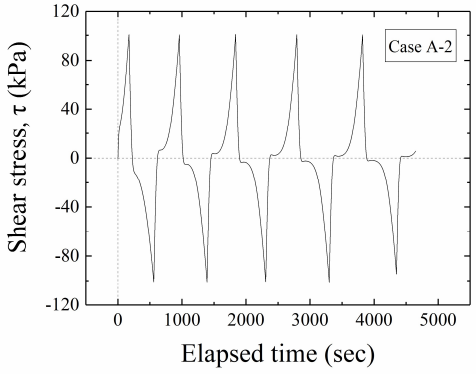

(c) Time history of shear stress

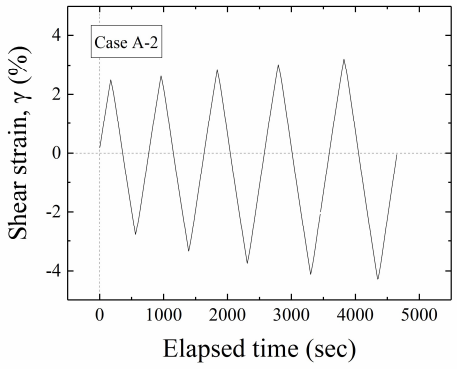

(d) Time history of shear strain

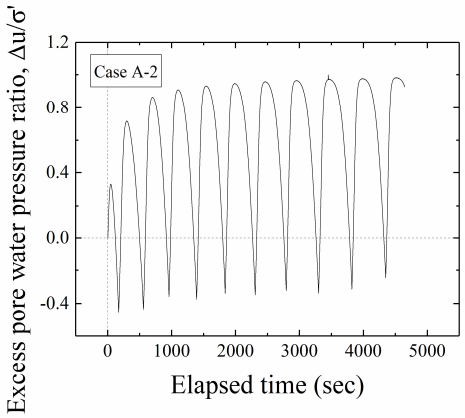

(e) Time history of excess pore water pressure ratio

Figure 4-3 Various relationships and time histories of case A-2 (2nd stage)

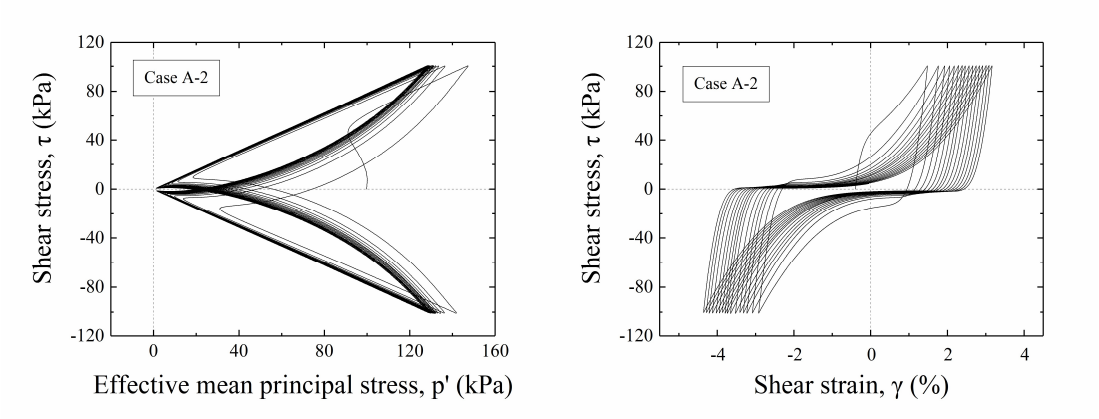

(a) Effective stress path (b) Stress-strain relationship

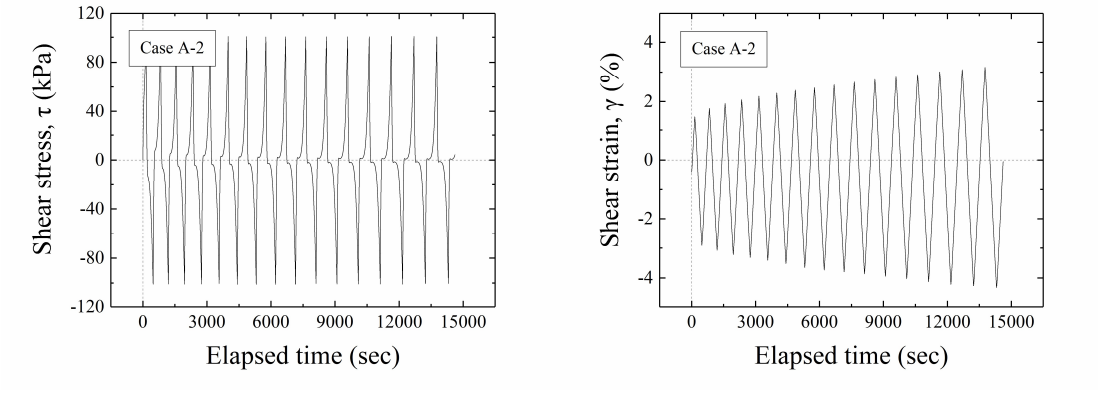

(c) Time history of shear stress (d) Time history of shear strain

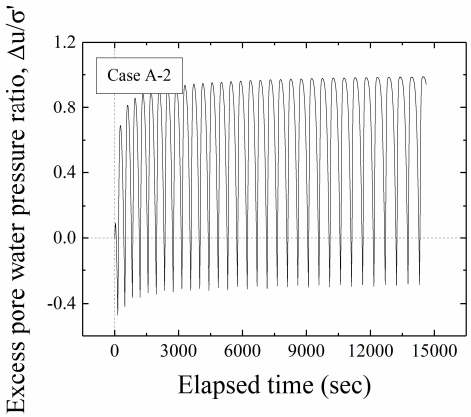

(e) Time history of excess pore water pressure ratio

Figure 4-4 Various relationships and time histories of case A-2 (3rd stage)

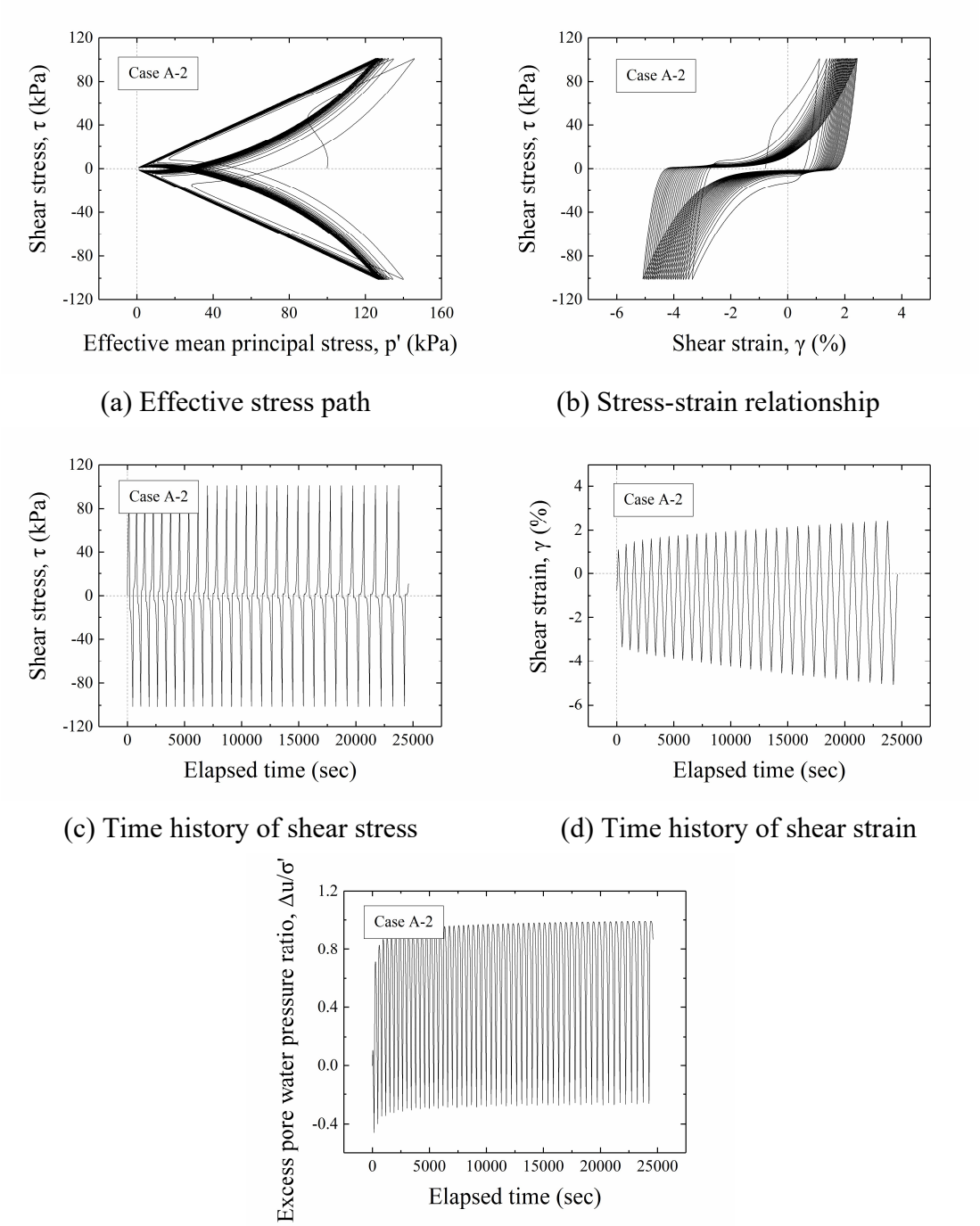

(a) Effective stress path

(b) Stress-strain relationship

(c) Time history of shear stress

(d) Time history of shear strain

(e) Time history of excess pore water pressure ratio

Figure 4-5 Various relationships and time histories of case A-2 (4th stage)

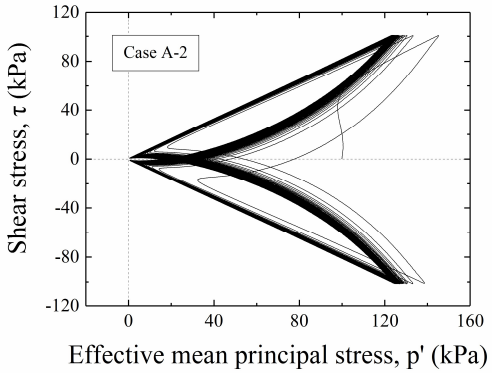

(a) Effective stress path

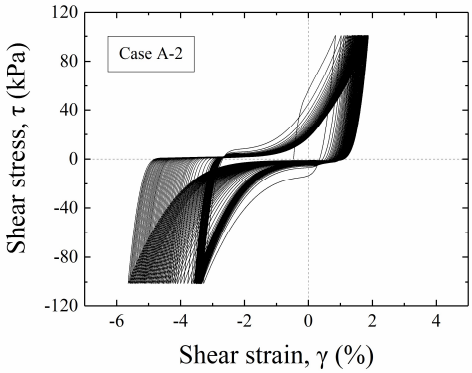

(b) Stress-strain relationship

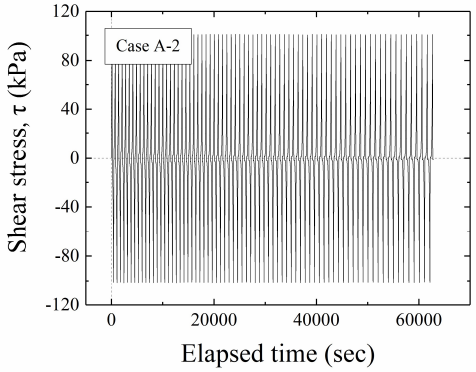

(c) Time history of shear stress

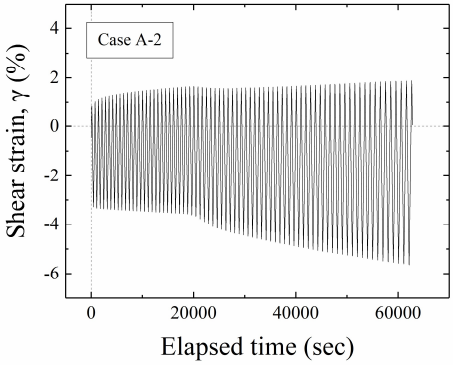

(d) Time history of shear strain

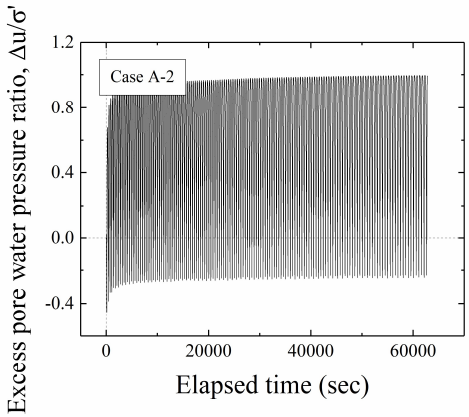

(e) Time history of excess pore water pressure ratio

Figure 4-6 Various relationships and time histories of case A-2 (5th stage)

Repeated liquefaction stages show similar dilatancy behavior as observed in the 1st stage. Even though the relative density of specimens increased after reconsolidations and repeated liquefaction, the first loading cycle in each stage shows a very similar behavior that it always induces a great reduction of effective stress (or increase of excess pore water pressure). In addition, it can be noticed that with such large excess pore water pressure accumulated in the first cycle, the initial liquefaction occurred very early in all repeated liquefaction stages while it still took more and more cycles to induce 7.5% double amplitude of shear strain.

From the results of case A-2, the increase of liquefaction resistance was observed from the first to the last liquefaction stage. As mentioned in the background, it was considered that pre-shear history, including the previous liquefaction history, could induce different effects on liquefaction resistance. Such a large amplitude of shear strain should have reduced the liquefaction resistance according to previous studies on loose or medium dense sand. Therefore, in order to investigate whether the increase of liquefaction resistance in this case was caused by the increase of relative density or pre-shear histories, case A-9 was carried out with same CSR of 1.00 and a higher initial relative density around 85%, which was even higher than the third stage of case A-2.

Figure 4-7 shows the relationship between relative density and liquefaction resistance represented by the number of cycles to induce 7.5% double amplitude of shear strain. It can be noticed that the relative density of the first stage of case A-9 was higher than the first three stages in case A-2, but its liquefaction resistance was similar to the 2nd stage of A-2 and lower than the 3rd stage. This result proved that the increases of liquefaction resistance during repeated liquefaction stages in case A-2 were not only because of the increase of relative density, but also the liquefaction and repeated liquefaction histories. This result suggests that liquefaction behavior especially the pre-shear effects may be different for sand specimens with different relative densities since

different behavior was reported by Wahyudi et al. (2015) and Aoyagi (2018) on medium dense sand.

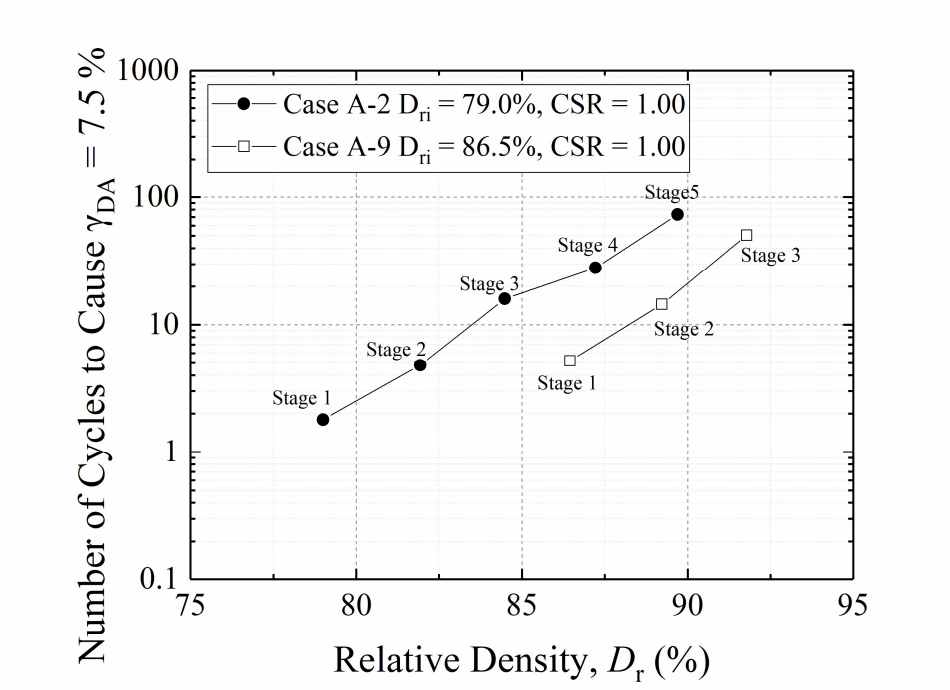

Figure 4-7 Relationship between relative density and liquefaction resistance

In case A-2, cyclic stress ratio of 1.00 was so large that the specimen quickly liquefied after a few cycles of cyclic loadings. In order to compare the differences of liquefaction and repeated liquefaction behavior of dense sand under different cyclic stress ratio, various relationships and time histories of case A-5 are shown from Figures 4-8 to 4-10.

With a relatively lower cyclic stress ratio applied in case A-5, the liquefaction characteristics changed. In this case, due to the lower cyclic stress ratio, the specimen did not exhibit obvious dilatancy as in case A-2. But the excess pore water pressures were similarly accumulated rapidly in the first several cycles in all the repeated liquefaction stages of this case. After comparing the stress-strain relationship between different liquefaction stages, it can be noticed that shear strain induced in early loading

cycles did not change a lot but after that, the accumulation speed of shear strain became slower in later liquefaction stages.

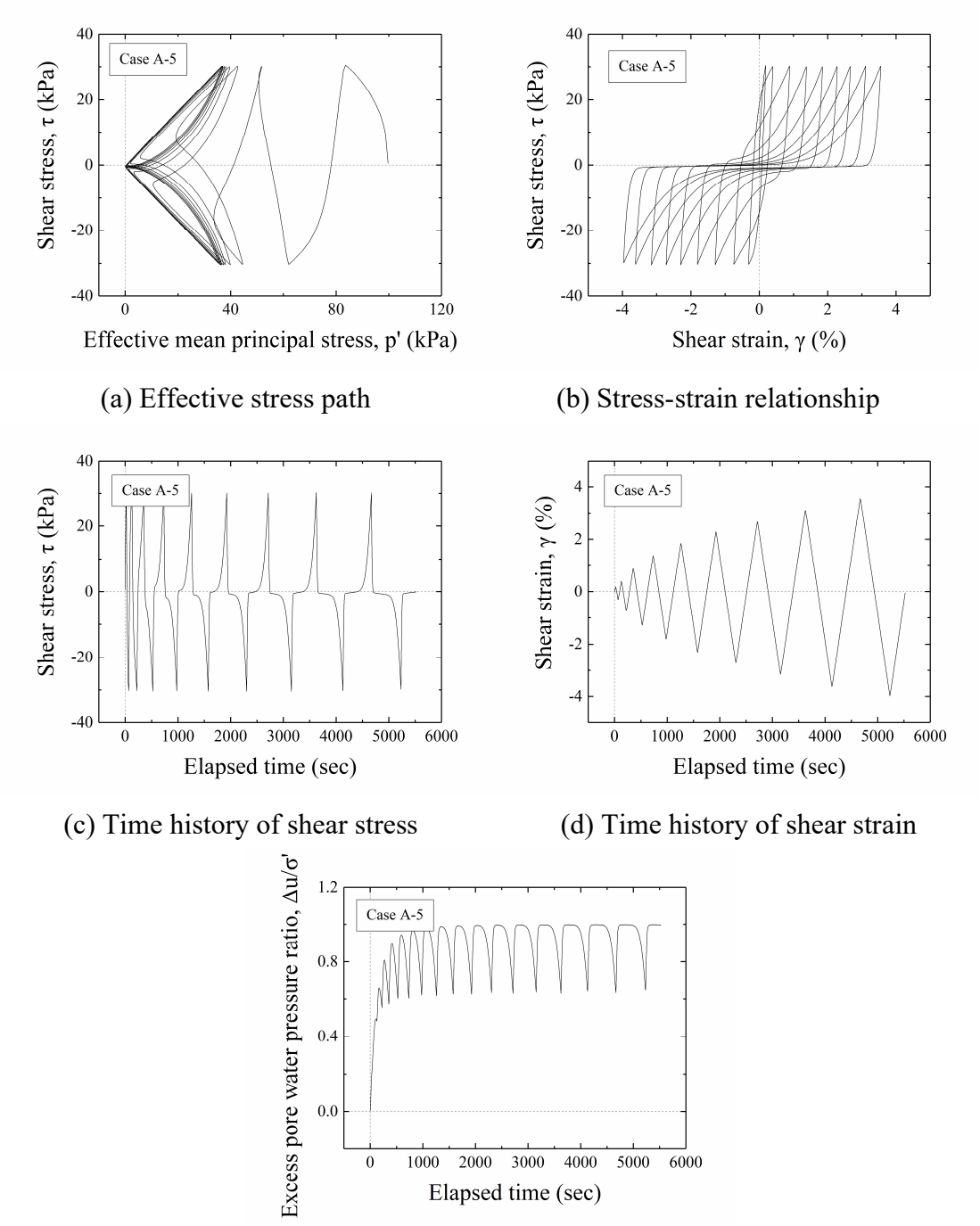

(a) Effective stress path

(b) Stress-strain relationship

(c) Time history of shear stress

(d) Time history of shear strain

(e) Time history of excess pore water pressure ratio

Figure 4-8 Various relationships and time histories of case A-5 (1st stage)

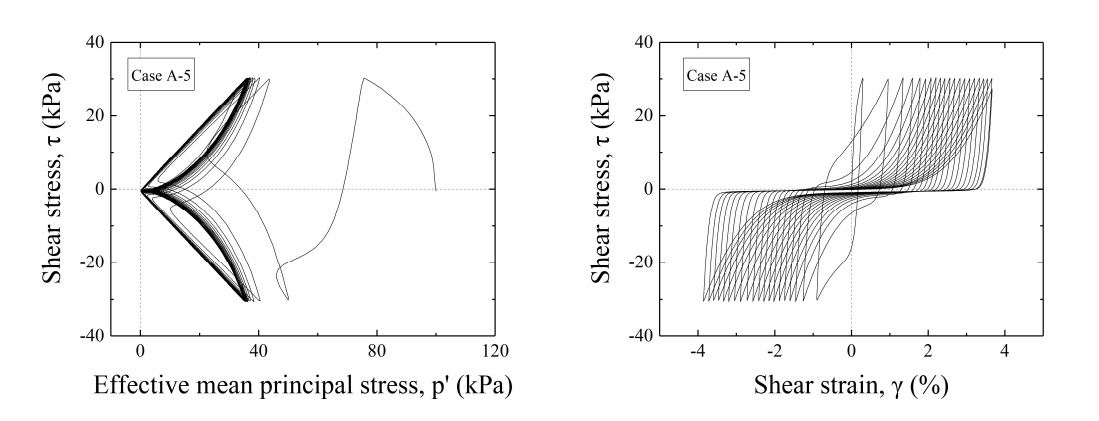

(a) Effective stress path (b) Stress-strain relationship

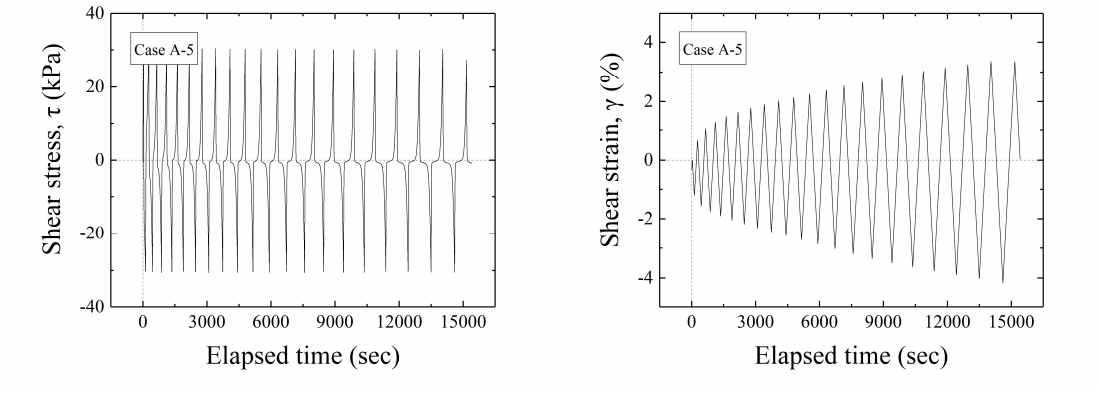

(c) Time history of shear stress (d) Time history of shear strain

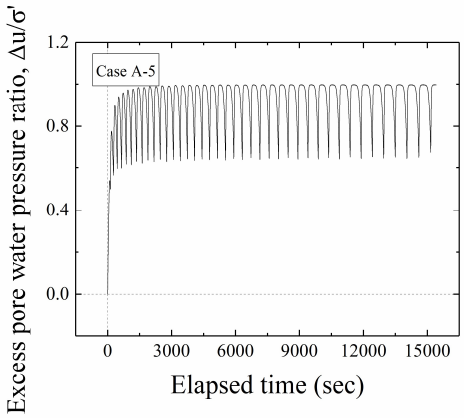

(e) Time history of excess pore water pressure ratio

Figure 4-9 Various relationships and time histories of case A-5 (2nd stage)

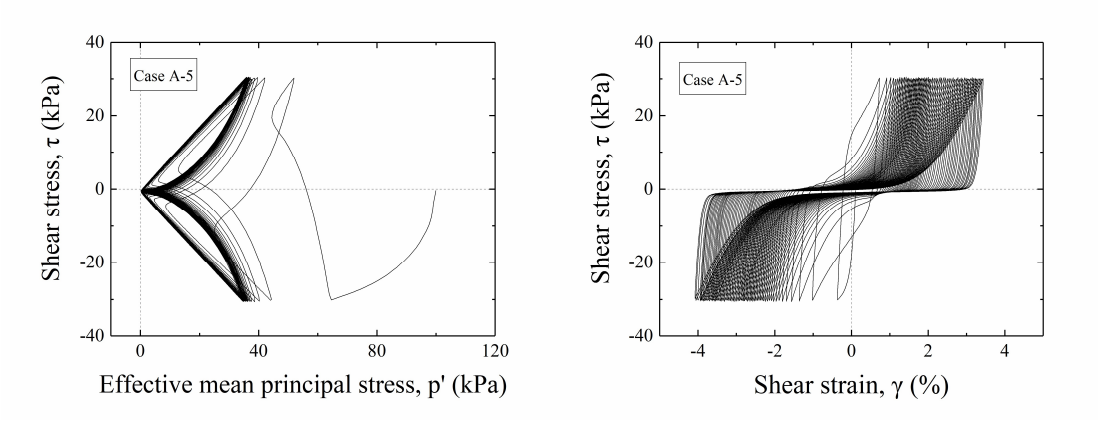

(a) Effective stress path

(b) Stress-strain relationship

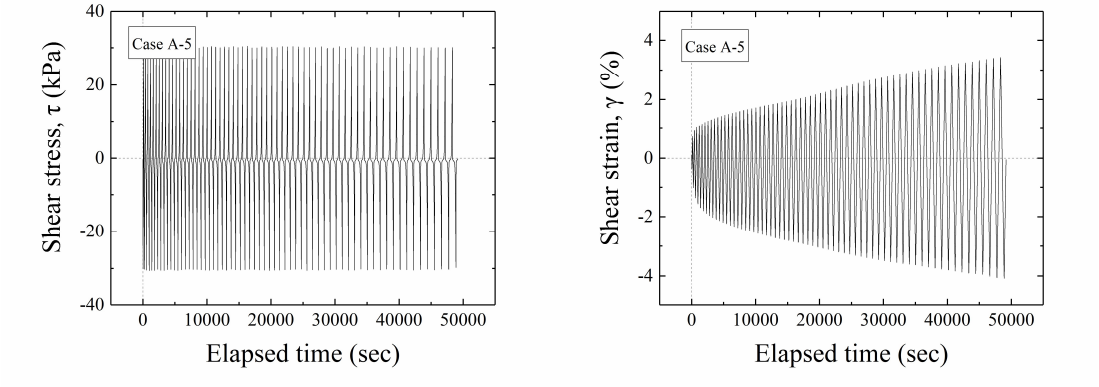

(c) Time history of shear stress

(d) Time history of shear strain

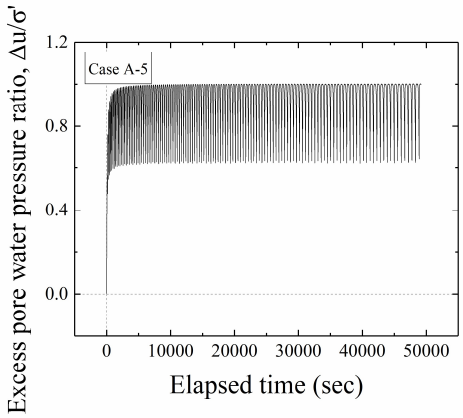

(e) Time history of excess pore water pressure ratio

Figure 4-10 Various relationships and time histories of case A-5 (3rd stage)

Figure 4-11 shows the liquefaction resistance curve of all cases in series A with similar initial relative density but different cyclic stress ratios. In this figure, the first liquefaction stage of each case is shown in green color, representing that there is no pre-shear or liquefaction history before this stage. In other words, stages after the first liquefaction stage are all affected by the liquefaction history before.

Figure 4-12 shows the change of relative density and liquefaction resistance of cases A-1 to A-5. Cases with different cyclic stress ratio generally showed consistent trends that with more liquefaction stages, the specimen became denser and stronger to liquefaction.

As introduced above, the increase of liquefaction resistance was not only because of the densification, but also induced by the liquefaction histories.

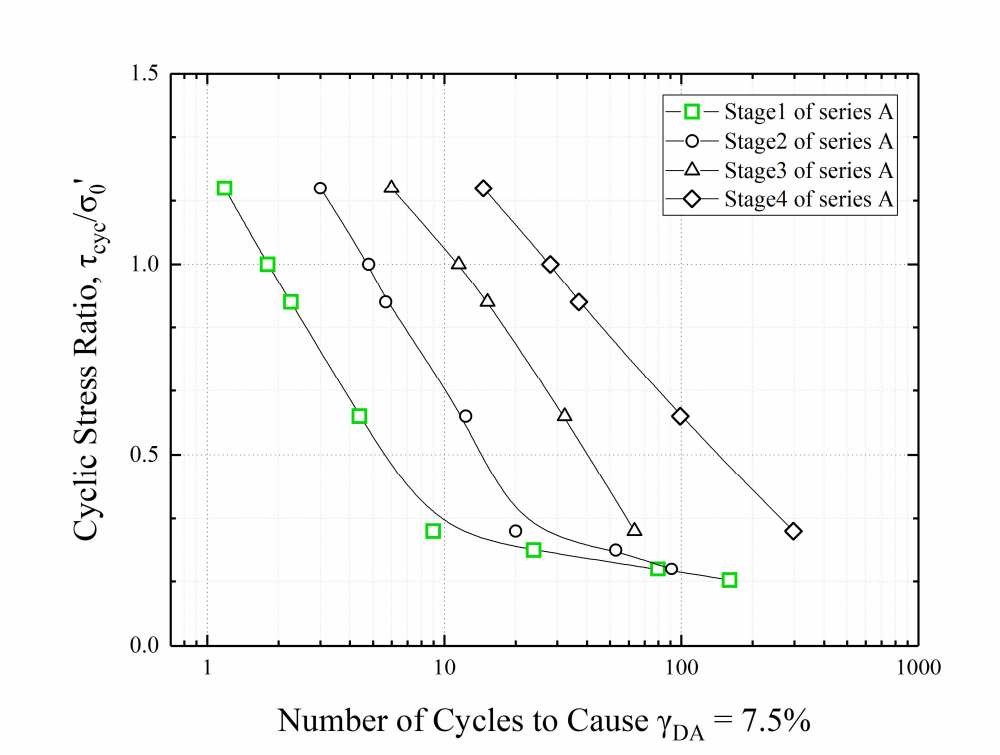

Figure 4-11 Liquefaction resistance curve of all stages

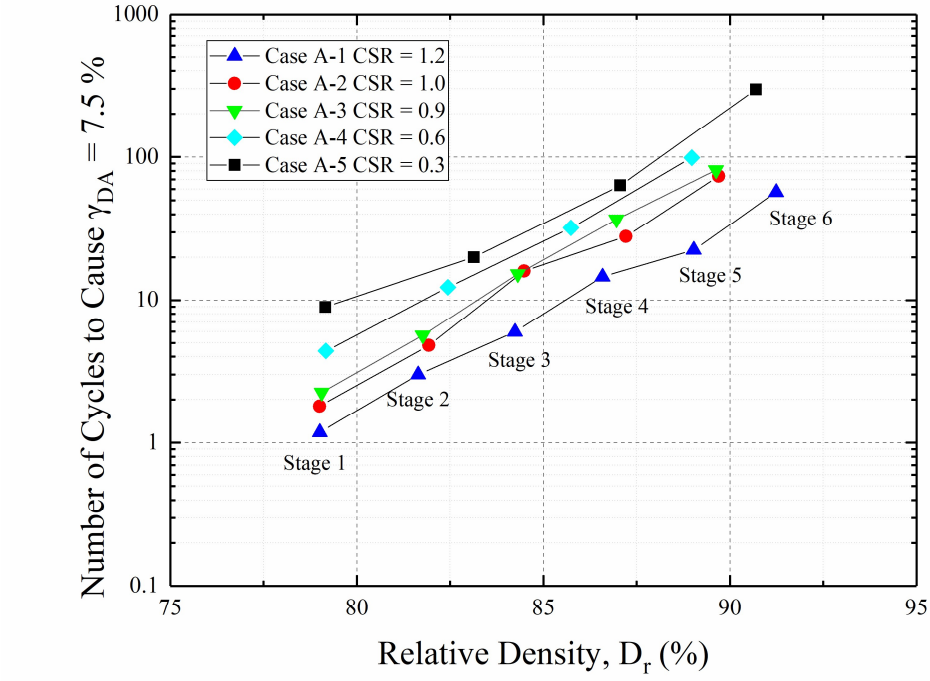

Figure 4-12 Relationship between relative density and liquefaction resistance

4.2.2 Liquefaction tests on small-scale torsional shear apparatus

For comparison purpose, a series of liquefaction tests were conducted on the small scale torsional shear apparatus as series B shown in Table 4-2. Liquefaction resistance curve drawn by these tests is shown in Figure 4-13 together with the one drawn by test series A. It can be noticed that in every single case there is some difference in liquefaction resistance between series A and B. But overall, these two series of tests generally show a similar trend in liquefaction resistance curve. This similarity is considered acceptable to conduct different liquefaction tests with these two apparatuses and make comparisons.

Table 4-2 Tests conditions of series B

Case ID	Initial relative density, D_{ri} (%)	Maximum double amplitude of shear strain, γ_{DAmax} (%)	Cyclic stress ratio, τ_{cyc}/σ_0'
B-1	81.0	7.5	1.00
B-2	78.8	7.5	0.60
B-3	80.9	7.5	0.30
B-4	79.6	7.5	0.20

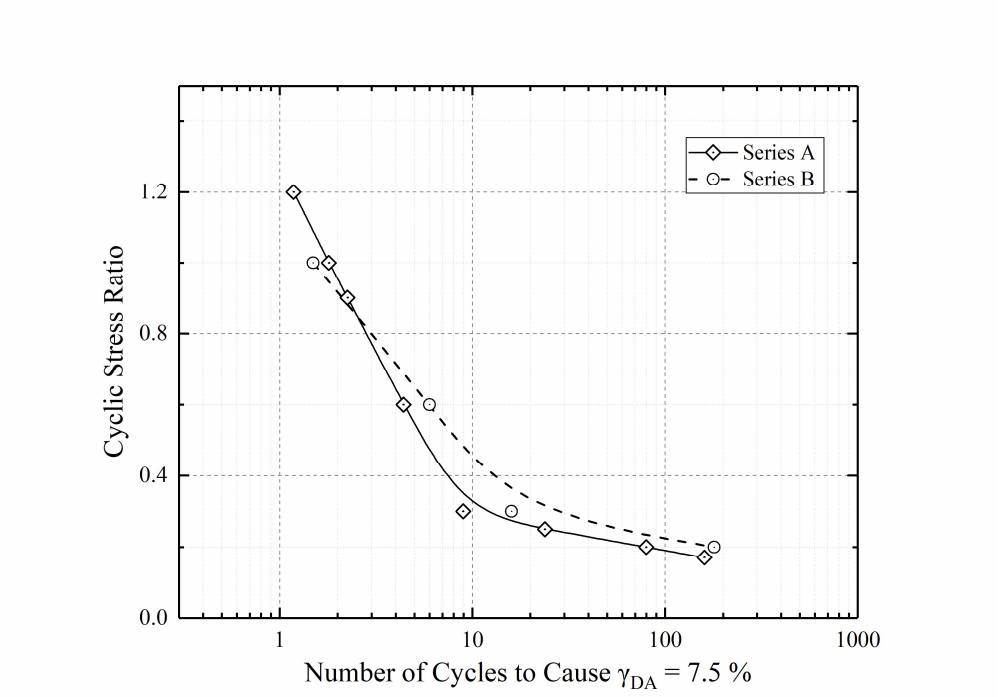

Figure 4-13 Comparison of liquefaction resistance between series A and B

4.3 Liquefaction tests with drained pre-shear history

In order to investigate the effects of pre-shear history, a series of liquefaction tests with pre-shear history under drained conditions were conducted with the mid-scale torsional shear apparatus. As labeled with series C, details of the tests are shown in Table 4-3.

Table 4-3 Test conditions of liquefaction tests with drained pre-shear history

Case ID	Initial relative density D_{ri} (%)	Relative density before the 1st stage of liquefaction test, D_{r0} (%)	Double amplitude of shear strain during pre-shear, γ_{DApre} (%)	Number of cycles during pre-shear, N_{Cpre}
C-1	77.8	79.2	0.20	100
C-2	78.3	81.2	0.60	100
C-3	79.1	82.9	0.60	200
C-4	73.3	80.5	0.60	500

In this series of tests, pre-shear histories were applied under drained conditions before the first stage of the liquefaction test. After that, the same repeated liquefaction tests were conducted as test series A introduced above. For comparison purpose, all the liquefaction test stages in series C applied the same cyclic stress ratio of 1.00 as in case A-2. In addition, considering the possible increase of relative density after different pre-shear programs, the initial relative densities of specimens were adjusted in order to reach a similar relative density before the first liquefaction stage.

Pre-shear history under drained conditions were applied a with constant double amplitude of shear strain in each case. Different double amplitudes of shear strain and the number of cycles were tested in different cases as shown in Table 4-3. The time

history of shear strain during pre-shear stage of case C-2 is shown in Figure 4-14 as an example.

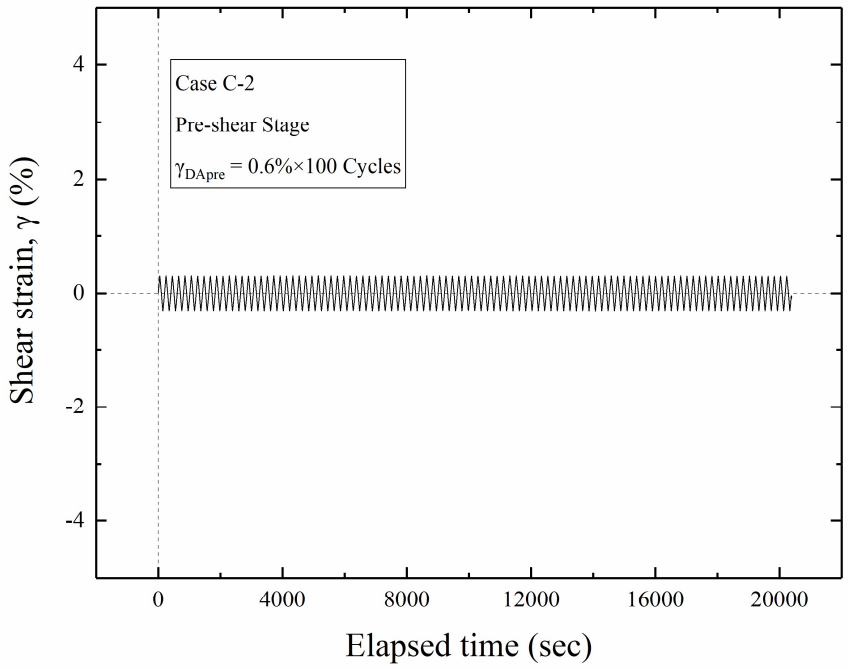

Figure 4-14 Time history of shear strain during pre-shear stage of case C-2

In order to investigate the effects of pre-shear history, the effective stress path and relationship between shear stress and shear strain of the first liquefaction stage of series C are presented together with those figures of case A-2 in Figures 4-15 and 4-16, respectively. In addition, the corresponding time histories of excess pore water pressure ratio are shown in Figure 4-17.

It can be seen that the pre-shear history in case C-1 did not affect a lot on the liquefaction resistance even though 100 cycles of cyclic loadings were conducted. However, with the increase in shear strain amplitude and number of loading cycles, the effects of pre-shear became more and more obvious. With the increase in strain amplitude and number of cycles, the most significant change can be observed in the effective stress paths. In repeated liquefaction test, the liquefaction history of the former

stage did not affect the accumulation of excess pore water pressure so that effective stress path in the first several loading cycles were very similar. However, different result can be observed that with the increase in strain amplitude and number of cycles of the pre-shear stage, the accumulation of excess pore water pressure became slower and the resistance for initial liquefaction (effective stress to be lower than 5% of the initial value) increased.

Meanwhile, the relationships between shear stress and shear strain were also influenced by different pre-shear histories. As observed in the repeated liquefaction tests series A, shear strain induced in the first cycle of different stages did not change significantly. But as shown in Figure 4-16, the shear strain of the first cycle was affected by different pre-shear histories.

Figure 4-18 shows the liquefaction resistance of the first stage in series C and all stages of series A. In this figure, liquefaction tests with no pre-shear histories were indicated in green, and the cases with small strain pre-shear history in drained condition were marked in red. Repeated liquefaction stages with liquefaction histories are indicated with black symbols. In this figure, the effects of different pre-shear histories can be observed more intuitively.

As mentioned in the background, with repeated liquefaction tests on medium dense sand, pioneer researchers found that the pre-shear history could only affect the liquefaction stage immediately after it. Therefore, repeated liquefaction tests were also conducted in series C after their first liquefaction stages. However, due to controlling mistake of the program, repeated liquefaction test was not successfully conducted in case C-2.

Figure 4-19 shows the relationship of relative density and liquefaction resistance (number of cycles to induce 7.5% double amplitude of shear strain) in case A-2 (as a reference) and test series C.

It can be noticed that the liquefaction resistance of the first stage increased with the increase of strain amplitude as well as the cyclic number of pre-shears. However, the influence of pre-shears seemed to only work on the liquefaction stage immediately after the pre-shear. In other words, it can be noticed that the liquefaction resistance in the second stages reduced to a similar value of the case without pre-shear history in case A-2.

These results indicate that the liquefaction resistance might be affected by its closest pre-shear history, or the full liquefaction history might eliminate the effect of the previous pre-shear. Similar behavior was also reported by Teparaksa (2017) on medium dense sand in triaxial shear test.

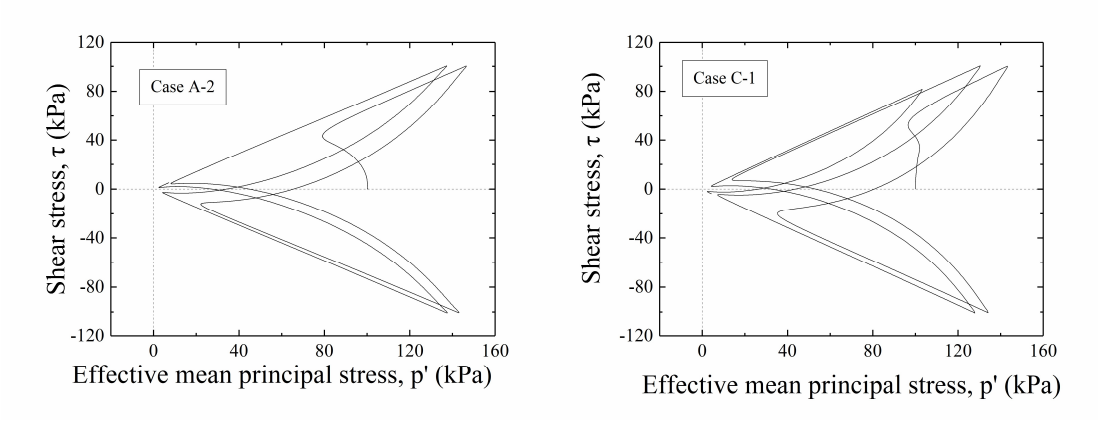

(a) Case A-2

(b) Case C-1

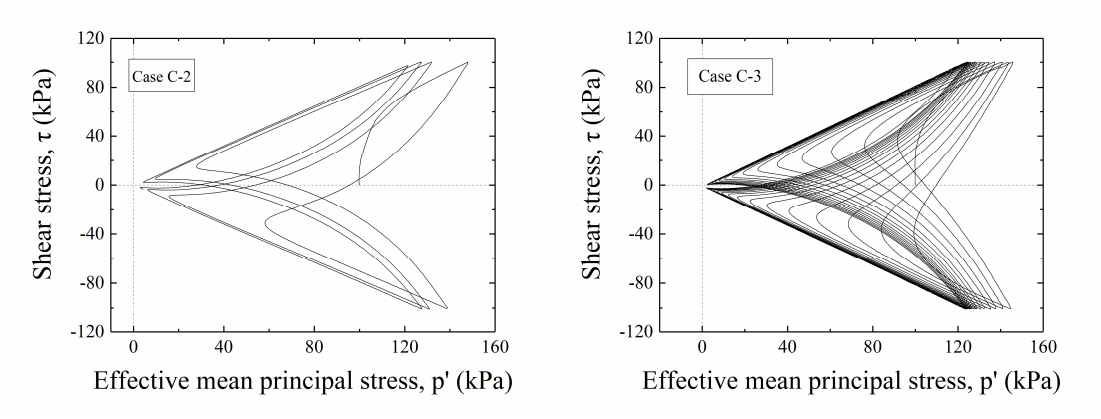

(c) Case C-2

(d) Case C-3

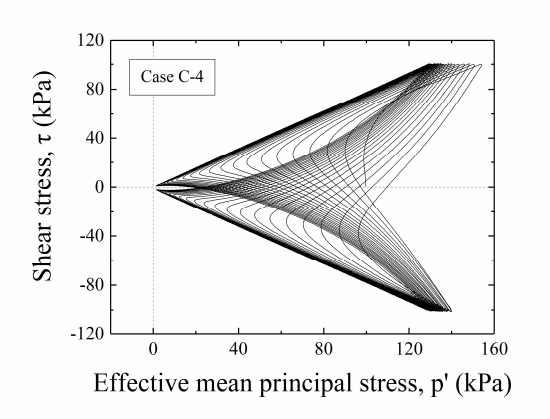

(e) Case C-4

Figure 4-15 Effective stress path of the 1st liquefaction stage

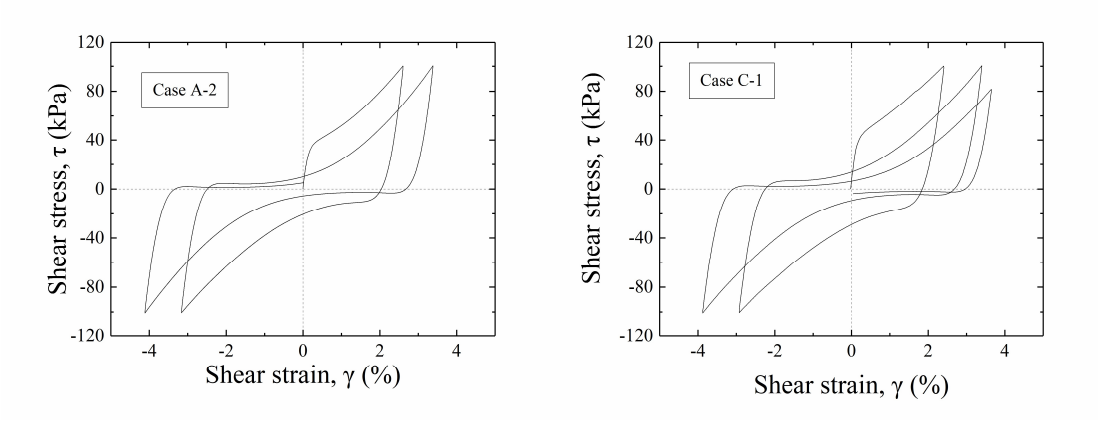

(a) Case A-2

(b) Case C-1

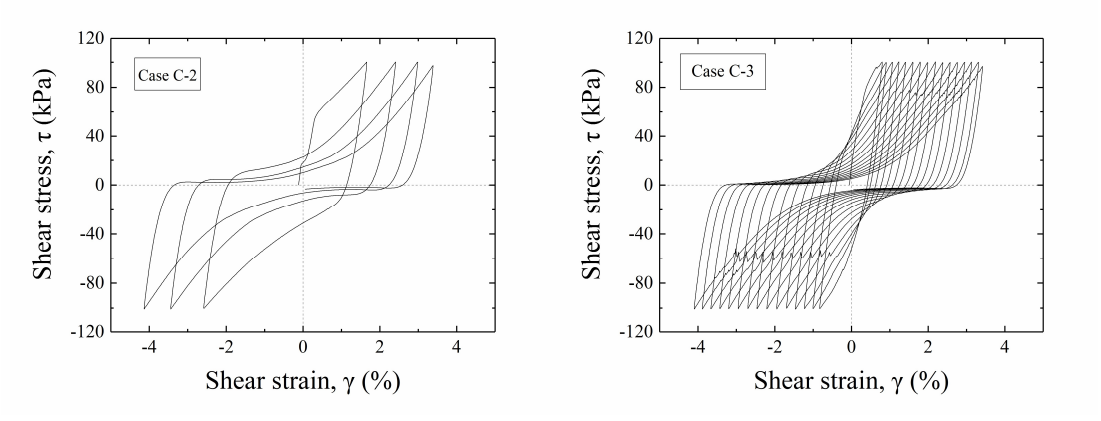

(c) Case C-2

(d) Case C-3

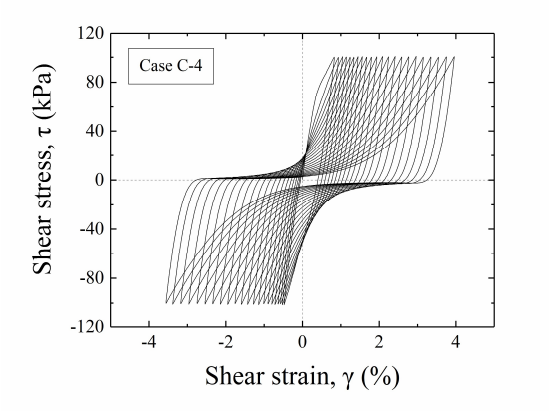

(e) Case C-4

Figure 4-16 Relationship between shear stress and shear strain of the 1st liquefaction stage

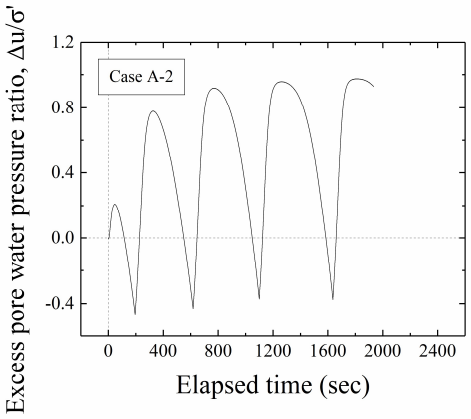

(a) Case A-2

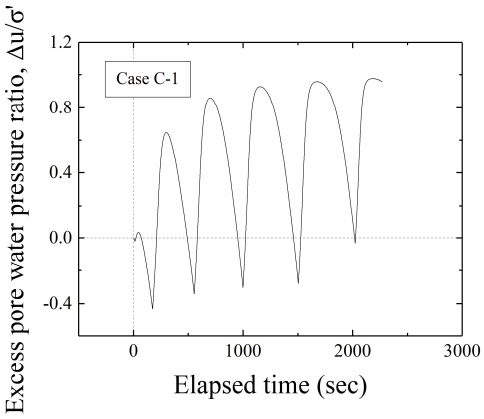

(b) Case C-1

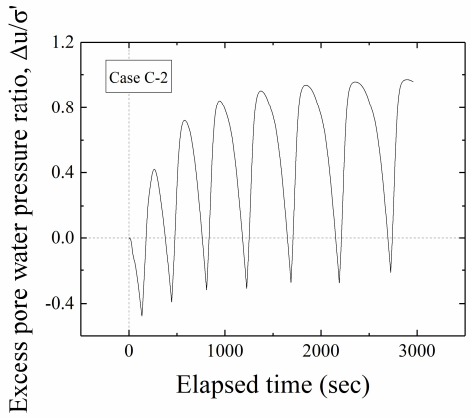

(c) Case C-2

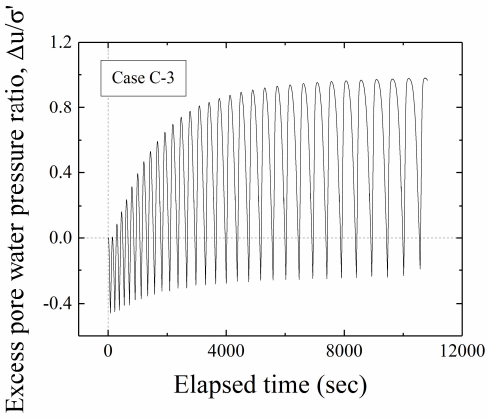

(d) Case C-3

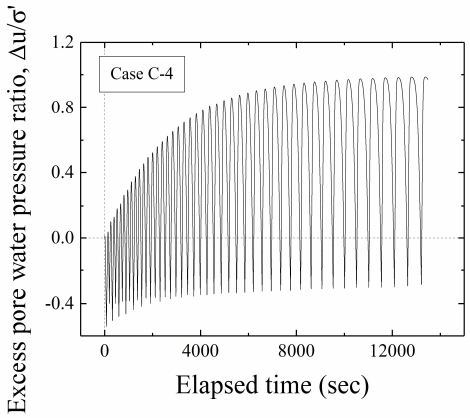

(e) Case C-4

Figure 4-17 Time histories of the excess pore water pressure ratio of the 1st liquefaction stage

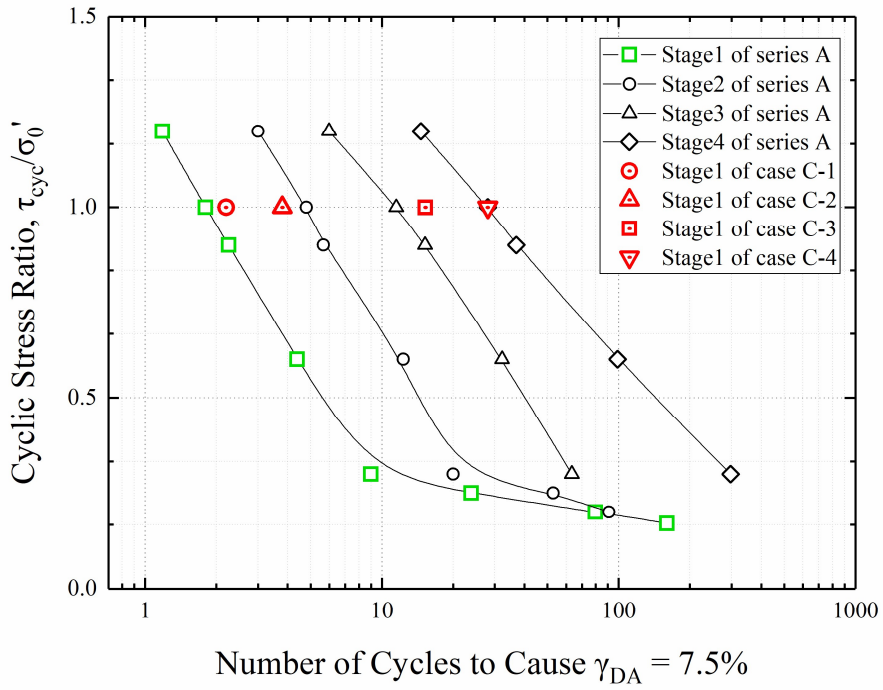

Figure 4-18 liquefaction resistance of the first stage in series C and all stages of series A

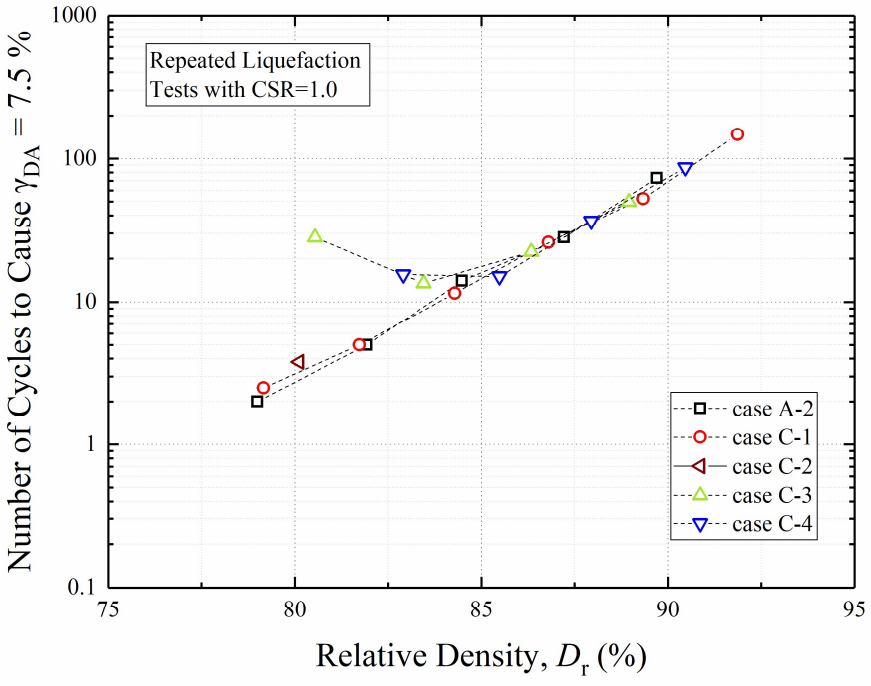

Figure 4-19 Relationship between relative density and liquefaction resistance in case A-2 and test series C

4.4 Liquefaction tests with undrained pre-shear histories

A series of repeated liquefaction tests were carried out with undrained pre-shear histories to investigate more details of the pre-shear effects. Details about the testing conditions are shown in Table 4-4.

Table 4-4 Test conditions of liquefaction tests with undrained pre-shear history

Case ID	Initial relative density D_{ri} (%)	Relative density before the 1st stage of liquefaction test, D_{r0} (%)	Number of pre-shear stages, N_{pre}	Cyclic stress ratio in liquefaction stages, τ_{cyc}/σ_0'
D-1*	78.5	79.2	1	1.00
D-2*	75.4	79.5	10	1.00
D-3*	72.1	79.1	18	1.00
D-4	73.3	80.5	18	0.90
D-5	73.0	79.6	18	1.00
D-6	72.4	79.2	18	1.20
D-7	73.1	80.2	18	1.60

* Cases D-1 to D-3 were carried out using the small-scale torsional shear apparatus.

As shown in Table 4-4, this series of tests was labeled as series D. In test series D, the specimen was subjected to the undrained pre-shear history before the first liquefaction stage. Under undrained conditions, cyclic loadings were applied to the specimen with a constant cyclic stress ratio. After the excess pore water pressure ratio reached 0.5, one stage of pre-shear completed. In cases D-1 to D-3, this kind of pre-shear was applied different times to investigate its influence. Between each pre-shear stage, reconsolidation was conducted to restore the initial effective stress. In later cases, tests

with different cyclic stress ratios during the following liquefaction tests were carried out to draw the liquefaction resistance curve.

In order to control the excess pore water pressure precisely, a relatively lower CSR was applied at the first pre-shear stage. However, in later cases with more pre-shear stages, CSR was increased stage by stage. That is because the former pre-shear history made it difficult for the accumulation of excess pore water pressure in the following stages. CSRs applied in different pre-shear stages are shown in Table 4-5.

Table 4-5 CSRs applied in different pre-shear stages

Stage No.	Case D-1	Case D-2	Cases D-3 to D-7
1	0.25	0.25	0.25
2		0.25	0.25
3		0.30	0.30
4		0.35	0.35
5		0.40	0.40
6		0.45	0.45
7		0.50	0.50
8		0.55	0.55
9		0.60	0.60
10	-	0.65	0.65
11			0.70
12			0.75
13			0.80
14		-	0.85
15			0.90
16			0.95
17			0.95
18			0.95

As typical examples, Figures 4-20 to 4-22 show the effective stress paths and the time histories of the excess pore water pressure ratio in the 3rd, 10th and 18th pre-shear stages of case D-3, respectively.

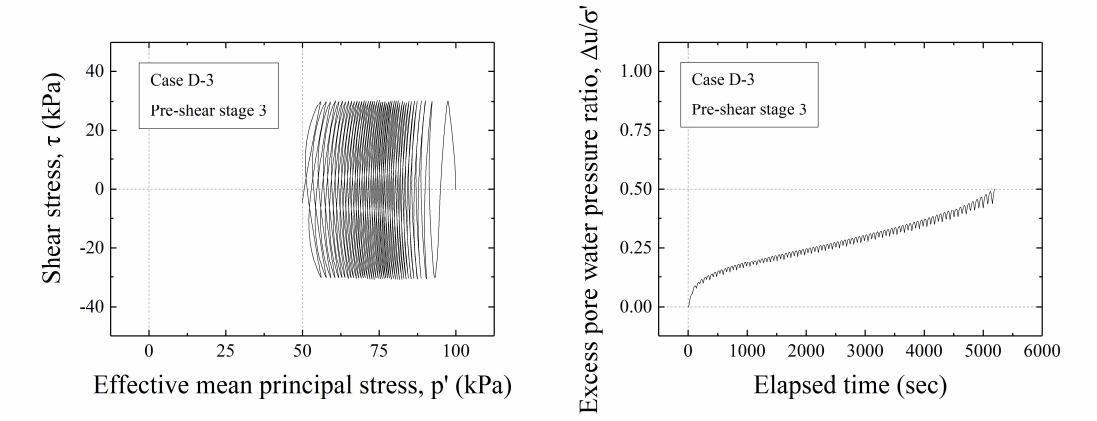

Figure 4-20 Effective stress path (left) and the time history of excess pore water pressure ratio (right) during undrained pre-shear stage (3rd stage)

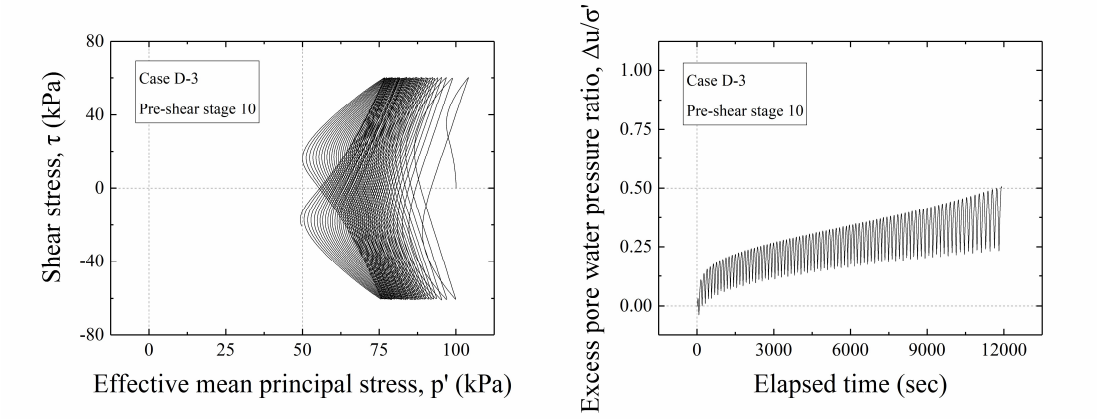

Figure 4-21 Effective stress path (left) and the time history of excess pore water pressure ratio (right) during undrained pre-shear stage (10th stage)

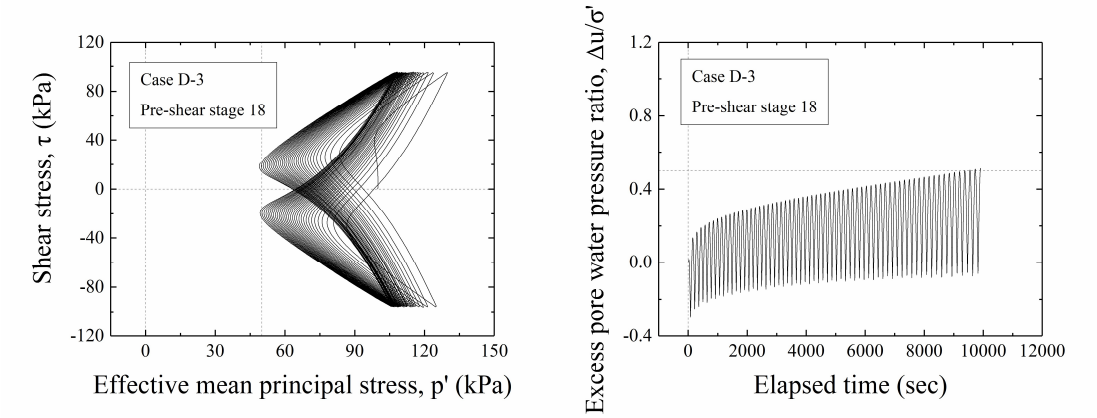

Figure 4-22 Effective stress path (left) and the time history of excess pore water pressure ratio (right) during undrained pre-shear stage (18th stage)

It can be observed that with the increase of liquefaction resistance and CSR during pre-shear stages, specimens tended to show positive dilatancy more and more obviously.

From the 10th pre-shear stage, phase transformation occurred in the first cycle of loadings.

For comparison, the effective stress path, stress-strain relationship, and time history of excess pore water pressure ratio of the first liquefaction stage in cases A-2 and D1 to D3 are shown in Figures 4-23 to 4-25, respectively. The results clearly show that the pre-shear effect in each pre-shear stage could be accumulated since with increasing number of stages, the liquefaction resistance increased significantly.

However, as mentioned above, the phase of effective stress path transformed from the first loading cycle after the 10th pre-shear stage. This kind of pre-shear was considered as a large strain pre-shear as proposed in the past studies on loose or medium dense sand. But different from the results observed from loose or medium dense sand, this kind of large strain pre-shear increased the liquefaction resistance on dense sand specimens in these cases. In addition, it can be noticed that the pre-shear histories affected the generation of excess pore water pressure and the accumulation of shear strain. This result is similar as observed in the liquefaction test with drained pre-shear introduced before.

For investigating the pre-shear effects on repeated liquefaction stages, the relationships between relative density and liquefaction resistance of different liquefaction stages are shown in Figure 4-26 including cases D-1 to D-3 and other cases introduced before. As concluded above, the pre-shear effects in drained conditions were eliminated after the first full liquefaction stage and they were considered to affect the liquefaction stage immediately after.

However, it can be observed from Figure 4-26 that the effects of undrained pre-shear not only affected the liquefaction resistance of the first liquefaction stage noticeably, the later stages were also affected. The effects of pre-shear histories were reduced after

the first liquefaction stage but not fully removed. Considering that the effects of pre-shear history can be accumulated in different stages, this result might be the possible explanation of the reason why old sand deposits have significantly high liquefaction resistances. During the long time period, small earthquakes with limited ground motions and excess pore water pressure generated strengthened the sand layer and the effects accumulated like in the pre-shear stages of the test. Even though the great earthquakes took place occasionally, the effects of small earthquakes partially remained and made the soil stronger and stronger.

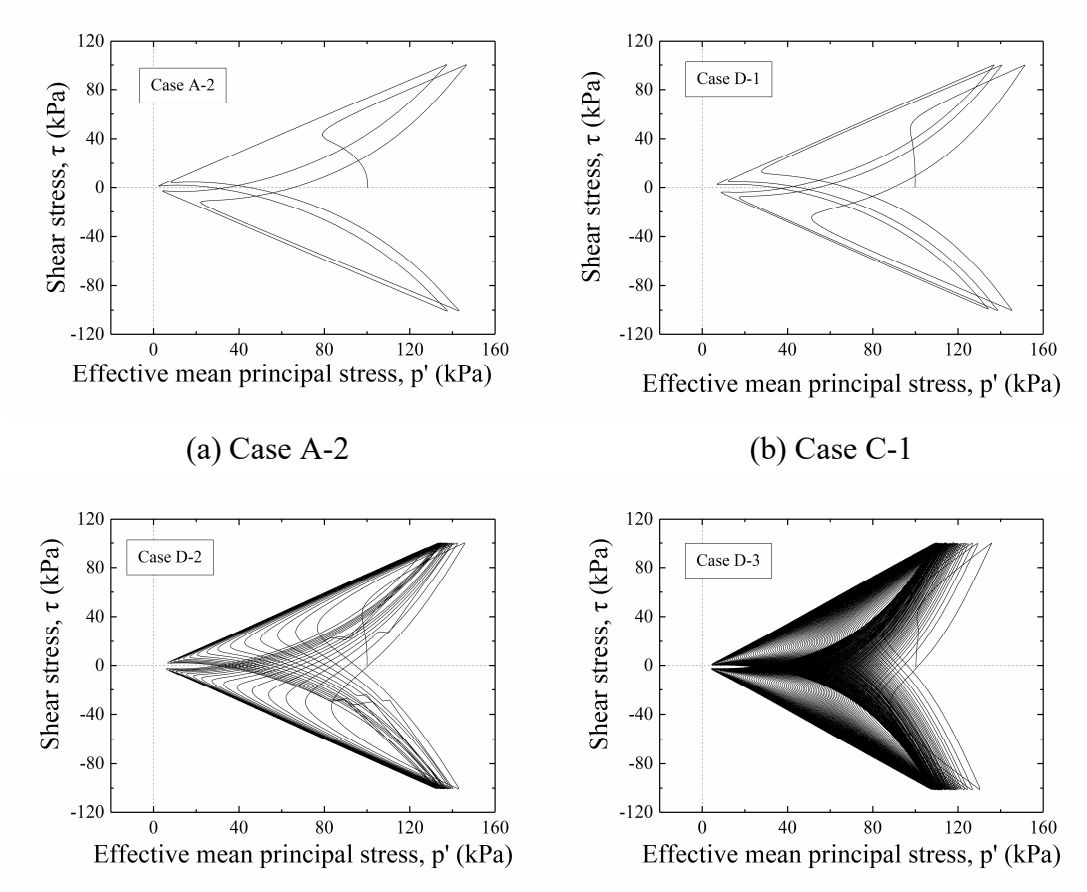

(a) Case A-2 (b) Case C-1

(c) Case C-2 (d) Case C-3

Figure 4-23 Effective stress paths of the 1st liquefaction stage

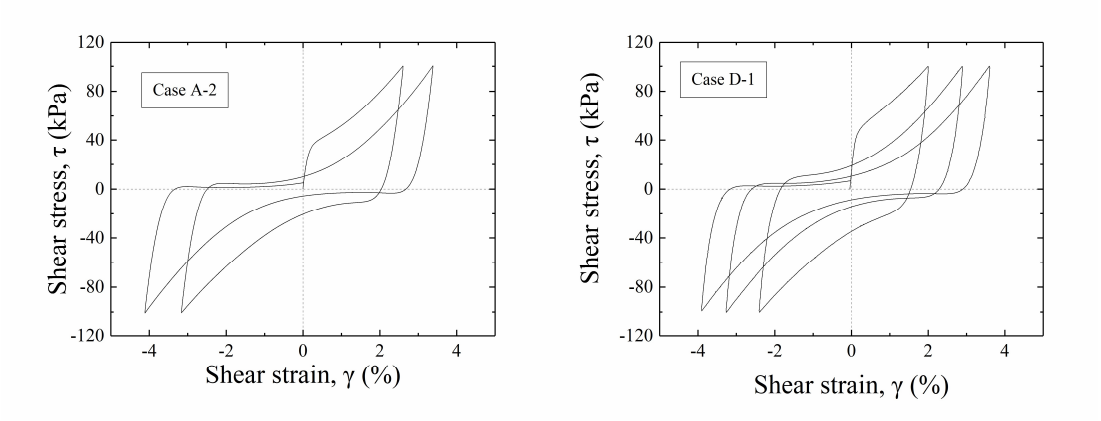

(a) Case A-2 (b) Case C-1

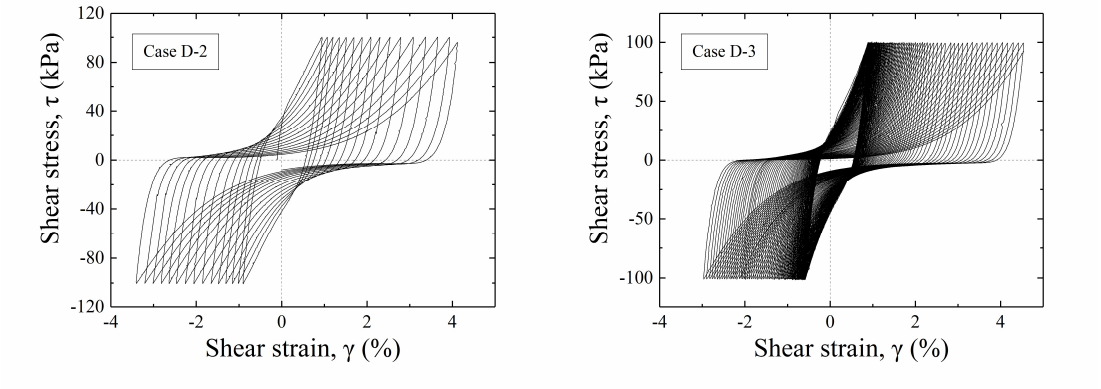

(c) Case C-2 (d) Case C-3

Figure 4-24 Relationships between shear stress and shear strain of the 1st liquefaction stage

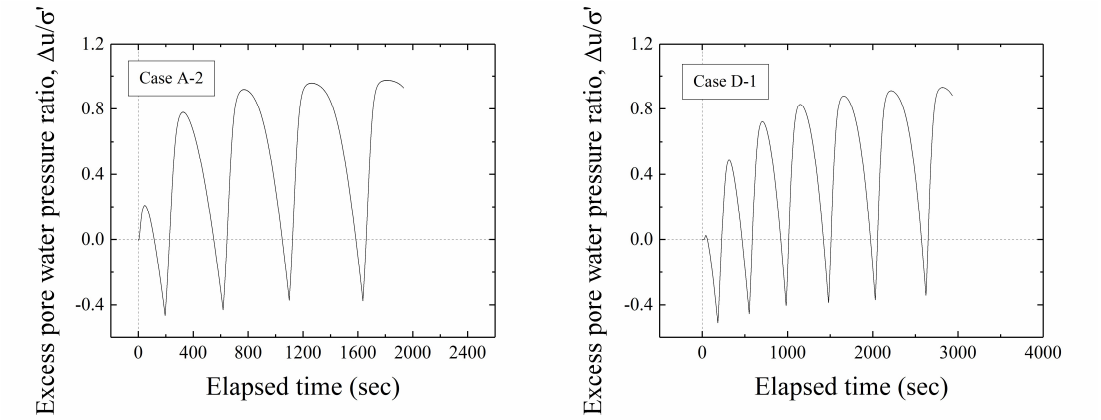

(a) Case A-2 (b) Case C-1

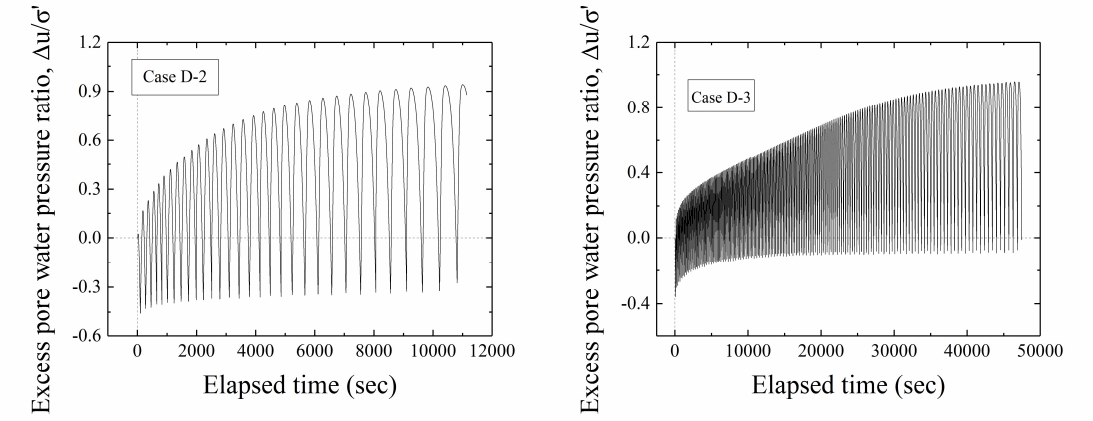

(c) Case C-2 (d) Case C-3

Figure 4-25 Time histories of the excess pore water pressure ratio of the 1st liquefaction stage

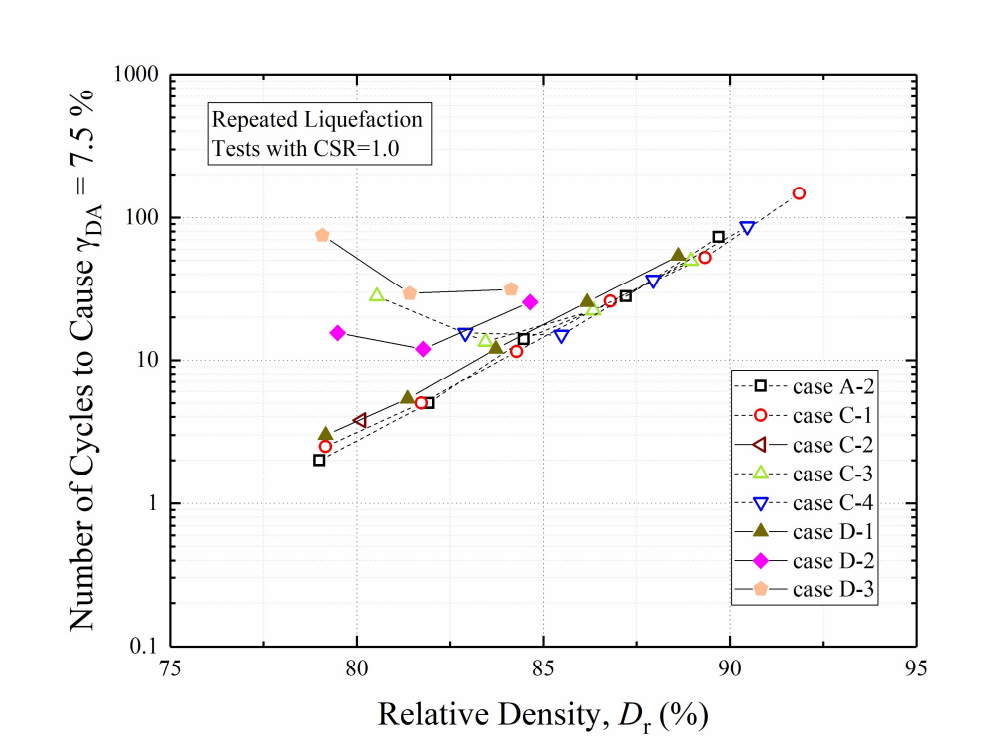

Figure 4-26 Relationship between relative density and liquefaction resistance in case A-2, test series C and cases D-1 to D-3

In order to draw the liquefaction resistance curve with high liquefaction resistance, liquefaction tests were carried out with the same pre-shear history but different CSRs in cases D4-D7.

Figure 4-27 shows the relationship between number of cycles to induce 7.5% double amplitude of shear strain and cyclic stress ratio including the first liquefaction stage of all cases introduced above (except for series B). For comparison purpose, the data of the 4th repeated liquefaction stage of series A are introduced in this figure as well.

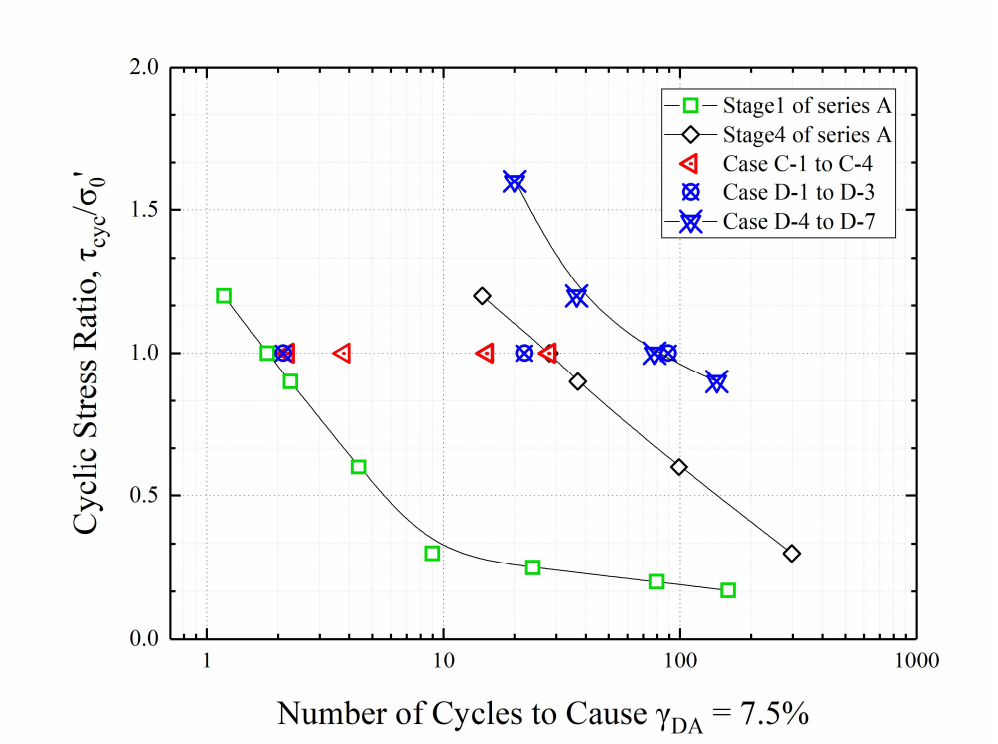

Figure 4-27 Relationship between liquefaction resistance and cyclic stress ratio

The liquefaction resistance of cases D-4 to D-7 were noticeably high as presented in this figure. The "partial liquefaction" histories with a large number of stages increased the liquefaction resistance much more remarkably than the "full liquefaction" histories in series A.

However, the results presented above are not enough to compare the difference of drained and undrained pre-shears since both drainage conditions and loading programs are different. Therefore, for quick comparison, an extra case of liquefaction test with drained pre-shear was carried out as case C-5.

In case C-5, the same loading program was employed as in case D-5 where 18 stages of "partial liquefaction" histories were applied to the sand specimen. But during these pre-shear loadings, the specimen was kept in drained condition as in test series C. After the pre-shear and reconsolidation, the specimen was subjected to same loading program as applied in case D-5 with a cyclic stress ratio of 1.00.

The test results of case C-5 was shown together with those of case D-5 in Figures 4-28 to 4-30. Except for the accumulation direction of shear strain, the results of these two tests were of great similarities. It seems that the same stress history dominated the effect of pre-shear even though the different drainage conditions induced different effective stress paths during pre-shear loadings as shown in Figure 4-31. Under the same shear stress history, the excess pore water pressure generated in the drained condition was negligible.

The liquefaction resistance point of case C-5 was added in Figure 4-32 after Figure 4-27. The liquefaction resistance is a little larger than case D-3 or D-5 but considering the inevitable natural deviation, the difference is not very significant.

However, only one case in comparison is not enough to draw the conclusion that the drainage condition has a negligible influence on the effects of pre-shear histories. Thus, further investigations are still necessary to be continued in the future.

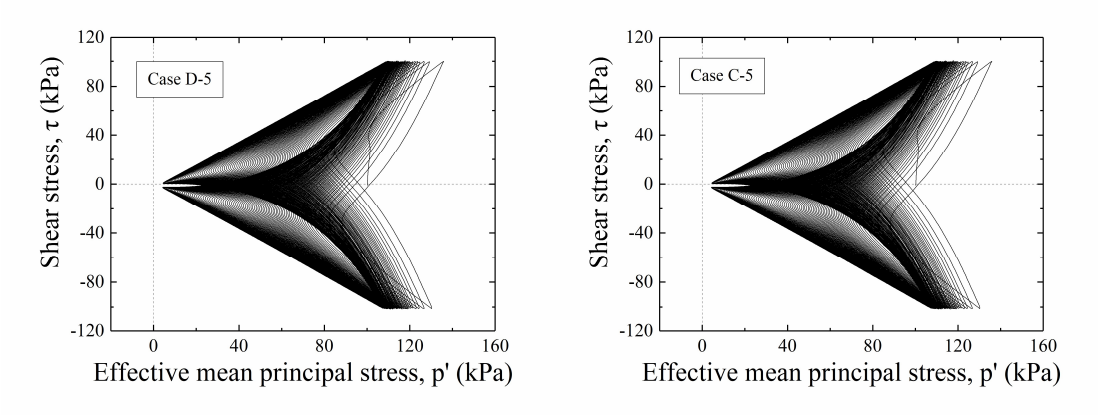

(a) Case D-5 (b) Case C-5

Figure 4-28 Effective stress paths of the 1st liquefaction stage

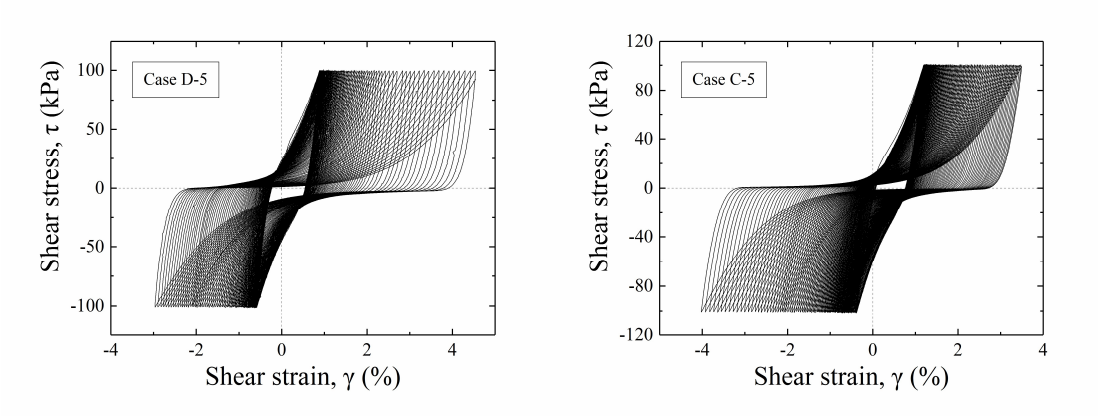

(a) Case D-5 (b) Case C-5

Figure 4-29 Relationships between shear stress and shear strain of the 1st liquefaction stage

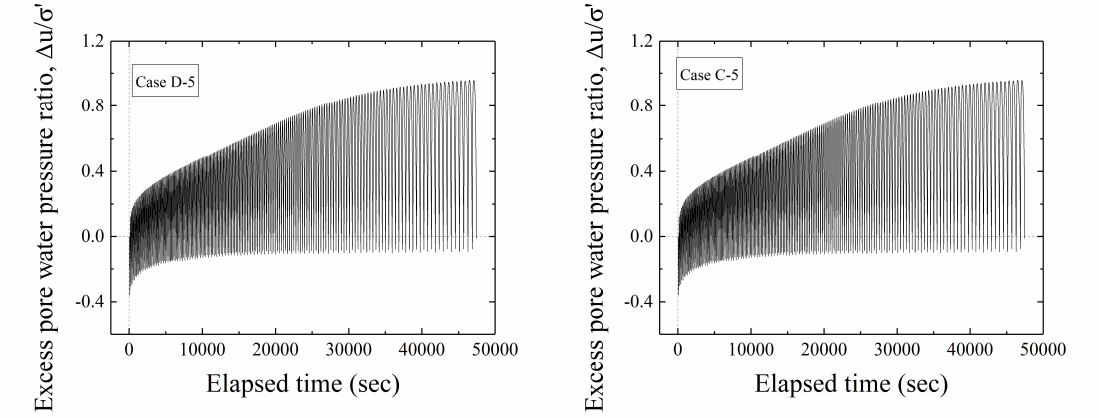

(a) Case D-5 (b) Case C-5

Figure 4-30 Time histories of the excess pore water pressure ratio of the 1st liquefaction stage

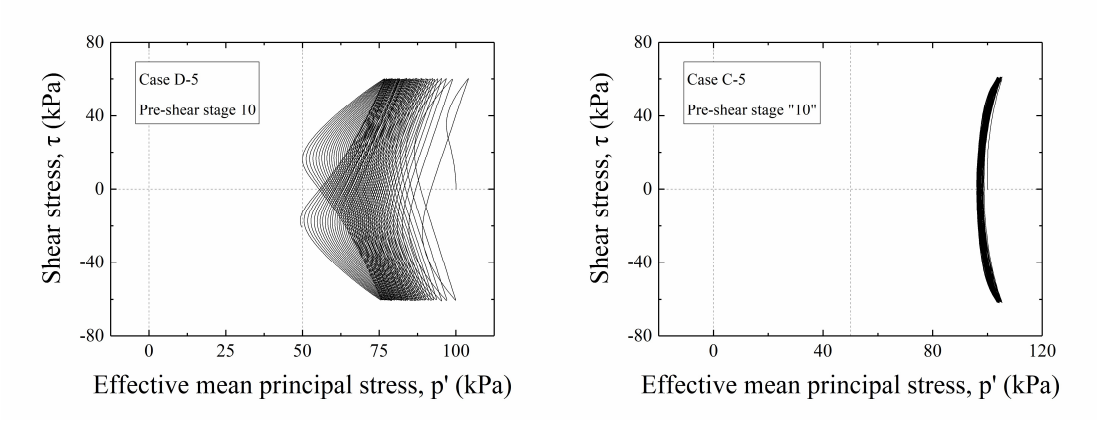

(a) Case D-5 (undrained) (b) Case C-5 (drained)

Figure 4-31 Effective stress paths of pre-shear stages under different drainage conditions

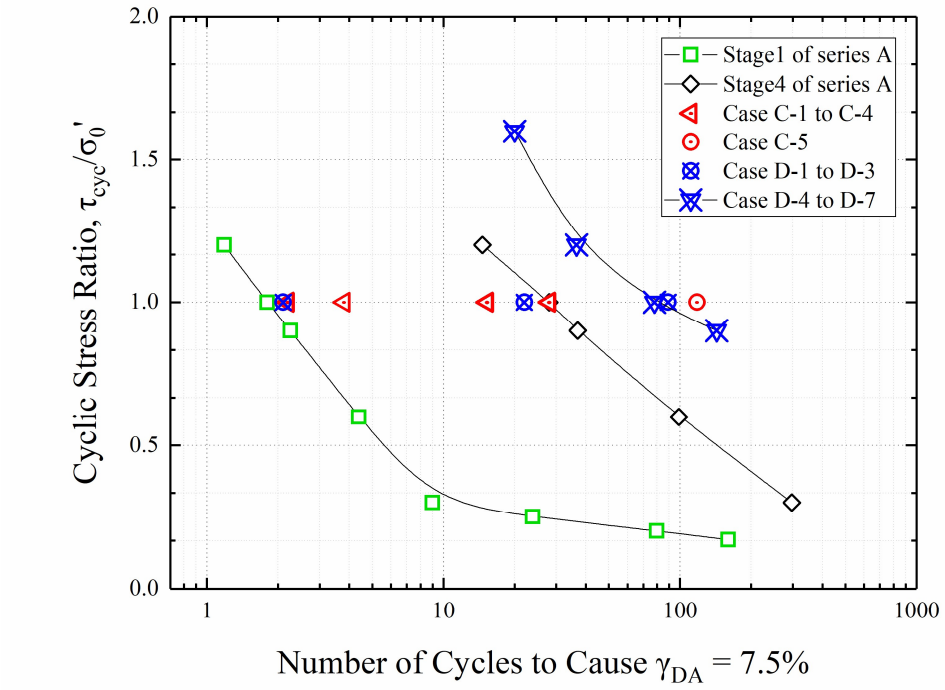

Figure 4-32 Relationship between liquefaction resistance and cyclic stress ratio

4.5 Summary

Four series of liquefaction tests were conducted in the torsional shear apparatus to investigate the effect of different kinds of pre-shear histories and the repeated liquefaction behavior after the pre-shear on dense sand specimens. The results of the torsional shear tests can be concluded as follows:

1. The liquefaction resistance in repeated liquefaction tests increased with liquefaction stages.

In the repeated liquefaction tests without pre-shear history, the specimen showed increasing liquefaction resistance during repeated liquefaction. This behavior is different from what was reported on medium dense sand by pioneer researchers.

2. Pre-shear history under drained conditions affected the liquefaction resistance of dense sand specimen differently with various loading programs.

In test series C, by conducting liquefaction tests with different drained pre-shears, it was found that both the amplitude of shear strain and the number of loading cycles affected the liquefaction resistance in the following liquefaction test. However, it was noticed that the pre-shear seemed to only affect the liquefaction stage immediately after, since the liquefaction resistance from the second stage reduced to the same level as the one with no pre-shear.

3. Pre-shear history under undrained conditions was found to affect the liquefaction resistance as well.

Tests with pre-shear history under undrained conditions were applied with a “partial liquefaction” history by inducing excess pore water pressure ratio to 0.5. It was found that this kind of pre-shear can be accumulated in different pre-shear stages. After 18 stages of pre-shear loadings, the sand specimen became extremely strong to

liquefaction even though it had similar relative density as the virgin sample in cases with no pre-shear. It was noticed that the complex pre-shear history could not be fully eliminated after the first liquefaction stage as in the drained pre-shear cases.

4. A simple comparison was made between pre-shear histories in different drainage conditions and no significant difference was found.

No significant difference was found by conducting tests with the same stress history but in different drainage conditions. It seemed that the accumulation of excess pore water pressure during the undrained condition did not affect the liquefaction resistance very much. However, due to the limited test numbers, it cannot be concluded that the drainage condition has no effect during the pre-shear stage. Further investigations based on more testing cases are still necessary to provide more evidence.

4.6 References

AOYAGI, Y., 2018. Analysis of multiple-liquefaction characteristics in torsional shear and stacked ring shear tests based on energy concept. *Ph.D. Thesis. Department of Civil Engineering, the University of Tokyo, Japan.*

TEPARAKSA, J., 2017. Comparison of sand behavior under repeated liquefaction in triaxial and shaking table tests. *Ph.D. Thesis. Department of Civil Engineering, the University of Tokyo, Japan.*

WAHYUDI, S., KOSEKI, J., SATO, T. and CHIARO, G., 2015. Multiple-liquefaction behavior of sand in cyclic simple stacked-ring shear tests. *International Journal of Geomechanics,* Vol. 16(5), pp. C4015001.

Chapter 5 Analysis of Pre-shear Effects Based on the Energy Concept

5.1 Introduction

In this chapter, analysis of the pre-shear effects based on the energy concept is introduced and discussed. Regarding the special liquefaction behavior of dense sand, a new method to distinguish the “negative impact” and “positive impact” of pre-shear histories was proposed. In addition, considering the versatility of the new method among different relative densities, further discussion was carried out based on the re-analysis of Dr. Aoyagi’s liquefaction tests data on medium dense sand.

5.2 Introduction of the dissipated energy concept

5.2.1 Dissipated energy equation of liquefaction test

Generally, the work can be described and computed as the following equation:

$$W = \int Fds \qquad (5\text{-}1)$$

where W represents the work, F represents the force and s represents the displacement in the direction of the force. In torsional shear test, the dissipated energy can be calculated based the stress-strain relationship curve by adjusting this equation. As shown in Figure 5-1, the energy dissipated in the red rectangular can be calculated with its bottom side length $\Delta\gamma$ and its height τ. The energy equation for triaxial and torsional shear test can be obtained by accumulating these little areas as the following equation (Wahyudi, 2014):

$$\sum \Delta W = \int q d\varepsilon = \int \tau d\gamma \qquad (5\text{-}2)$$

where $\sum \Delta W$ is the dissipated energy of the unit of soil due to the plastic deformation during cyclic loadings, q and ε are the deviator stress and vertical displacement in undrained triaxial tests on saturated specimens, τ and γ are the shear stress and shear strain in undrained torsional shear tests on saturated specimens conducted by keeping the specimen height constant and inner and outer cell pressures equal to each other, respectively.

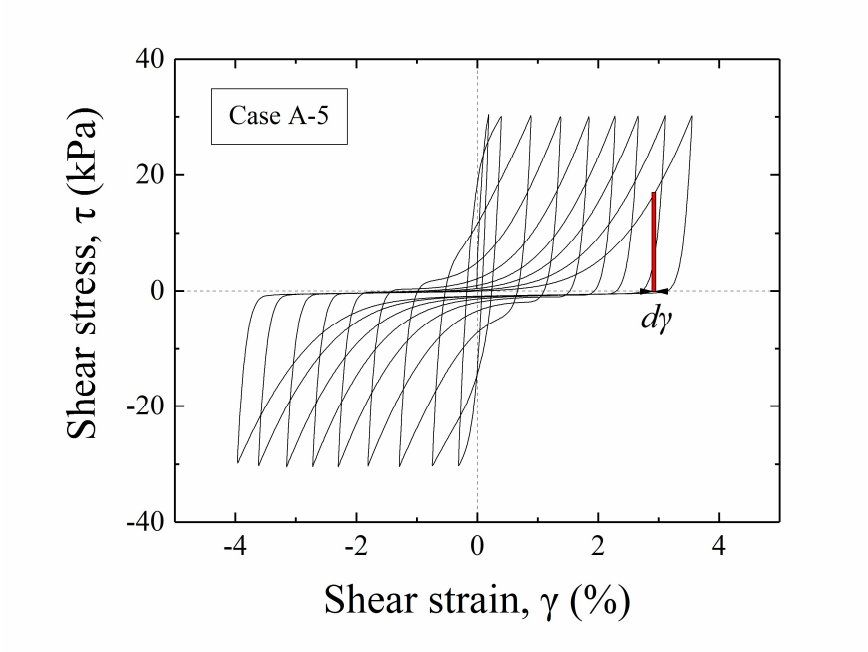

Figure 5-1 Dissipated energy calculation in torsional shear test

5.2.2 Modified dissipated energy equation

Aoyagi (2016, 2018) modified the energy equation by normalizing the shear stress by its corresponding effective stress during cyclic loadings. The modified energy equation is as follows:

$$\sum \frac{\Delta W}{p'} = \int \frac{\tau_{corr.}}{p'_{corr.}} d\gamma \qquad (5\text{-}3)$$

where $\tau_{corr.}$ and $p'_{corr.}$ are the corrected shear stress and shear strain, respectively. In order to compute the normalized dissipated energy, it is necessary to correct the shear stress and shear strain. As shown in Figure 5-2, in some cases of liquefaction test, the effective stress path did not pass through the coordinate origin. Koseki et al. (2005) suggested that this might be due to the effect of interlocking and error in measuring. Therefore, in order to compute the ratio of shear stress divided by effective stress, they need to be corrected as follows:

$$\tau_{corr.} = \tau + \Delta\tau \qquad (5\text{-}4)$$

$$p'_{corr.} = p' + \Delta p' \qquad (5\text{-}5)$$

where $\Delta\tau$ and $\Delta p'$ are the correction values obtained from the effective stress path close up shown in Figure 5-2.

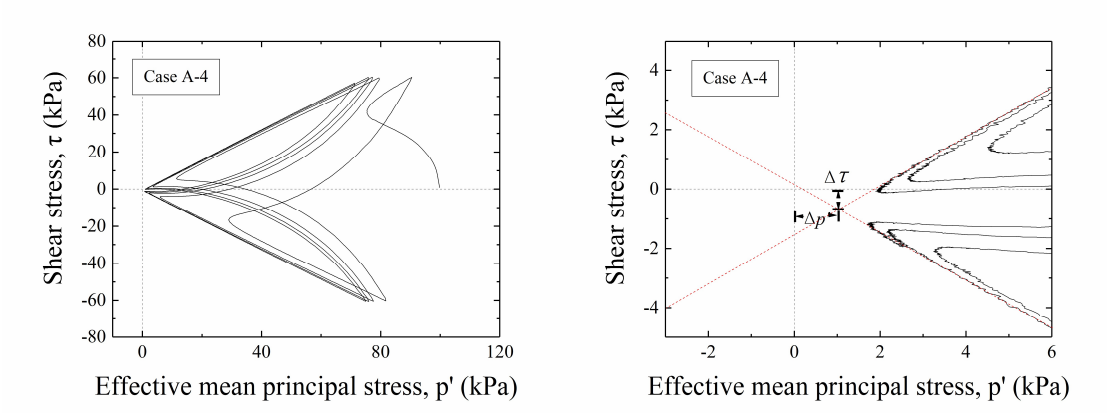

Figure 5-2 Effective stress path (left) and its close-up near the origin

The relationships between the normalized shear stress and shear strain before and after the correction are shown in Figure 5-3. It can be seen that the relationship became more reasonable after the correction. With this correction, test results with different degrees of possible error during measuring could become more uniform.

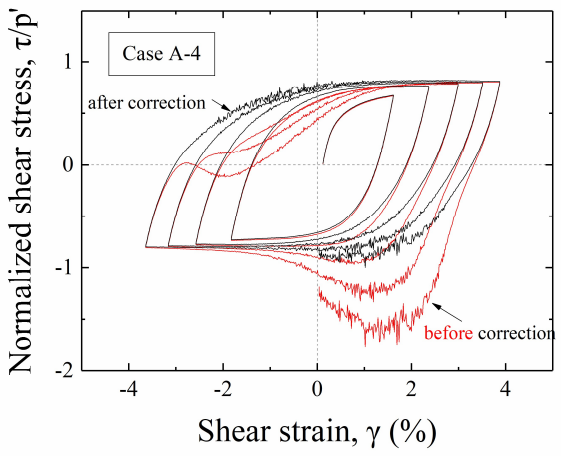

Figure 5-3 Relationship between normalized shear stress and shear strain before and after the correction

5.2.3 Accumulated shear strain

In the analysis with dissipated energy concept, the accumulated shear strain is very important in describing the progress of energy dissipation. As shown in Figure 5-4, the accumulated shear strain in torsional shear test can be calculated as:

$$\sum\gamma = \int \left|\frac{d\gamma}{dt}\right| dt \qquad (5\text{-}6)$$

where γ is the shear strain and t is the elapsed time during the loading.

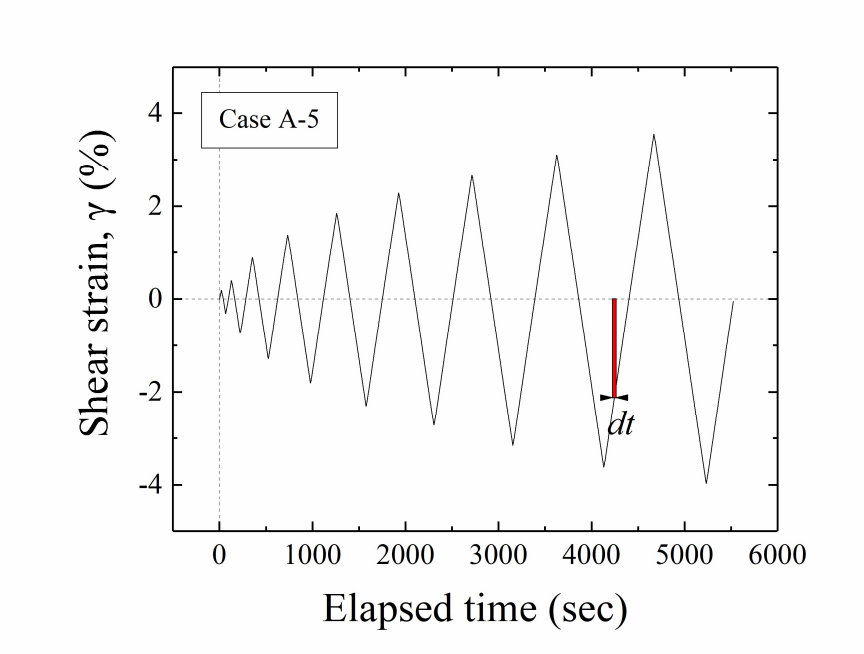

Figure 5-4 Calculation of the accumulated shear strain

5.3 Analysis and discussions

5.3.1 Applications in the past

Wahyudi, et al. (2015) applied the dissipated energy method to investigate the repeated liquefaction behavior of medium sand in the stacked rings shear tests. By plotting the relationship between dissipated energy and the accumulated shear strain, three turning points can be found on the relationship as shown in Figure 5-5 as an example. He found that these points corresponded with the starting point of phase transformation, the starting point of rapid accumulation of shear strain and the point that initial liquefaction occurred. Considering the different behavior of sand before and after the second point, he divided the dissipated energy into the positive impact and negative impact. The positive impact was considered to improve the liquefaction resistance while the negative one reduced the resistance.

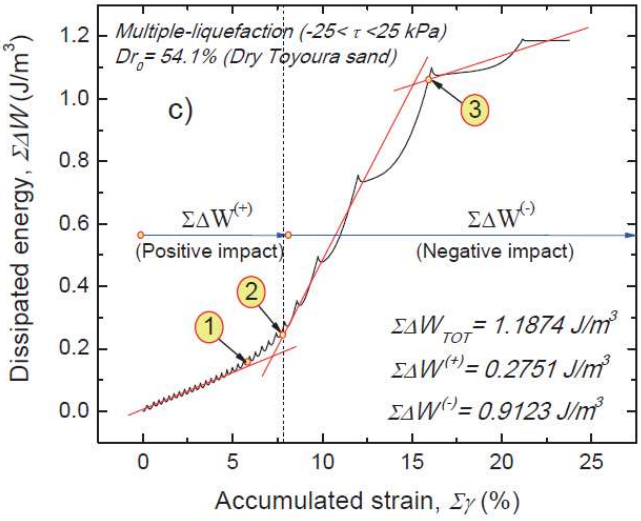

Figure 5-5 Relationships between dissipated energy and accumulated shear strain (Wahyudi, et al., 2015)

Aoyagi (2018) analyzed the multiple liquefaction behavior of medium dense sand with normalized dissipated energy approach. With the boundary of the line of phase transformation, he suggested that the "positive impact" accumulated before the phase transformation could increase the re-liquefaction resistance and the "negative impact"

could reduce the re-liquefaction resistance. With further analysis, he found a possible relationship between the re-liquefaction resistance and the combination of "positive impact" and "negative impact", which provided the possibility for estimating the re-liquefaction resistance through energy approach.

5.3.2 Energy analysis results of liquefaction tests on dense sand

The dissipated energy and normalized dissipated energy during the pre-shear stages and liquefaction stages were calculated to study their relationship with the liquefaction resistance.

Repeated liquefaction tests without pre-shear (Test series A)

In this series of test, the dissipated energy and normalized dissipated energy during each repeated liquefaction test were calculated and the results of case A-2 are shown in Figures 5-6 to 5-9.

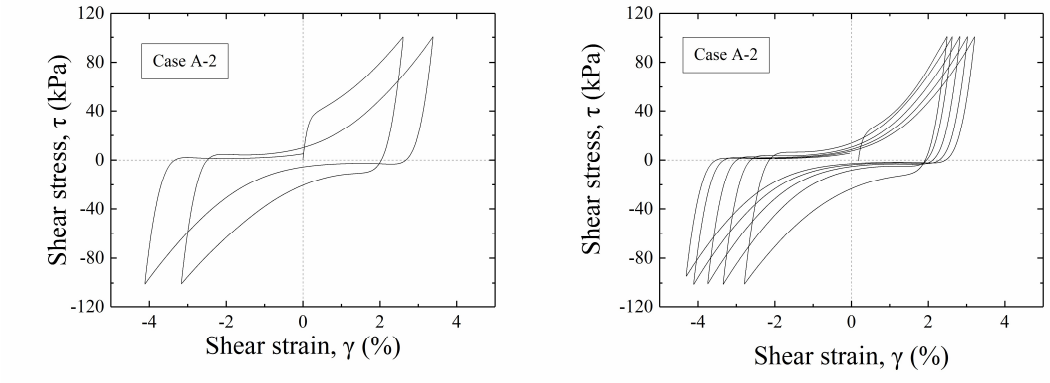

(a) stage 1 (b) Stage 2

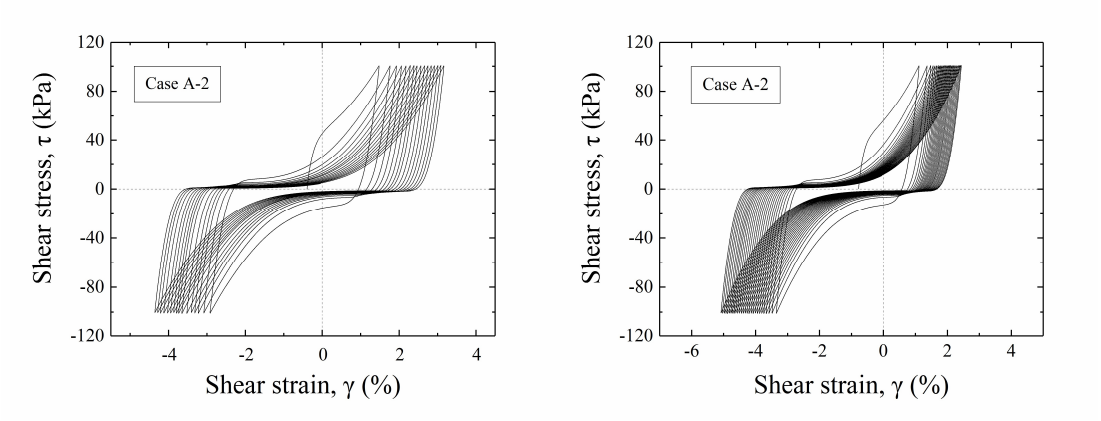

(c) stage 3 (d) Stage 4

Figure 5-6 Relationship between shear stress and shear strain in different liquefaction stages in case A-2

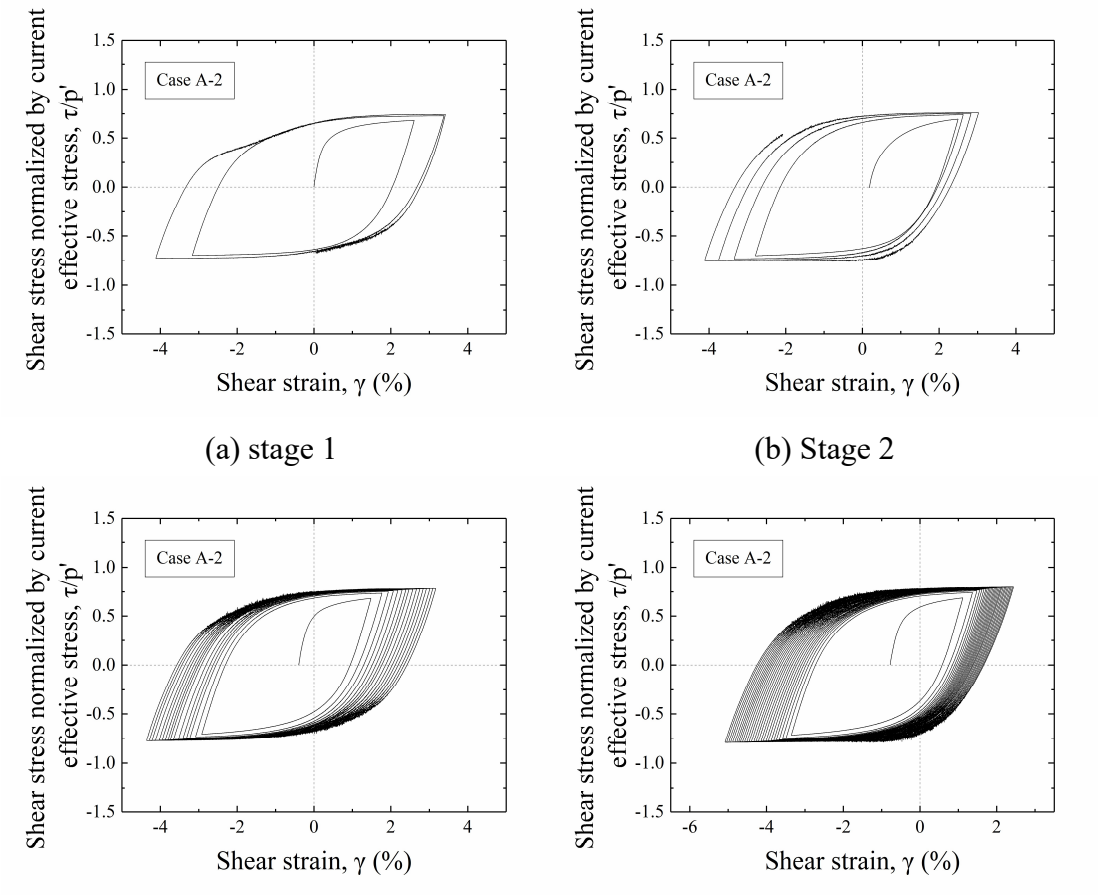

(a) stage 1 (b) Stage 2

(c) stage 3 (d) Stage 4

Figure 5-7 Relationship between normalized shear stress and shear strain in different liquefaction stages in case A-2

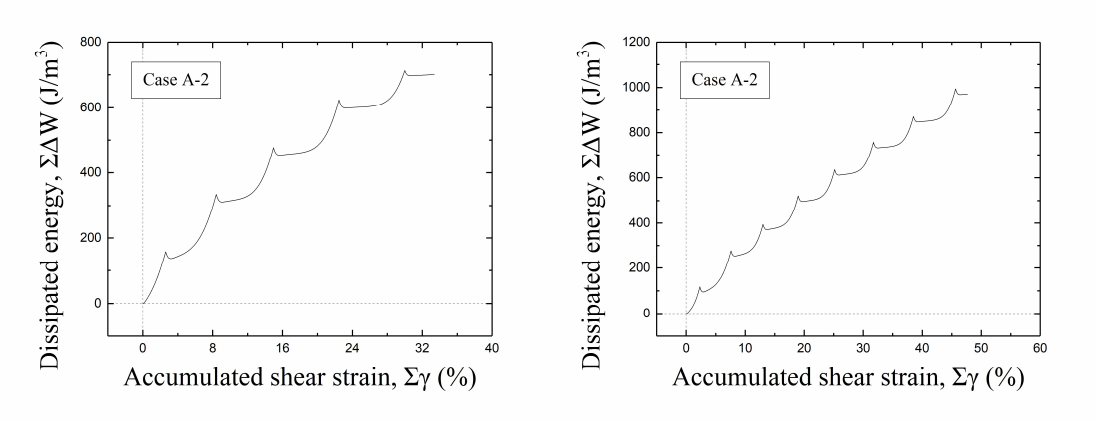

(a) stage 1 (b) Stage 2

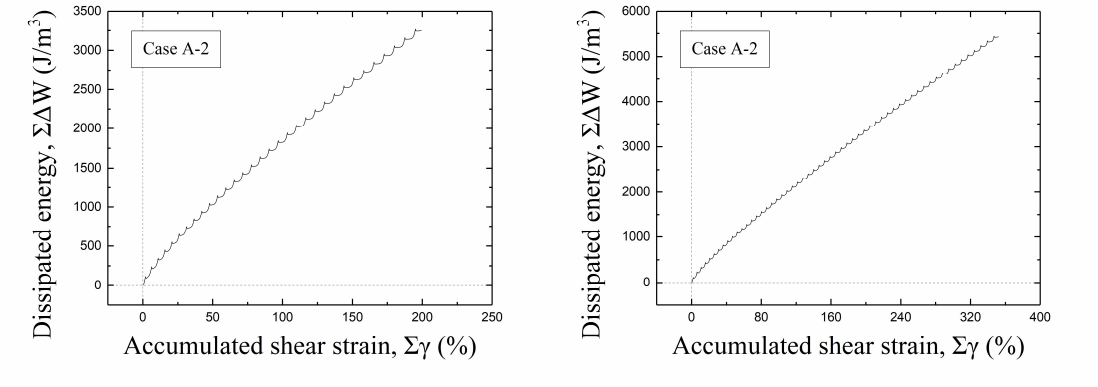

(c) stage 3 (d) Stage 4

Figure 5-8 Dissipated energy during different liquefaction stages in case A-2

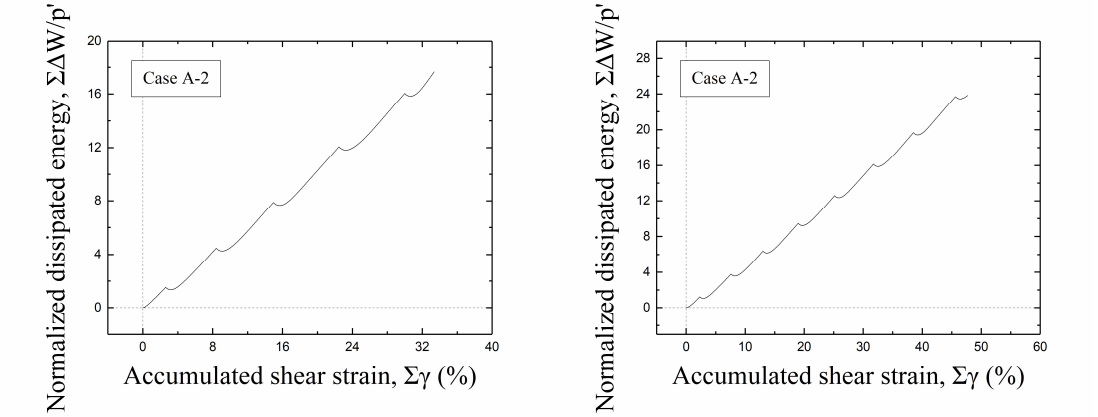

(a) stage 1 (b) Stage 2

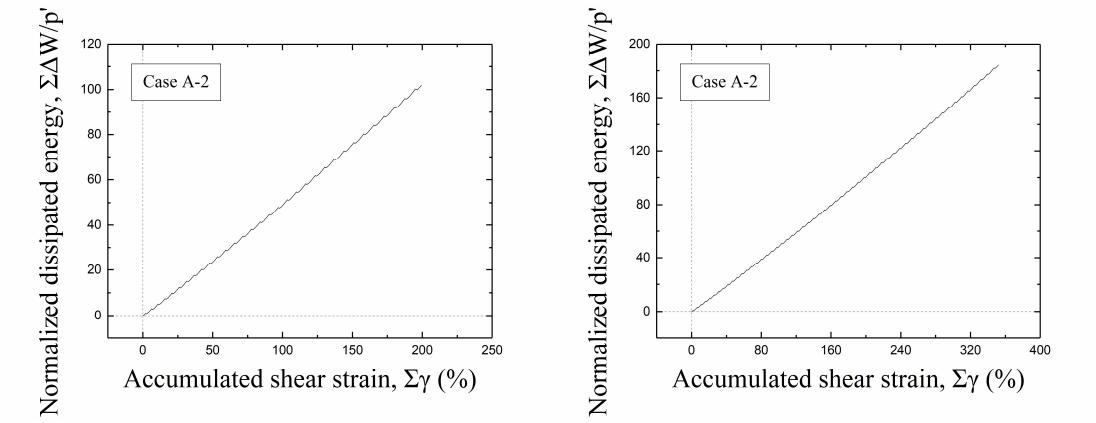

(c) stage 3 (d) Stage 4

Figure 5-9 Normalized dissipated energy during different liquefaction stages in case A-2

In this case, it can be observed that with the increase of liquefaction stages, the liquefaction resistance increased noticeably as introduced in the 4th chapter. However, there is no obvious change in the relationship between dissipated energy or normalized dissipated energy and the accumulated shear strain. Within one stage, a tri-linear relationship between dissipated energy and accumulated shear strain and a bi-linear relationship between the normalized one and accumulated shear strain were reported by Aoyagi (2018) on medium dense sand. However, similar relationship did not appear on the dense sand.

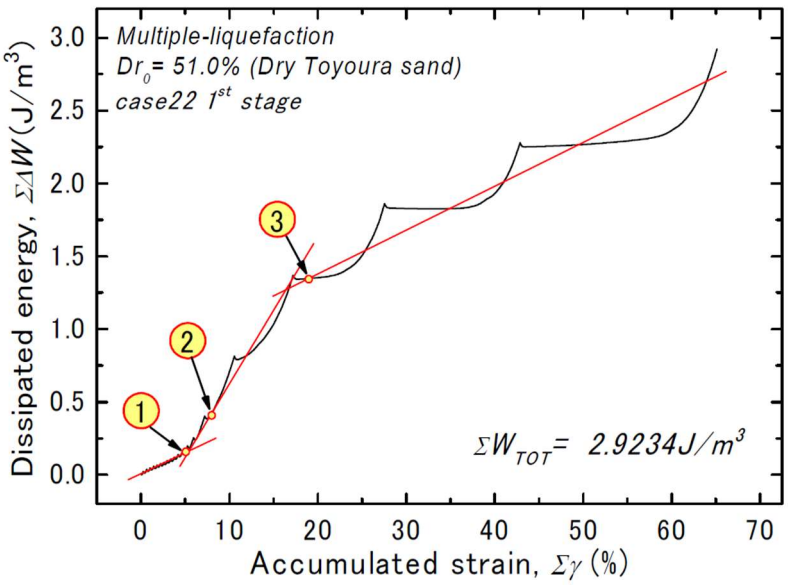

Figure 5-10 Relationship between dissipated energy and accumulated shear strain (Aoyagi, 2018)

Because of the large cyclic stress ratio employed on the dense sand specimen, very high excess pore water pressure generated in the first several cycles with a large shear strain induced. It can be observed that the accumulation speed of shear strain gradually decreased from the first cycle to the last one, and there is no sudden change like observed in the case of medium dense sand. The effective stress path in Figure 5-11 shows that the line of phase transformation was passed in the first cycle of loading due to the large CSR.

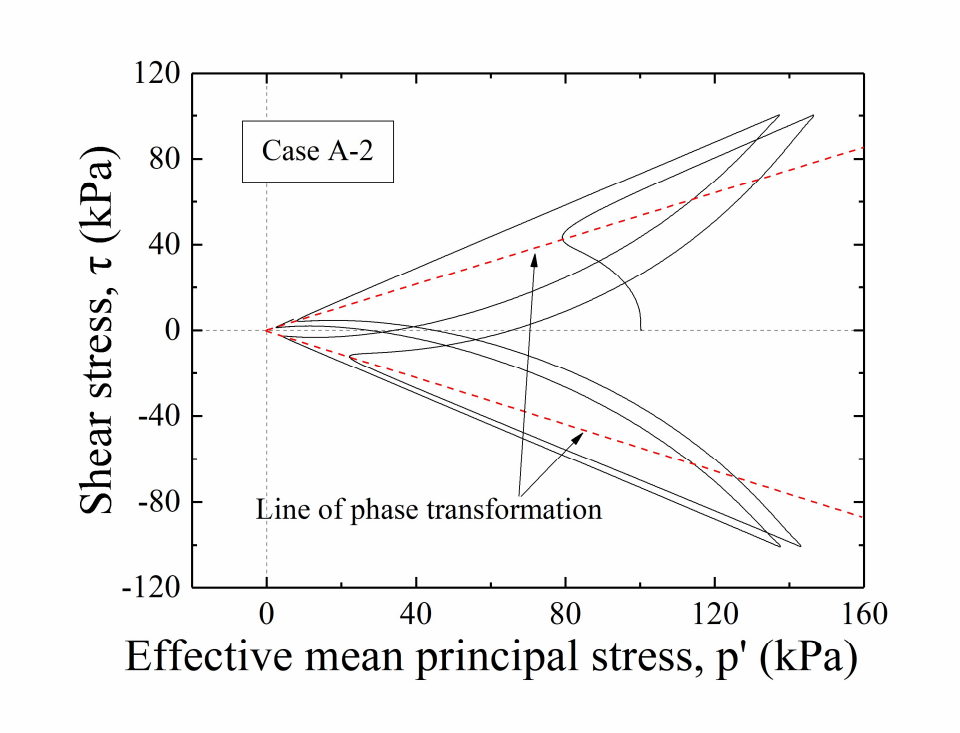

Figure 5-11 The line of phase transformation

As introduced in the 4th chapter, the repeated liquefaction resistance increased not only because of the increase of relative density, but also because of the former liquefaction history. This result indicated the different liquefaction properties between dense sand and loose or medium dense sand. As reported by Ishihara and Okada (1978), "large strain histories" after phase transformation could reduce the liquefaction resistance of the medium dense sand specimen. Aoyagi (2018) also found that the dissipated energy accumulated after the line of phase transformation had a negative impact on its re-liquefaction resistance.

Based on the research results on medium dense sands, the liquefaction history in case A-2 should be considered as a "large strain history" and all energy dissipated during this history was the "negative impact". But the result of increase in liquefaction resistance indicated that new methods are necessary to distinguish the "positive impact" and the "negative impact" on dense sand.

Liquefaction tests with drained pre-shear histories (Test series C)

Since the repeated liquefaction stages in this series of tests were similar as in series A, this part of analysis and discussions is focused on the pre-shear stage.

As an example, the time history of shear strain, effective stress path, stress-strain relationship, dissipated energy, normalized stress-strain relationship and normalized dissipated energy of the pre-shear stage in case C-2 are shown in Figure 5-12 from (a) to (f), respectively. It can be noticed that due to the drained condition, excess pore water pressure was not accumulated a lot. Therefore, both dissipated energy and normalized dissipated energy accumulated almost linearly due to the constant shear strain and nearly constant shear stress and effective stress.

As reported in the 4th chapter, with the increase of pre-shear strain amplitude and number of pre-shear cycles, the liquefaction resistance increased. Obviously with the increase in these parameters, the accumulated energy and normalized energy increased as well. The relationship between the liquefaction resistance and total dissipated energy or normalized dissipated energy from cases C-1 to C-4 are plotted in Figures 5-13 and 5-14. With more energy dissipated during the pre-shear, the liquefaction resistance tended to be larger in the later liquefaction stage.

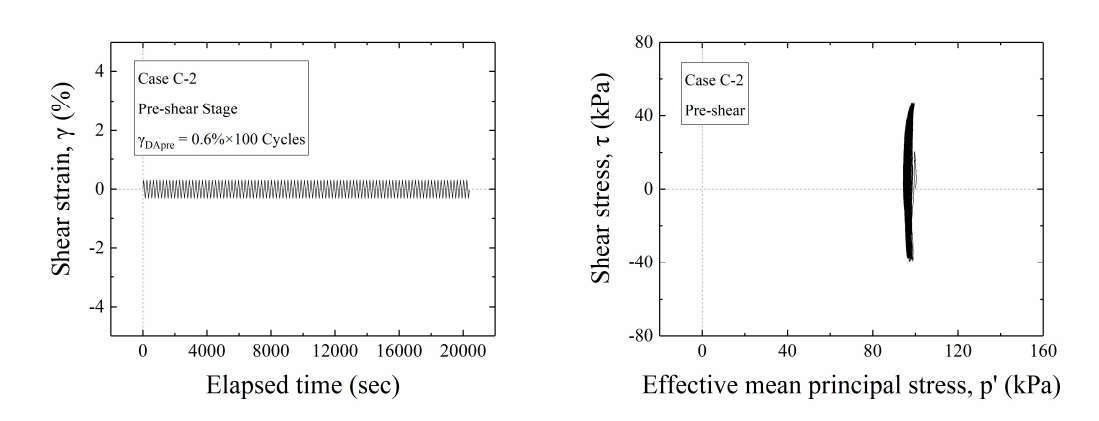

(a) Time history of shear strain (b) Effective stress path

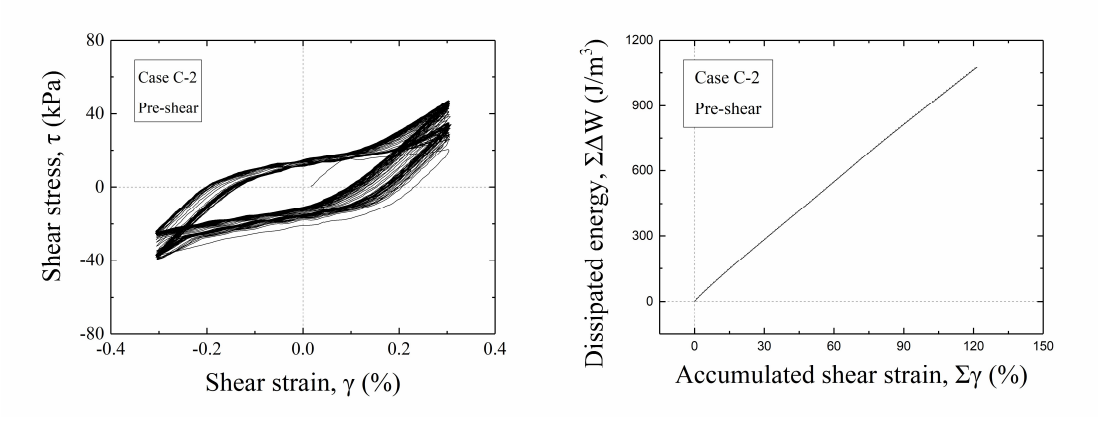

(c) Stress-strain relationship (d) Dissipated energy

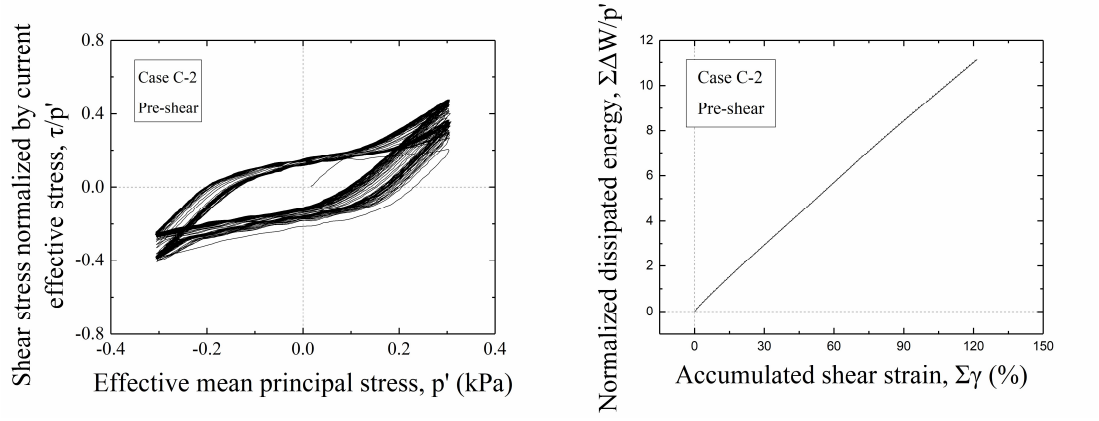

(e) Normalized stress-strain relationship (f) Normalized dissipated energy

Figure 5-12 Relationships during the pre-shear stage of case C-2

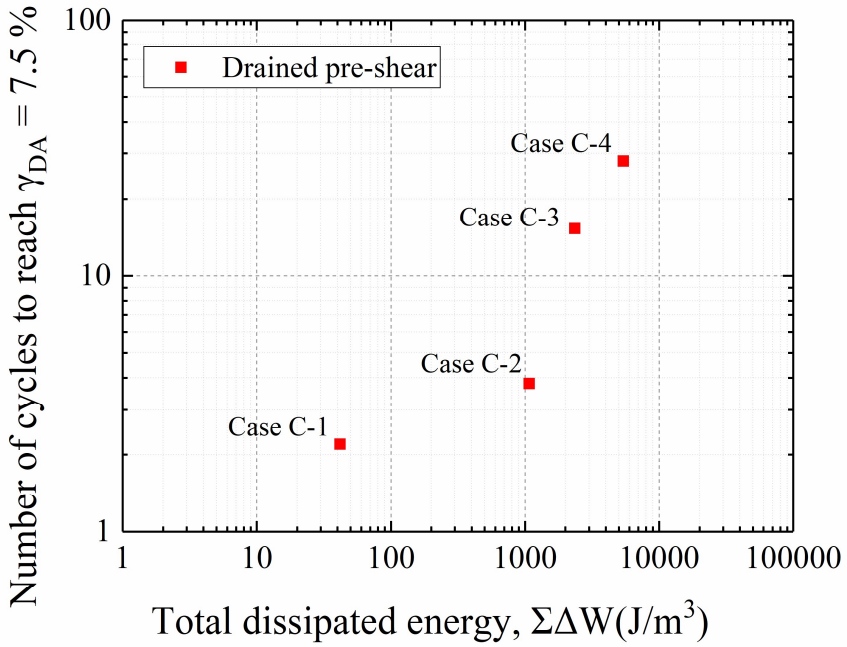

Figure 5-13 Relationship between dissipated energy during drained pre-shear and liquefaction resistance after pre-shear

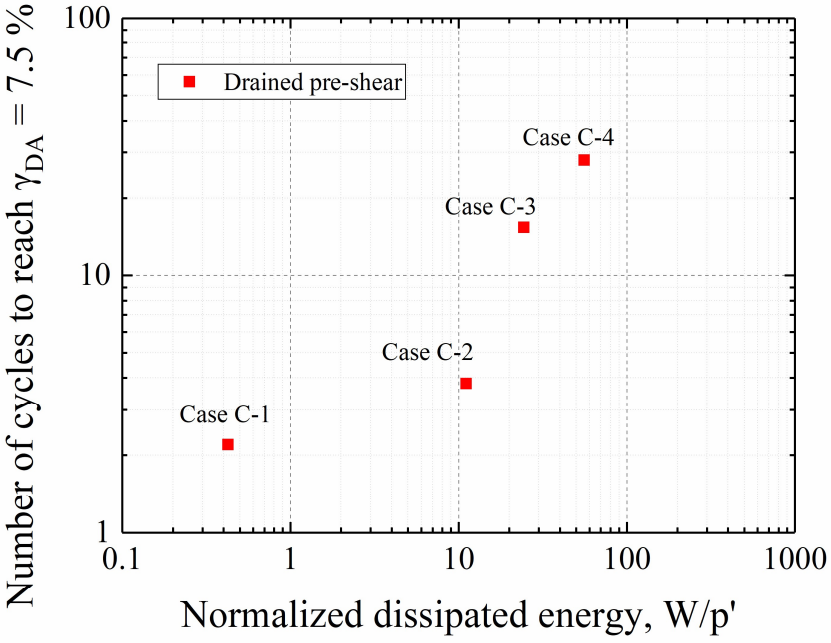

Figure 5-14 Relationship between normalized dissipated energy during drained pre-shear and liquefaction resistance after pre-shear

Liquefaction tests with undrained pre-shear histories (Test series D)

As concluded in the 4th chapter, the pre-shear effects in different undrained pre-shear stages can be accumulated. Therefore, analysis and discussions in this part will be based on this conclusion.

As examples, the data and analysis results of the 3rd, 10th and 18th pre-shear stages in case D-3 are shown in Figures 5-15 to 5-17. With the increase of cyclic stress ratio, shear strain became larger and more energy was dissipated.

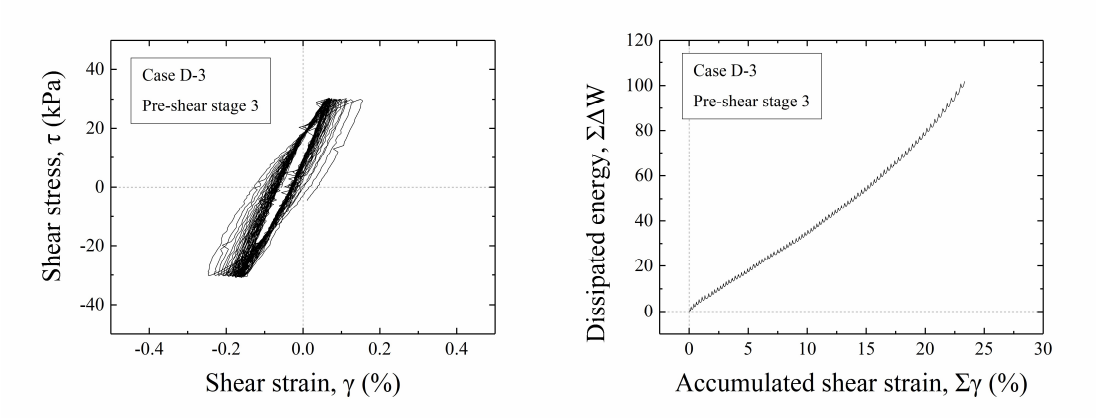

(a) Stress-strain relationship (b) Dissipated energy

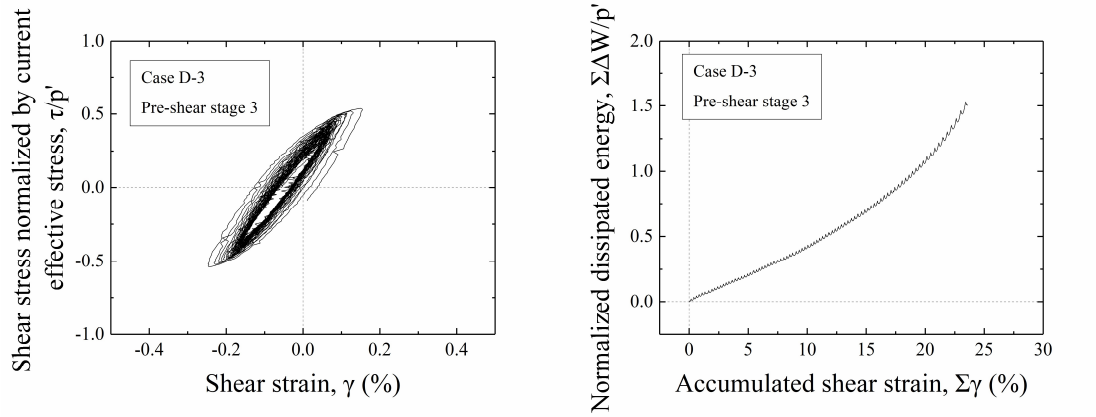

(c) Normalized stress-strain relationship (d) Normalized dissipated energy

Figure 5-15 Relationships during the pre-shear stage of case D-3 (3rd stage)

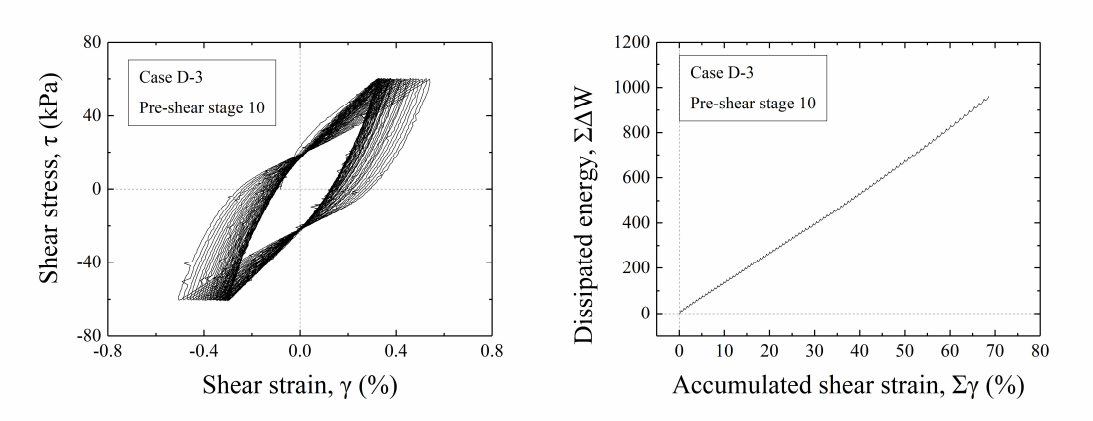

(a) Stress-strain relationship (b) Dissipated energy

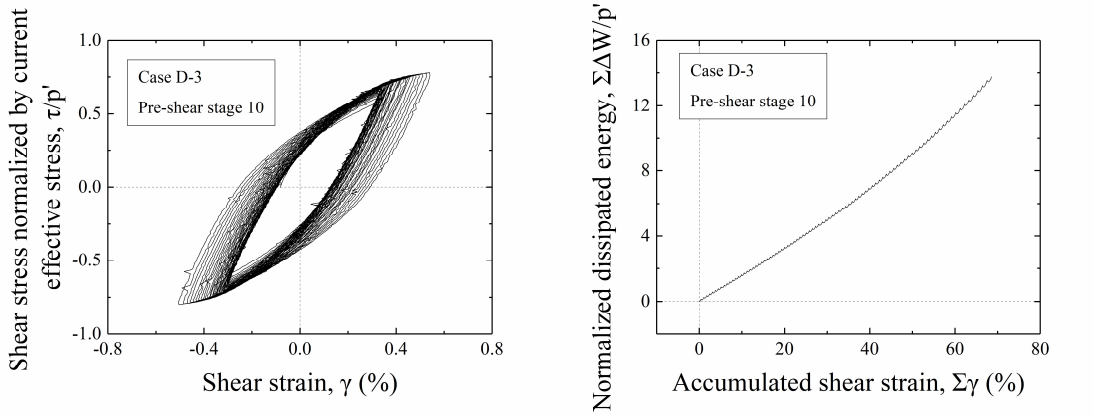

(c) Normalized stress-strain relationship (d) Normalized dissipated energy

Figure 5-16 Relationships during the pre-shear stage of case D-3 (10^{th} stage)

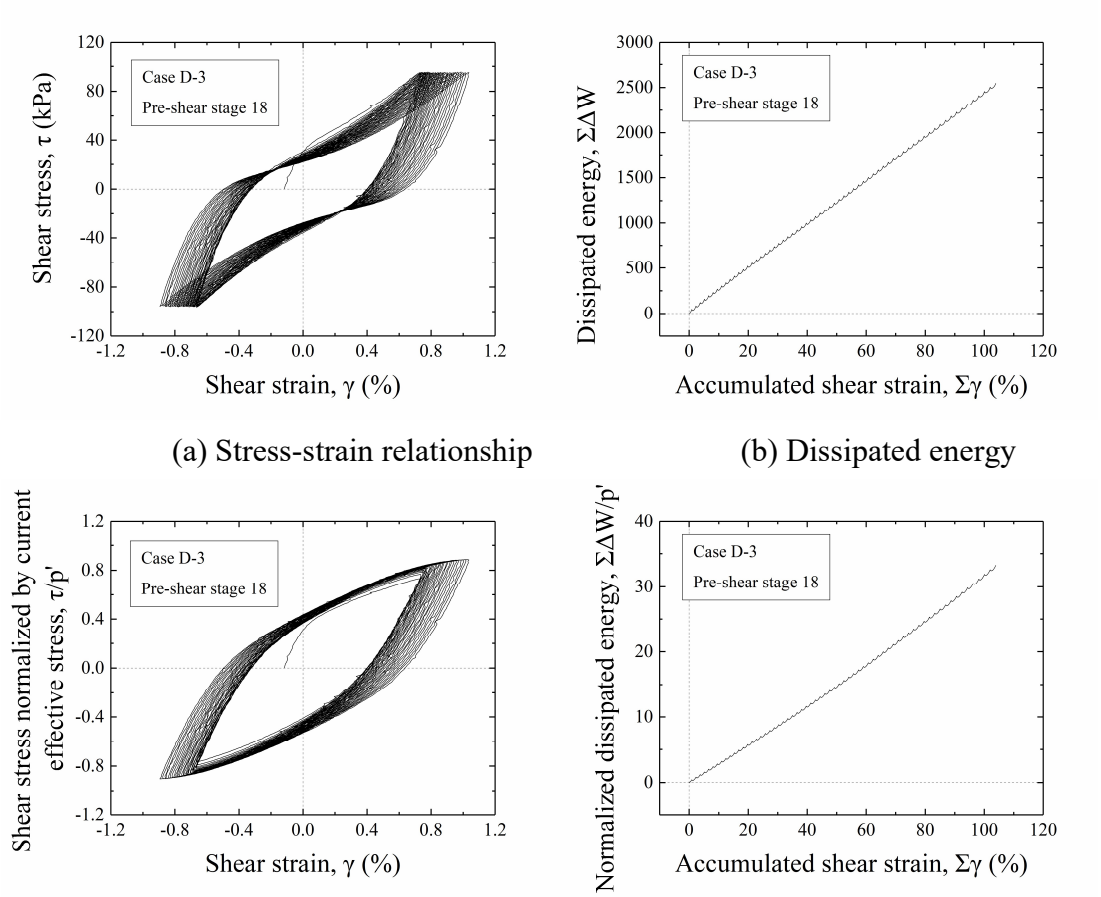

(a) Stress-strain relationship (b) Dissipated energy

(c) Normalized stress-strain relationship (d) Normalized dissipated energy

Figure 5-17 Relationships during the pre-shear stage of case D-3 (18^h stage)

In order to investigate the effect of total dissipated energy during all pre-shear stages, the dissipated energy and normalized dissipated energy during all pre-shear stages in cases D-1 (1 stage), D-2 (10 stages) and D-3 (18 stages) were summed up, respectively. The results are shown in Figures 5-18 and 5-19. It can be observed that the liquefaction resistance was related with the dissipated energy as well as the normalized one as plotted in full-logarithmic axis. But the data points were not enough to conclude the possible existence of the linear relationship.

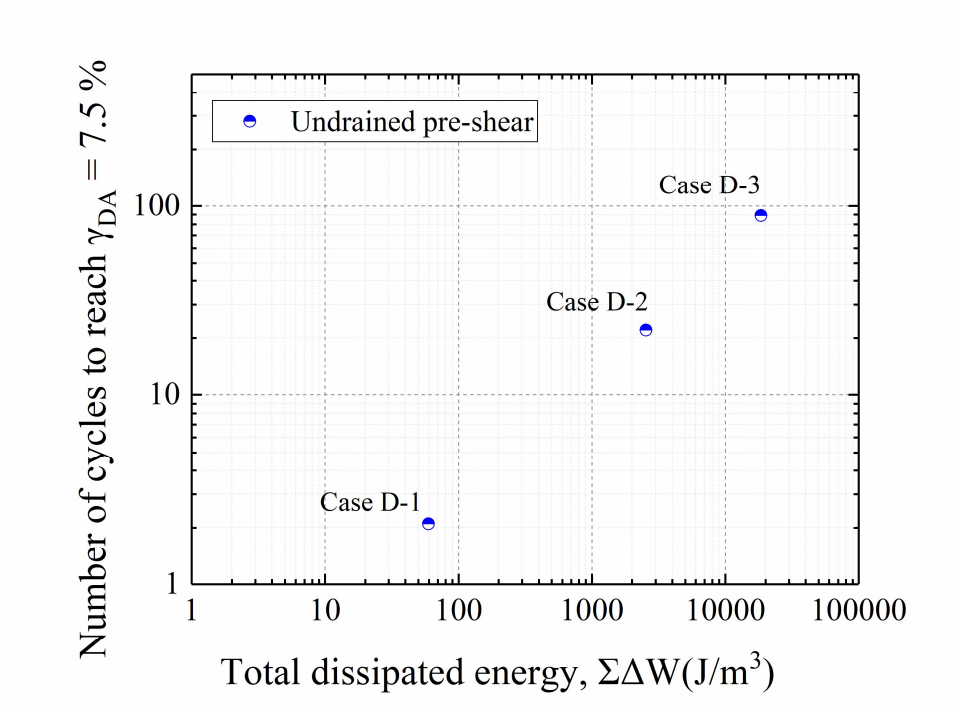

Figure 5-18 Relationship between dissipated energy during undrained pre-shear and liquefaction resistance after pre-shear

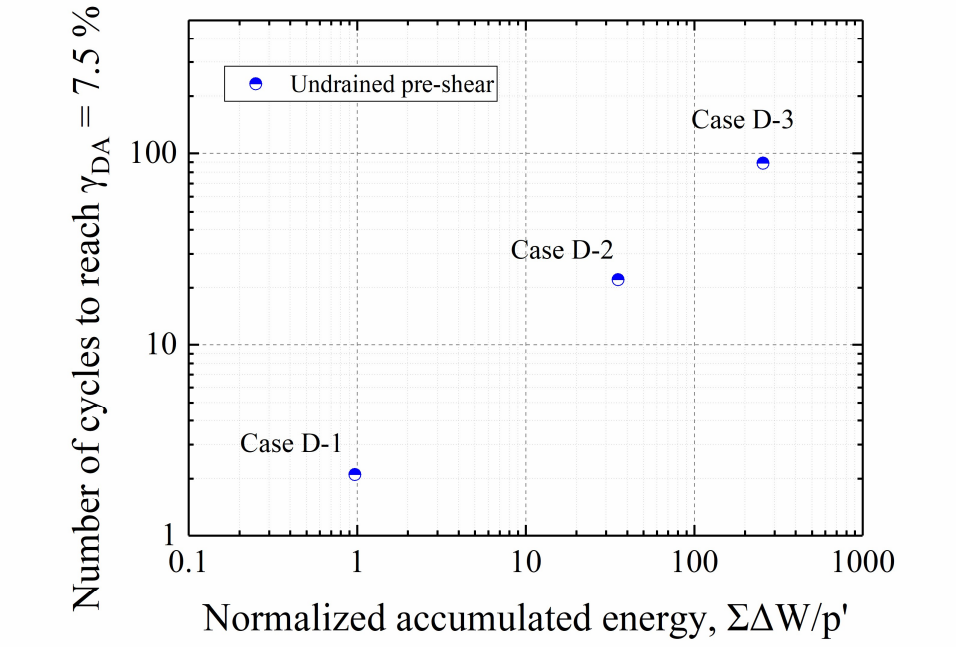

Figure 5-19 Relationship between normalized dissipated energy during undrained pre-shear and liquefaction resistance after pre-shear

Comparisons and discussions

As introduced in the 4th chapter, cases C-5 and D-5 were carried out with the same pre-shear program in different drainage conditions, but their liquefaction resistance did not show much difference. However, from the energy point of view, it is considered that the dissipated energy and normalized dissipated energy accumulated during their pre-shear stages should be very different since the stress paths were different. Figures 5-20 and 5-12 show the accumulated dissipated energy and normalized dissipated energy in all pre-shear stages of cases C-5 and D-5.

The results of calculation show that the dissipated energy did not differ a lot but the normalized dissipated energy in the undrained case (D-5) was much larger than in the drained case. This is because that due to the drained condition, the effective stress kept in a high level during the pre-shear of case C-5. However, neither dissipated energy nor the normalized one shows any similar relationship with the liquefaction resistance as shown in other cases mentioned above. The dissipated energy and normalized dissipated energy were large in case D-5 but its liquefaction resistance was lower than in case C-5.

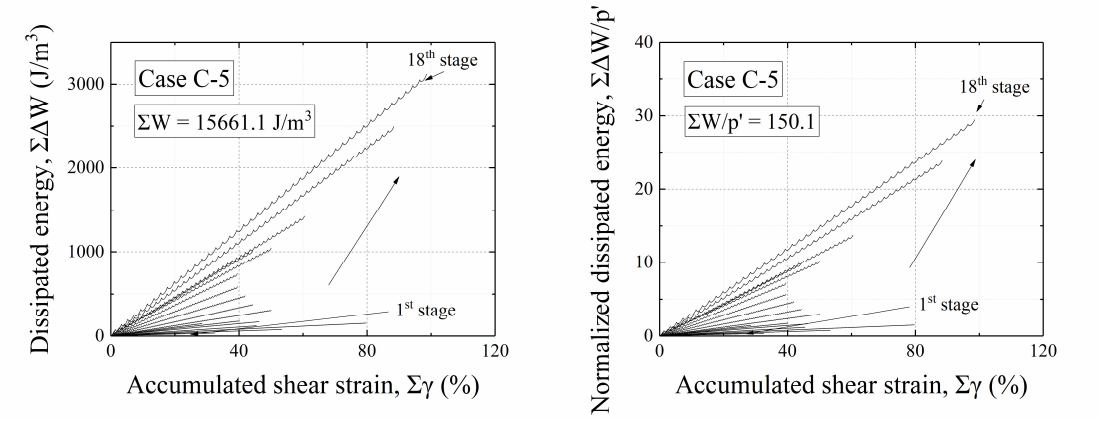

(a) Dissipated energy *(b) Normalized dissipated energy*

Figure 5-20 Dissipated energy and normalized dissipated energy during the pre-shear stages of case C-5

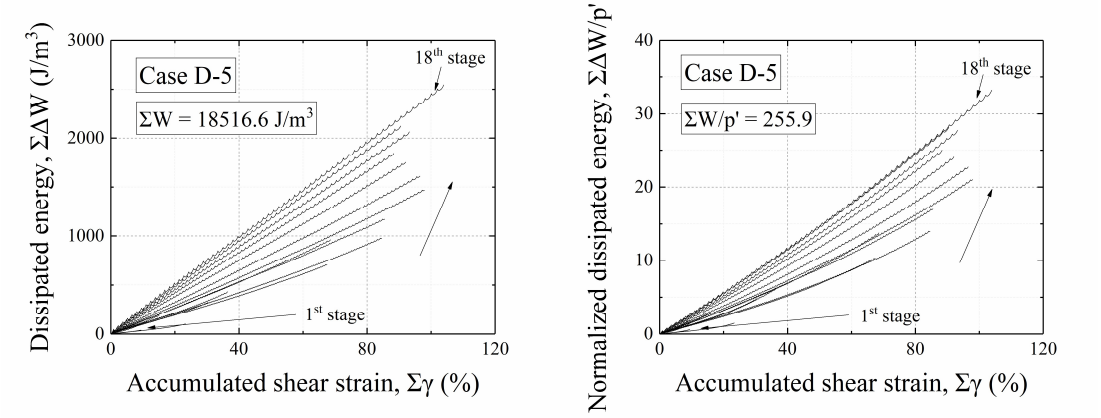

(a) Dissipated energy (b) Normalized dissipated energy

Figure 5-21 Dissipated energy and normalized dissipated energy during the pre-shear stages of case D-5

For further investigation, the results of all drained pre-shear and undrained pre-shear cases with the same liquefaction test CSR of 1 are plotted together in Figures 5-22 and 5-23. In addition, the results of the repeated liquefaction stages are also plotted considering their former liquefaction stage as a full liquefaction history.

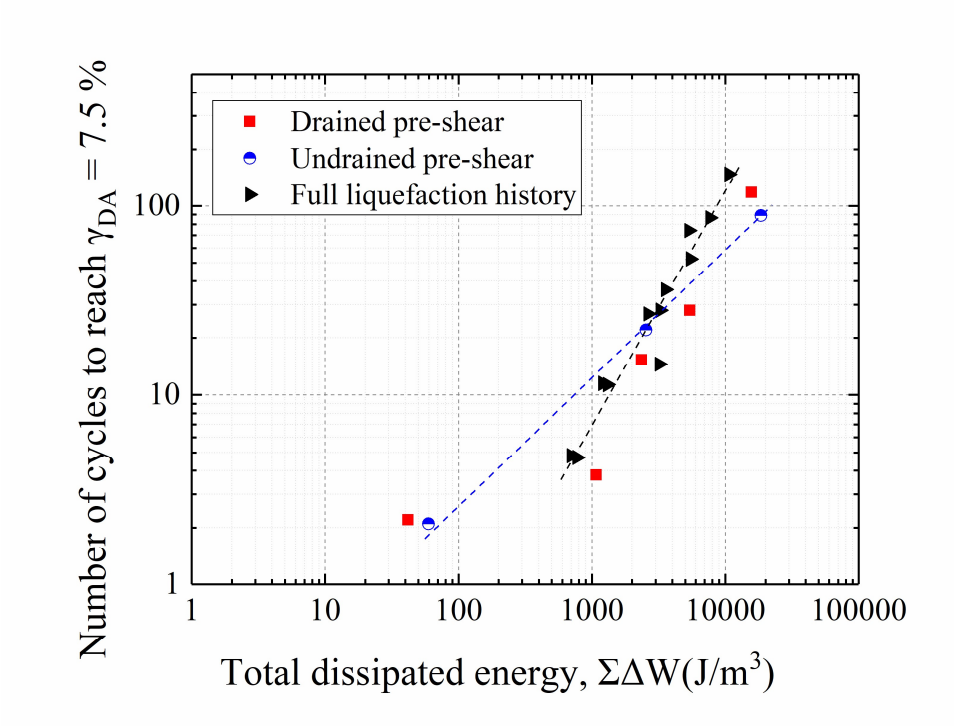

Figure 5-22 Relationship between dissipated energy during pre-shear and liquefaction resistance after pre-shear

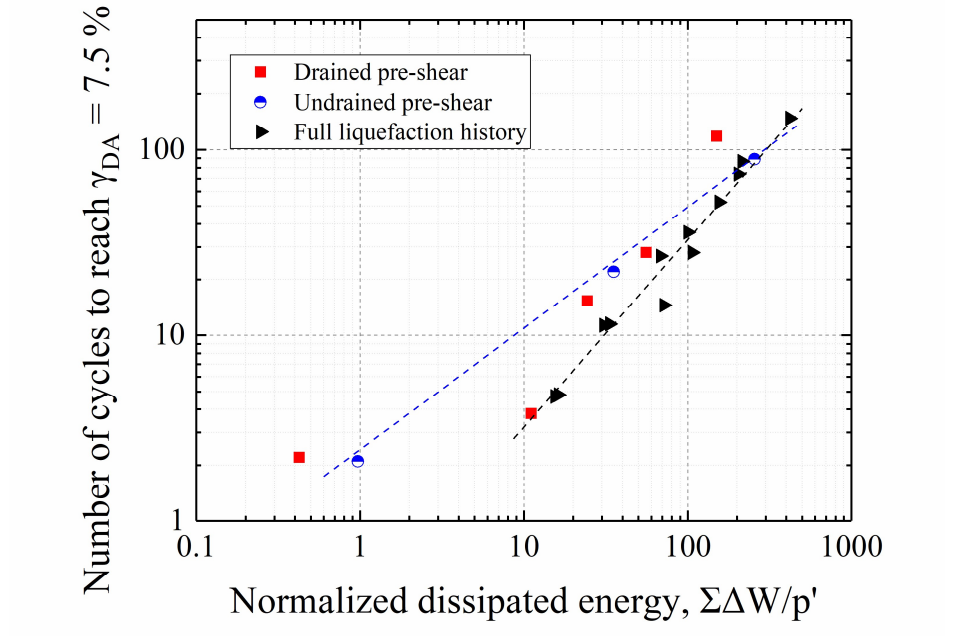

Figure 5-23 Relationship between normalized dissipated energy during undrained pre-shear and liquefaction resistance after pre-shear

It can be observed that the energy dissipated during full liquefaction histories was also related with the liquefaction resistance. However, the relationship is not consistent with those in series C or D. On one hand, this difference might be due to the different relative densities in different repeated liquefaction stages. During the repeated liquefaction stages, the liquefaction resistance was not only influenced by the liquefaction history but also the increase of relative density. On the other hand, the "positive impact" and "negative impact" are also considered to be one possible reason that resulted in the difference.

5.3.3 Proposal of a new method to distinguish the "positive impact" and "negative impact"

As mentioned above, pre-shear under different drainage condition had very different normalized dissipated energy but similar effects on the liquefaction resistance. Besides, the full liquefaction histories and other pre-shear histories also showed different relationships between dissipated energy and the effects on liquefaction resistance. These differences might be due to the "positive impact" and "negative impact" among the dissipated energy or normalized dissipated energy.

However, in dense sand cases, phase transformation occurred quite early due to the high cyclic stress ratio and there is no sudden change in the accumulation speed of shear strain. It indicates that the method for distinguishing different impacts that proposed by Aoyagi (2018) is not suitable for the dense sand cases since the pre-shear after phase transformation still increased the liquefaction resistance. Therefore, in this part, a new method to distinguish different impacts will be proposed and discussed.

In pioneer studies, the line of phase transformation was used as a border to distinguish different impacts of dissipated energy due to different behaviors of sand before and after the line of phase transformation. However, it can be observed from the effective

stress path that after the phase transformation, the sand still behaves differently at different sides of the line in every loading cycle. Therefore, different impacts of dissipated energy are considered to exist in these different behaviors during every cycle of loading.

In one cycle of loading, the sand shows negative dilatancy before reaching the line of phase transformation and dissipated energy in this part is considered as the "positive impact". After the shear stress becomes large enough (beyond the line of phase transformation), the sand starts to show positive dilatancy and the dissipated energy is considered as the "negative impact". As shown in Figure 5-24, two horizontal lines are drawn through the phase transformation points on the effective stress path. With these two lines, the relationship of shear stress and shear strain is divided into three parts. In this figure, dissipated energy calculated in the top and bottom parts is considered as the "negative impact" while the rest in middle is the "positive impact".

As for the calculation of normalized dissipated energy, the two boundary lines are decided by the normalized shear stress at the points where stress path crosses the line of phase transformation (shown in Figure 5-25).

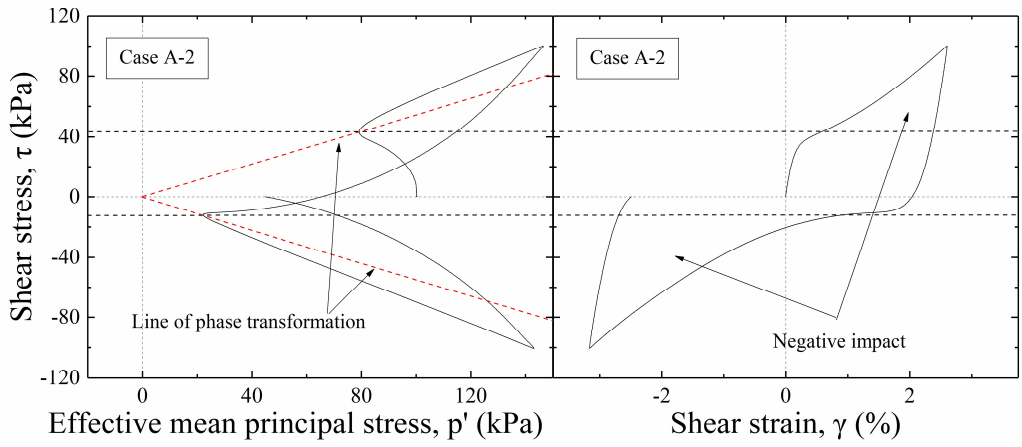

Figure 5-24 Definition of the "positive" and "negative impact" in dissipated energy

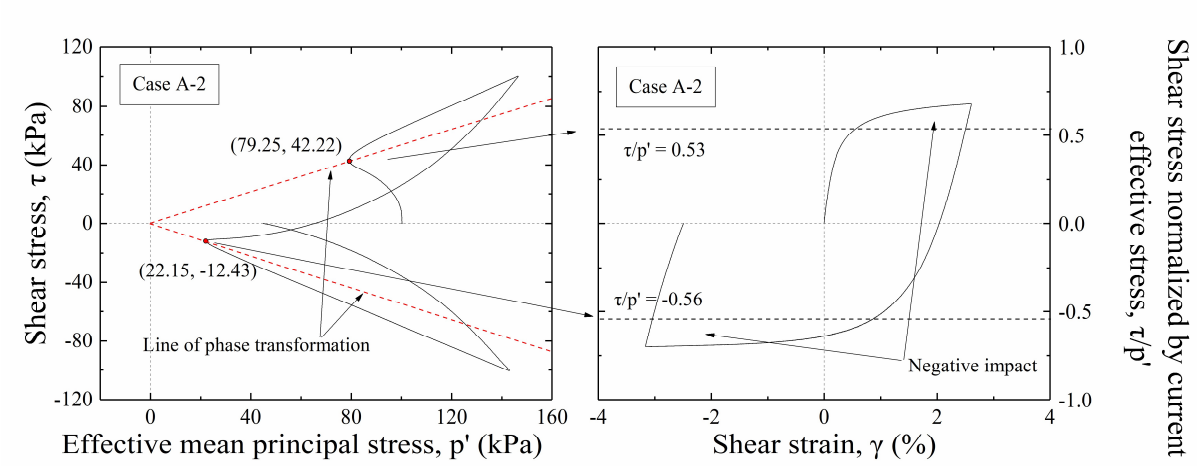

Figure 5-25 Definition of the "positive" and "negative impact" in normalized dissipated energy

By applying the new method, the "negative dissipated energy" and "positive dissipated energy" are calculated and plotted in Figure 5-26 with the vertical axis showing the liquefaction resistance after shear history. Similarly, the "negative impact" and "positive impact" in the normalized dissipated energy are calculated and plotted in Figure 5-27. In addition, During the calculation, the dissipated energy and normalized dissipated energy in the drained pre-shear are all considered as "positive", since phase transformation never occurred during these pre-shear loadings.

As shown in the sections that are picked up and plotted in Figures 5-28 and 5-29, it can be observed that the relationship between the "positive impact" of normalized dissipated energy and liquefaction resistance in Figure 5-29 is much consistent to each other than that with the dissipated energy in Figure 5-28. In addition, even though the "negative impact" has a similar scale as the "positive" one, its effect is quite negligible.

Overall, with the new method distinguishing the "positive impact" and "negative impact", it is found that the liquefaction resistance is relating to the "positive impact" of the normalized dissipated energy while the "negative" one does not affect much on the test results on dense sands.

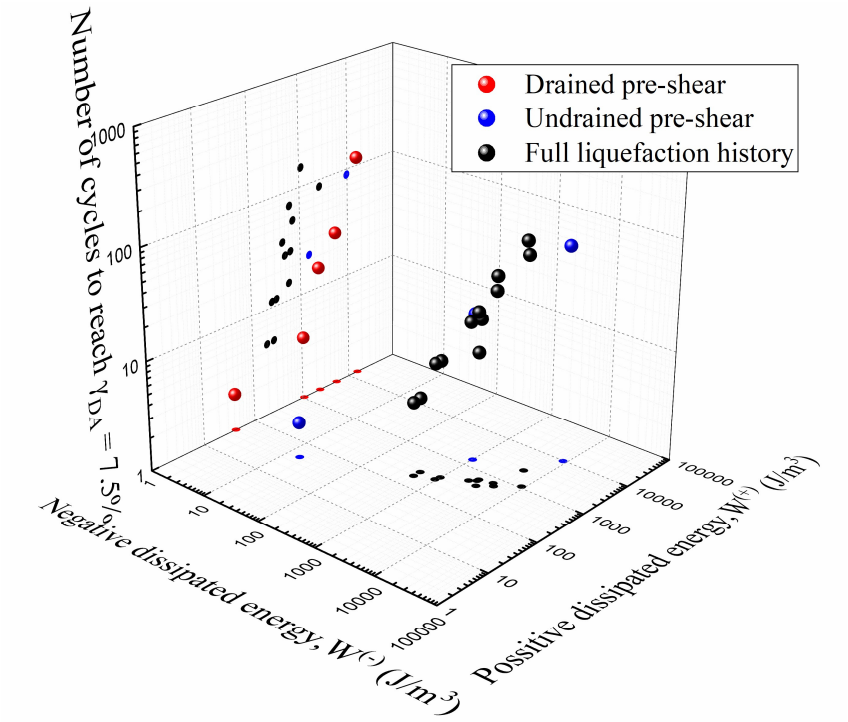

Figure 5-26 Relationship between "negative dissipated energy", "positive dissipated energy" and the liquefaction resistance

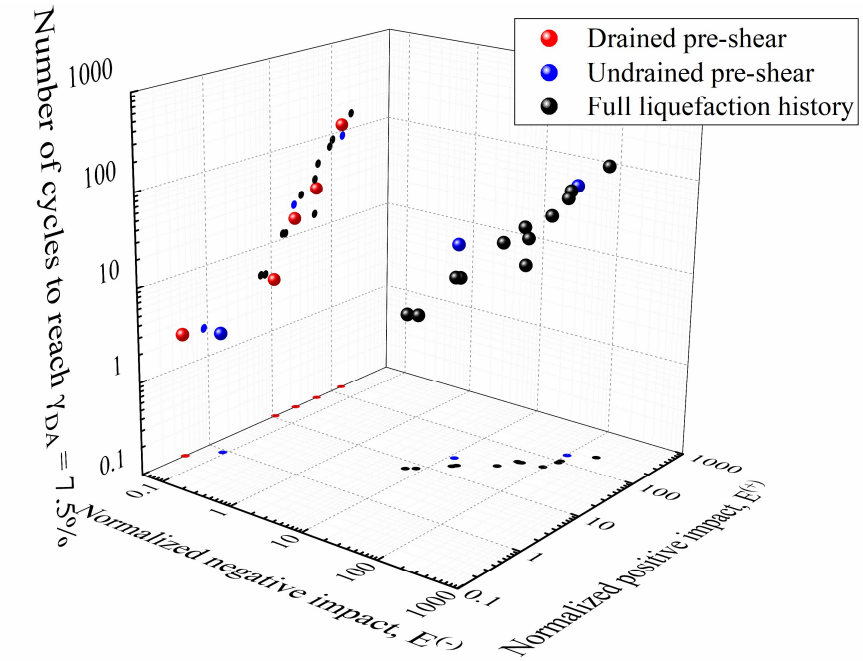

Figure 5-27 Relationship between "negative impact", "positive impact" and the liquefaction resistance

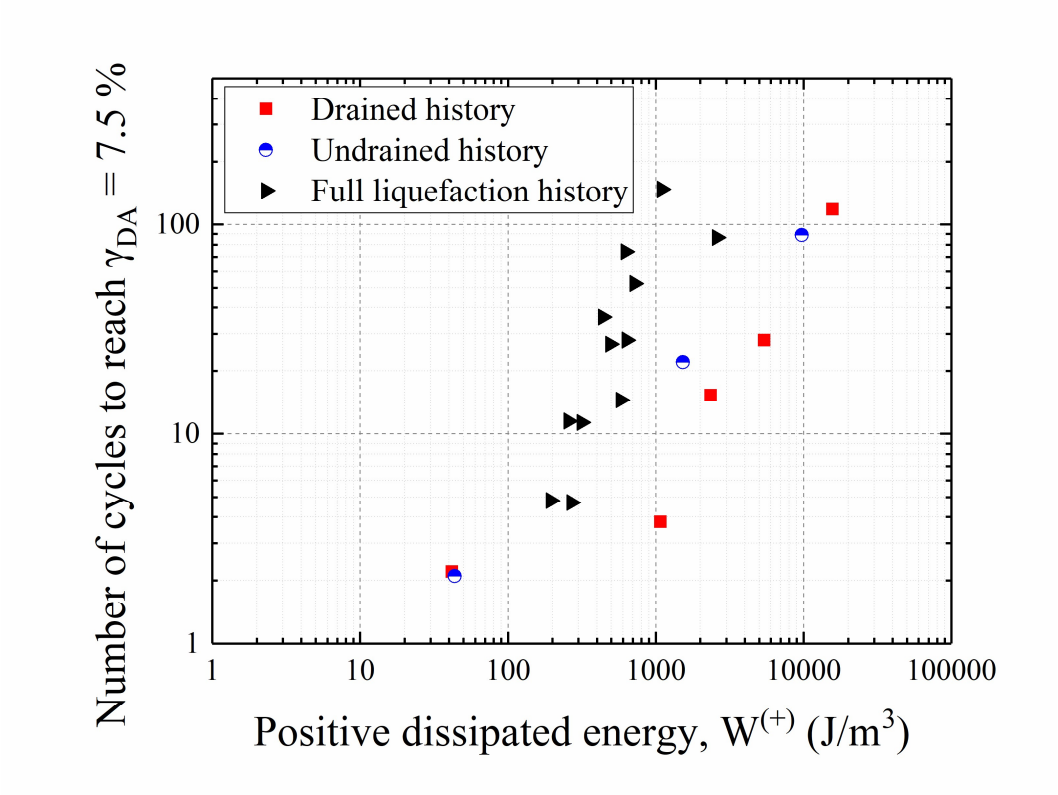

Figure 5-28 Relationship between "positive dissipated energy" and liquefaction resistance

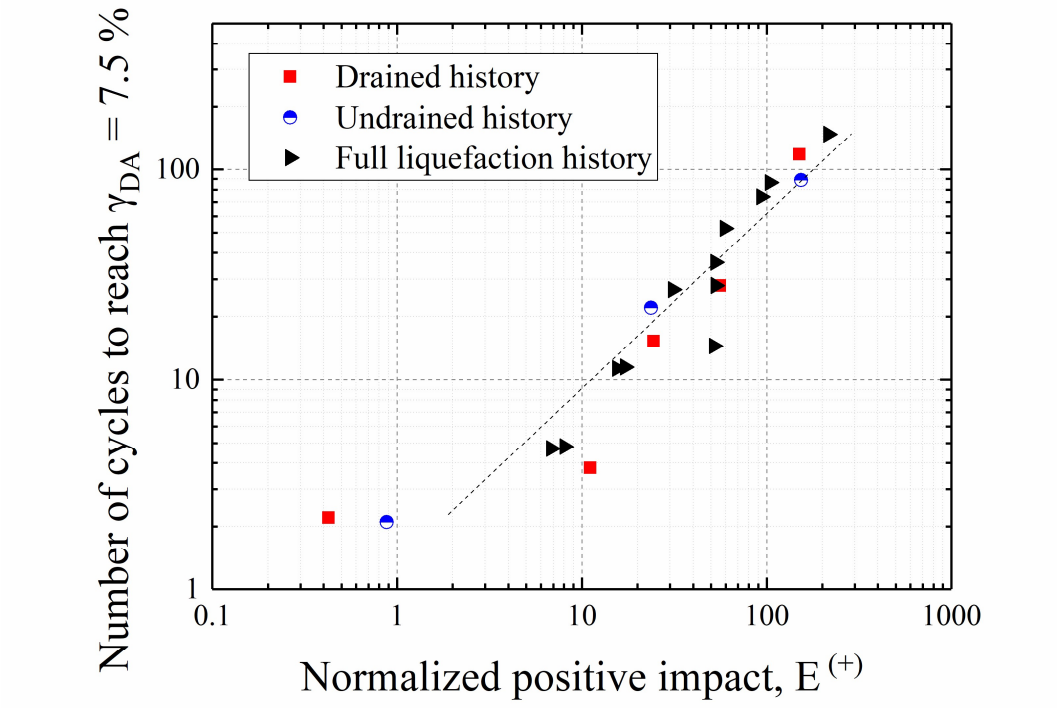

Figure 5-29 Relationship between "positive impact" and liquefaction resistance

5.3.4 Verification of the applicability of the new method on medium dense sand

The new method to distinguish the "positive impact" and "negative impact" is introduced and discussed based on the analysis results on the liquefaction tests on dense sand. However, it is also important to verify the applicability of the new method on medium dense sand. Therefore, in this part, by re-analyzing the repeated liquefaction tests carried out on medium dense sand using the small-scale torsional shear apparatus by Aoyagi (2018), the applicability of the new method will be discussed.

The details of repeated liquefaction tests carried out on medium dense Toyoura sand specimens are shown in Table 5-1.

Table 5-1 Details of repeated liquefaction tests on medium dense sand

Case ID	Initial relative density D_{ri} (%)	Maximum double amplitude of shear strain, γ_{DAmax} (%)	Initial effective stress, p_i' (kPa)	Cyclic stress ratio in liquefaction stages, τ_{cyc}/σ_0'
TS-36	60.4	2.0	100	0.25
TS-34	60.0	5.0	100	0.25
TS-26	47.2	2.0	100	0.25
TS-38	50.3	2.0	50	0.25
TS-34	60.0	5.0	100	0.25
TS-30	50.3	5.0	100	0.25

As shown in Table 5-1, these repeated liquefaction tests were carried out with different maximum double amplitude of shear strain, while keeping the same cyclic shear stress ratio. Therefore during the analysis and discussion in this part, the liquefaction resistance will be represented by the number of cycles to reach 2.0% double amplitude

of shear strain. The different shear strain amplitudes will be considered as different pre-shear histories. The energy analysis results are shown in Figures 5-30 to 5-33.

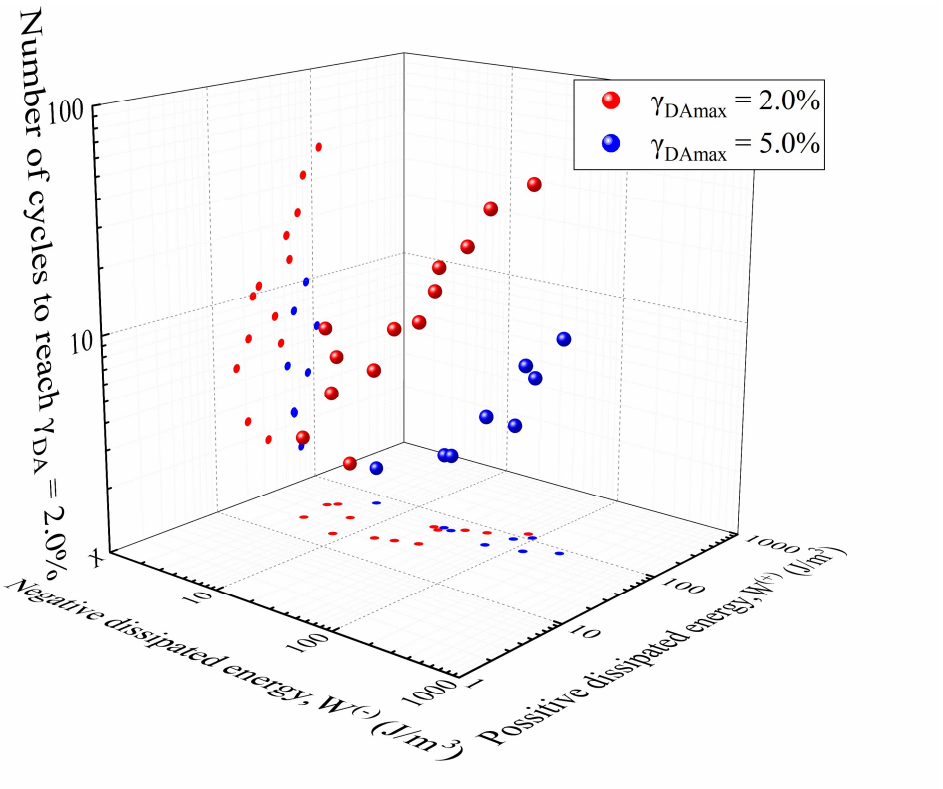

Figure 5-30 Relationship between "negative dissipated energy", "positive dissipated energy" and the liquefaction resistance

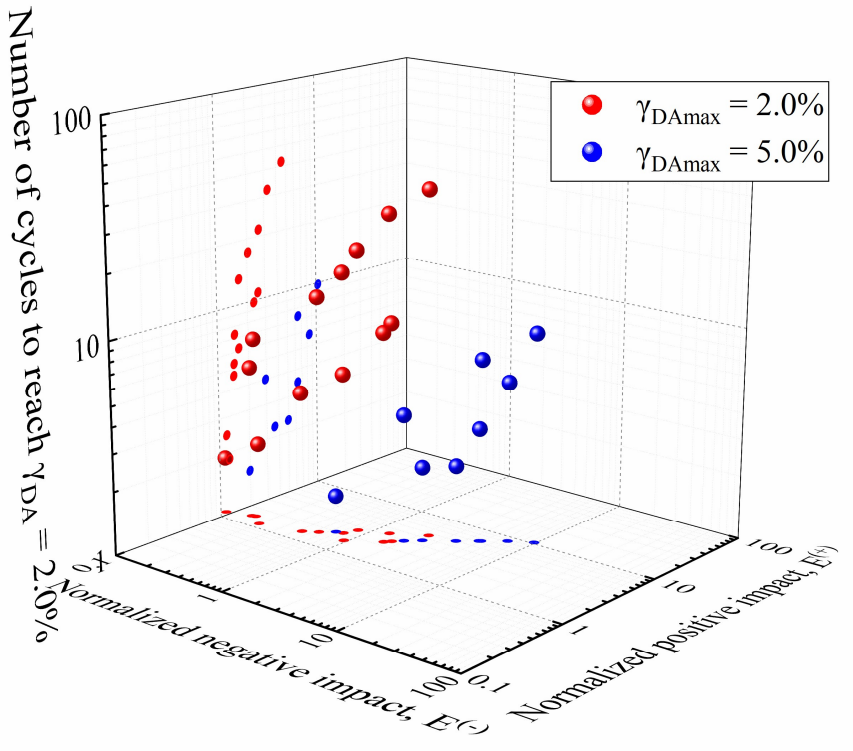

Figure 5-31 Relationship between "negative impact", "positive impact" and the liquefaction resistance

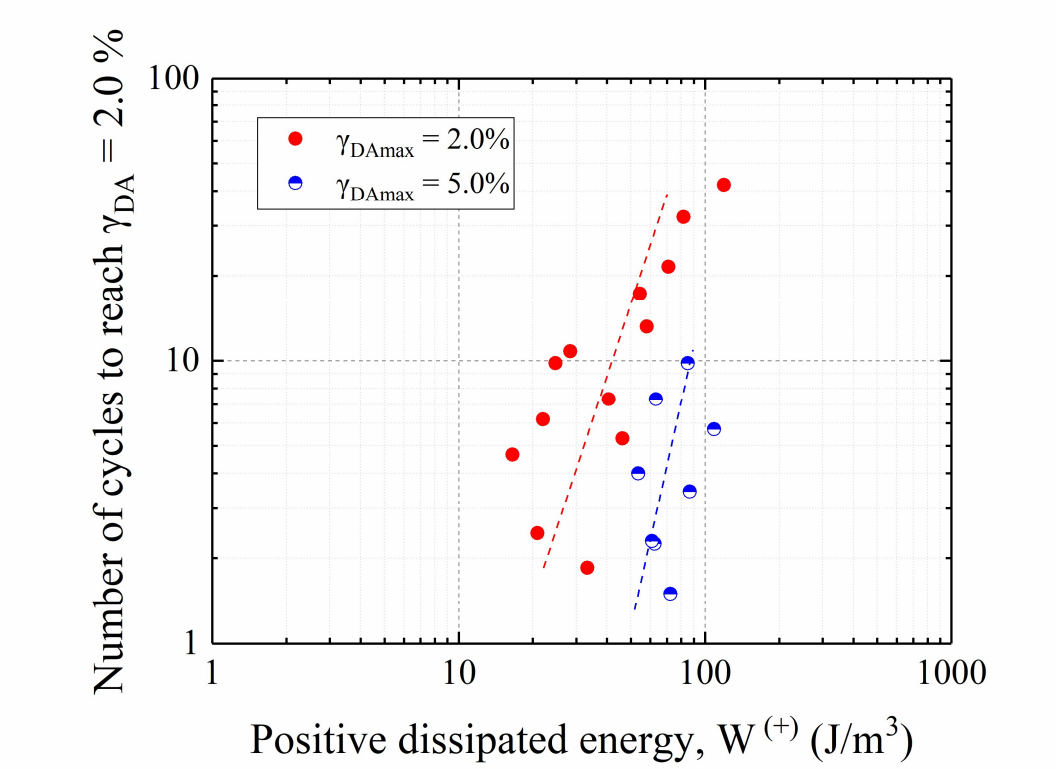

Figure 5-32 Relationship between "positive dissipated energy" and liquefaction resistance

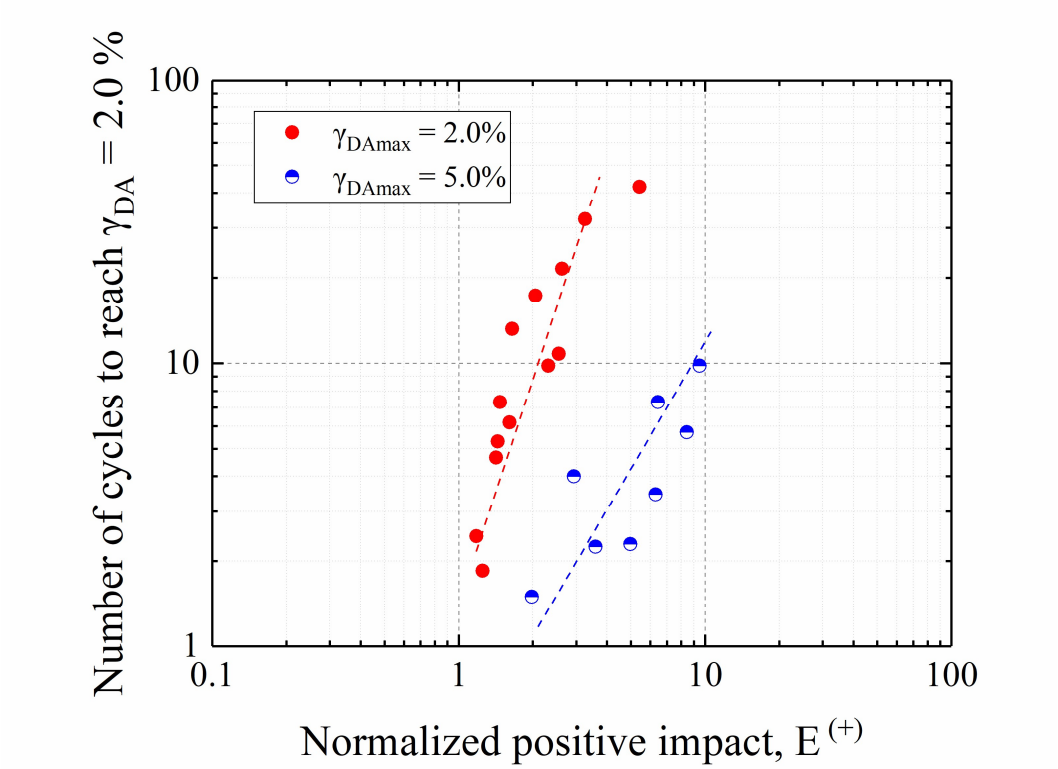

Figure 5-33 Relationship between "Normalized positive impact" and liquefaction resistance

Similar as the results of dense sand, the normalized positive impact shows better correlation with the liquefaction resistance than the non-normalized energy. However, it can be noticed from Figure 5-33 that cases with different shear strain amplitudes did not show consistent relationship between the "positive impact" and the liquefaction resistance, due possibly to the effects of negative impact that was found to be negligible in the cases of dense sands.

As shown in Figures 5-34 and 5-35 (2D version of Figures 5-30 and 5-31), the liquefaction resistance in the next liquefaction stage was not simply related with the "positive dissipated energy" or the "positive normalized impact". In order to consider the influence of the "negative impact", a new parameter "net impact" is defined as the linear combination of the "positive impact" and "negative impact":

$$W_{net.} = W^{(+)} + n \times W^{(-)} \qquad (5\text{-}6)$$

$$E_{net.} = E^{(+)} + n \times E^{(-)} \qquad (5\text{-}7)$$

where:

$W_{net.}$: "net impact" of dissipated energy (noted as net dissipated energy).

$W^{(+)}$: "positive impact" of dissipated energy.

$W^{(-)}$: "negative impact" of dissipated energy.

$E_{net.}$: "net impact" of normalized dissipated energy (noted as normalized net impact).

$E^{(+)}$: "positive impact" of normalized dissipated energy.

$E^{(-)}$: "negative impact" of normalized dissipated energy.

n: constant used to determine the influence of "negative impact".

As shown in the analysis results of dense sand cases, the effect of "negative impact" was so negligible that the constant "n" could be considered as "0". As for the medium dense sand cases, the constant "n" is considered to be a positive value. As trials, 0.3, 0.6 and 0.9 are assigned to "n" and the relationships between the "net impact" (without

and with normalization) and the liquefaction resistance (number of cycles to reach 2% double amplitude of shear strain) are shown in Figures 5-36 to 5-38.

It can be observed that with consideration of the negative impact, the relationships between the "normalized net impact" and the liquefaction resistance becomes more consistent in cases with different histories. However, the non-normalized ones become even worse.

Another possible reason that resulted in the inconsistency might be the different consolidation condition applied in Aoyagi's liquefaction tests. In this series of repeated liquefaction tests, anisotropic consolidation with K_0 = 0.5 was employed. The consolidation progress might also induce some influence on the liquefaction resistance of sand, but it was difficult to be expressed by the energy or normalized energy.

On the other hand, as reported by Tatsuoka (1982), sand with over 80% relative density behaves quite differently compared with loose sand or medium dense sand. Therefore, other special modifications may be necessary while applying the new method on loose sand in further study.

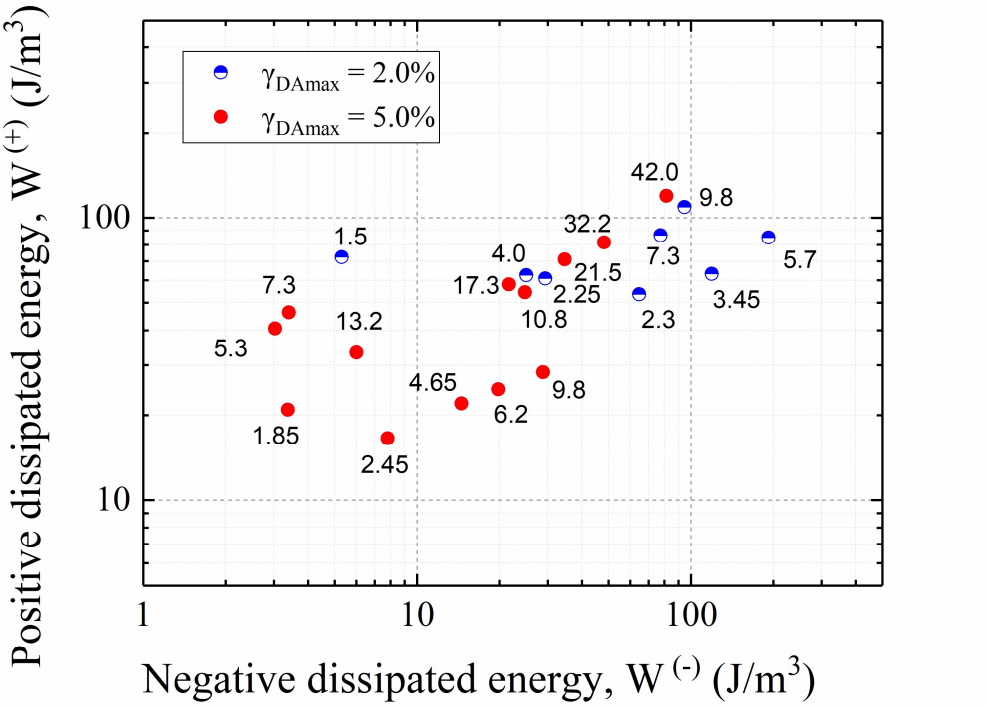

Figure 5-34 Relationship between "negative dissipated energy", "positive dissipated energy" and the liquefaction resistance (2D plot)

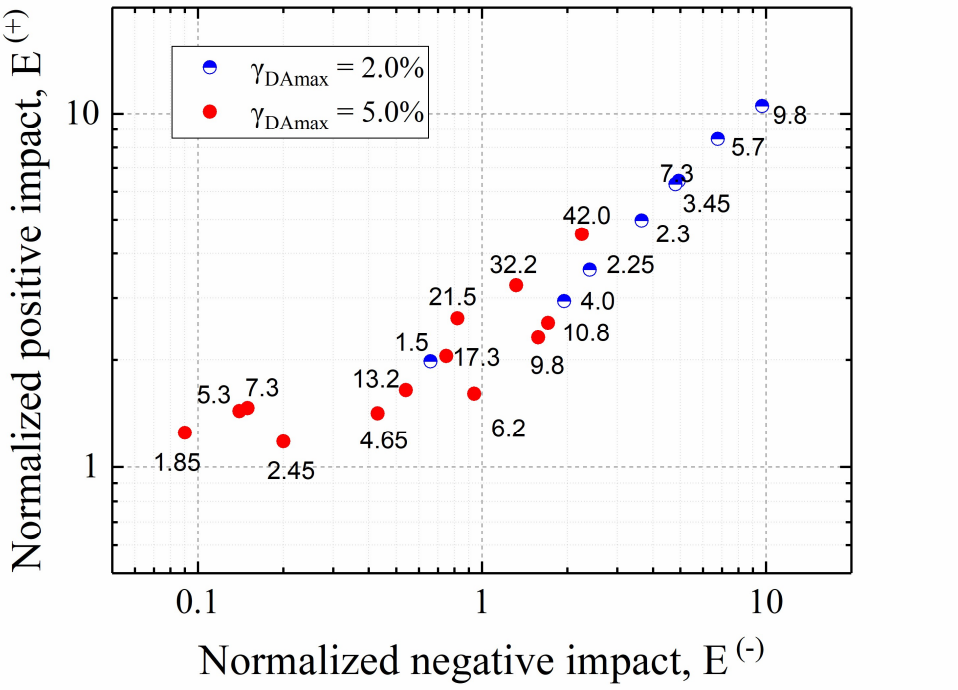

Figure 5-35 Relationship between "negative impact", "positive impact" and the liquefaction resistance (2D plot)

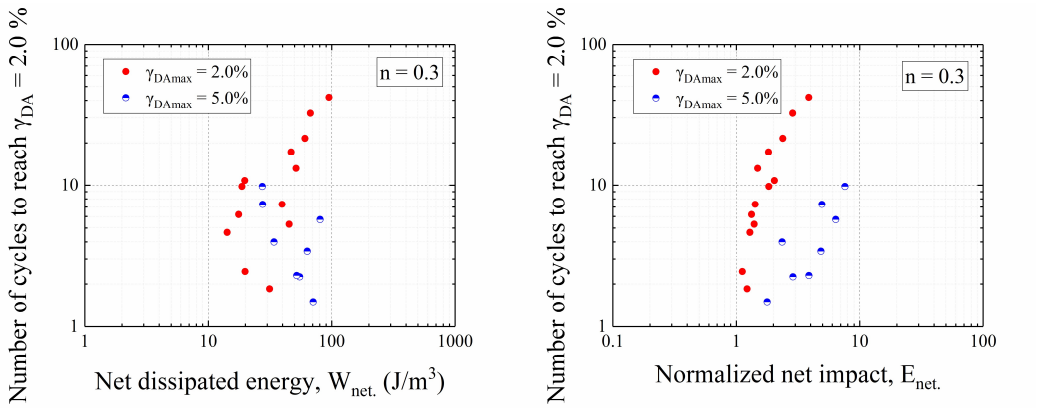

(a) Dissipated energy (b) Normalized dissipated energy

Figure 5-36 Relationship between "net dissipated energy", "normalized net impact" and the liquefaction resistance (n = 0.3)

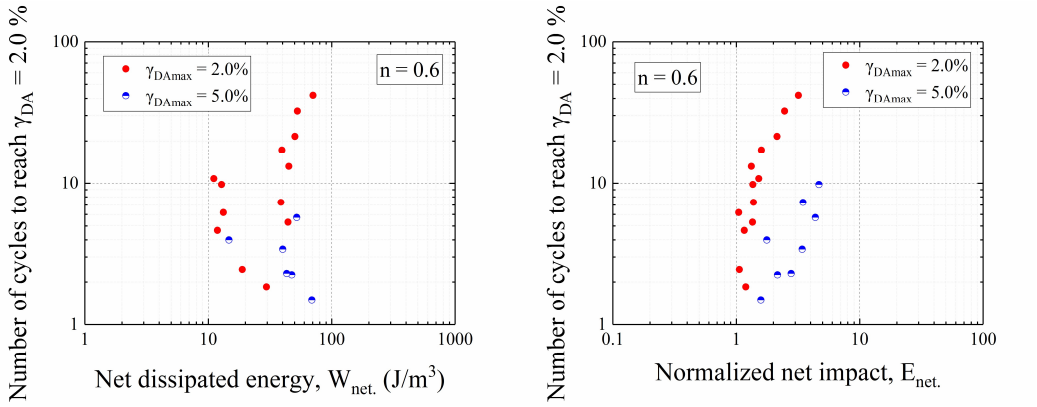

(a) Dissipated energy *(b) Normalized dissipated energy*

Figure 5-37 Relationship between "net dissipated energy", "normalized net impact" and the liquefaction resistance (n = 0.6)

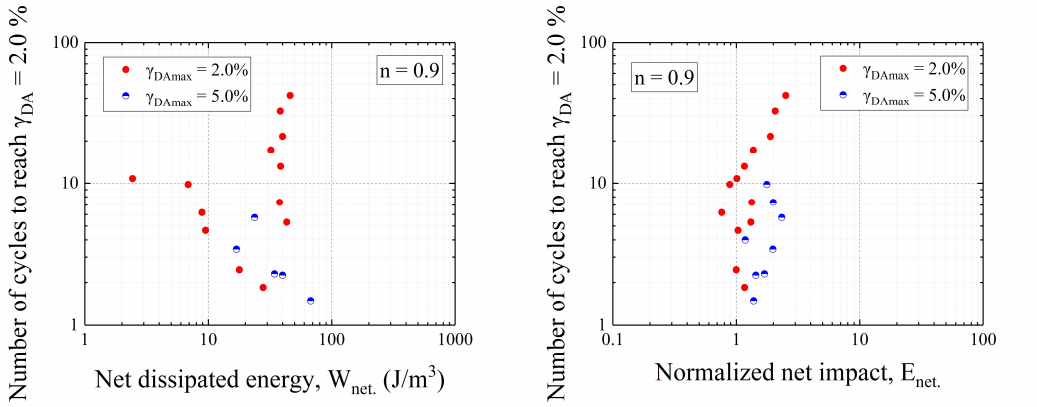

(a) Dissipated energy (b) Normalized dissipated energy

Figure 5-38 Relationship between "net dissipated energy", "normalized net impact" and the liquefaction resistance (n = 0.9)

5.4 Summary

From the analysis of the liquefaction test on dense sand and re-analysis on Aoyagi's data based on the energy concept, several conclusions can be made as follows:

1. With the increase of repeated liquefaction stages, the total dissipated energy and normalized dissipated energy increased. However, the accumulated shear strain and dissipated energy or normalized dissipated energy did not show the similar tri-linear or bi-linear relationship as reported in medium dense sand cases.

2. Due to the large cyclic stress ratio applied in the liquefaction tests on dense sand, the phase transformed in very early loading cycles. This kind of history was considered as the "negative impact" which could reduce the repeated liquefaction resistance based on the tests results of medium dense sand. However, the increase in repeated liquefaction resistance of dense sand indicated that the liquefaction properties were different between dense sands and medium dense or loose ones.

3. In the liquefaction tests with drained pre-shear histories, it was found that with more energy dissipated during the pre-shear, the liquefaction resistance tended to be stronger in the liquefaction stage after pre-shear.

4. Liquefaction tests with undrained pre-shear history showed similar results as the drained one. With more pre-shear stage, the total dissipated energy and normalized dissipated energy increased while the liquefaction resistance increased as well.

5. Analysis of the two cases with same pre-shear program but in different drainage conditions showed that due to the difference of excess pore water pressure, the normalized dissipated energy differed a lot. However, the similar liquefaction

resistance in the two cases indicated that the "effect part" of dissipated energy or normalized dissipated energy was similar. Therefore, new method is necessary to distinguish the different "impact".

6. By plotting the dissipated energy or normalized dissipated energy in all cases together, it was found that relationships between dissipated energy or normalized dissipated energy and liquefaction resistance were not consistent in different kinds of pre-shear histories. It might be because of the different proportion of "positive impact" and "negative impact" in the dissipated energy of different cases.

7. In order to compute the "positive impact" and "negative impact" of dissipated energy and normalized dissipated energy, a new method was proposed. With the boundary determined by the line of phase transformation, every cyclic loading cycle was divided into three parts. The parts with a shear stress or normalized shear stress beyond the boundary were considered as the "negative impact" due to the positive dilatancy. The rest parts showing negative dilatancy were considered as the "positive impact".

8. After calculating the "positive impact" and "negative impact" using the new method, it was found that the relationship between the liquefaction resistance and "normalized positive impact" became more consistent. However, the relationship between the liquefaction resistance and "positive dissipated energy" was still scattered.

9. In order to verify the applicability of the new method, re-analysis of the liquefaction tests on medium dense sand by Aoyagi was conducted. However, although cases with same shear histories showed the correlation between liquefaction resistance and the "positive impact", the relationships were not consistent in cases with different shear history. Then the "net impact" was introduced by considering the "negative impact" on medium dense sand. It was found that with consideration of the negative impact, the relationships between the "normalized net impact" and the liquefaction resistance

became more consistent in cases with different histories. However, the non-normalized ones become even worse.

5.5 Reference

AOYAGI, Y., WAHYUDI, S., KOSEKI, J., SATO, T. and MIYASHITA, Y., 2016. Behavior of multiple-liquefaction under small to large strain levels and its analysis based on dissipated energy. *JSCE Journal of Earthquake Engineering*, Vol. 72(4), pp. I_167-I_176 (in Japanese).

AOYAGI, Y., 2018. Analysis of multiple-liquefaction characteristics in torsional shear and stacked ring shear tests based on energy concept. *Ph.D. Thesis. Department of Civil Engineering, The University of Tokyo, Japan* (in Japanese).

ISHIHARA, K. and OKADA, S., 1978. Effects of stress history on cyclic behavior of sand. *Soils and Foundations,* Vol. 18(4), pp. 31-45.

KOSEKI, J., YOSHIDA, T. and SATO, T., 2005. Liquefaction properties of Toyoura sand in cyclic tortional shear tests under low confining stress. *Soils and Foundations,* Vol.45(5), pp. 103-113.

TATSUOKA, F., MURAMUTSU, M., SASAKI, T., 1982. Cyclic undrained stress-strain behavior of dense sands by torsional simple shear test. *Soils and Foundations*, Vol. 22 (2), pp. 55-70.

WAHYUDI, S., 2014. Cyclic simple shear tests using stacked-rings on multiple liquefaction properties of sands. *Ph.D. Thesis. Department of Civil Engineering, The University of Tokyo, Japan.*

WAHYUDI, S. and KOSEKI, J., 2015. Analysis of re-liquefaction properties based on energy approach. *Bulletin of ERS, Institute of Industrial Science, University of Tokyo*, Vol. 48. pp. 52-61.

Chapter 6 Application of Energy Concept to Estimate Liquefaction Resistance Curve Based on Result from a Single Test

6.1 Introduction

In this chapter, the energy concept will be applied to estimate the liquefaction resistance curve based on a single liquefaction test. During this new attempt, the "positive impact" of normalized dissipated energy introduced in the 5th chapter is employed to modify the liquefaction resistance curve that is obtained by a single liquefaction test.

6.2 Liquefaction resistance curve obtained by a single test

The liquefaction resistance curve is widely used to quantitatively evaluate the liquefaction resistance of sands. As typically shown in Figure 6-1, the liquefaction resistance curve is generally obtained by a series of liquefaction tests on sand specimens. Generally, these tests should be carried out on sand specimens under the same (or very similar) conditions (i.e. relative density, consolidation condition, etc.) but using different cyclic stress ratios. However, unlike the reconstituted specimen, the contents of natural sand samples are so complex that the repeatability of liquefaction test may be not good. For example, as shown in Figure 6-2, two specimens liquefied at the same number of cycles under different cyclic stress ratios (Kiyota el al., 2009).

Koseki et al. (2019) proposed a method to estimate the liquefaction resistance curve via a single liquefaction test. For example, in a typical liquefaction test shown in Figure 6-3, it takes 85 cycles of cyclic loading with cyclic shear stress of 12 kPa to induce liquefaction (effective stress reduced to 0) from the starting point “a” with an initial effective stress of 100 kPa. At the point of “b”, due to the 30 cycles of undrained loading, the effective stress reduced by 30% to 70 kPa. It can be considered that from point “b”, with the “new” cyclic stress ratio of 12/70, it takes 55 cycles of loading to induce the liquefaction. Similarly, it can also be considered that from point c, with another new cyclic stress ratio, another number of cycles is taken to induce the liquefaction. Therefore, several different points can be obtained in the single test to draw the liquefaction resistance curve.

However, considering that the cyclic loadings in the early loading stage can change the soil particle structures, the liquefaction resistance curve obtained from a single test may be different from the typical one as shown in Figure 6-4. Thus, appropriate modification is necessary.

By defining a correction parameter $N_{cr} = N_{c2}/ N_{c1}$, Koseki et al. (2019) suggested that if the relationship between N_{cr} and the normalized dissipated energy can be quantitatively calculated, the modification will be available for different kinds of liquefaction cases.

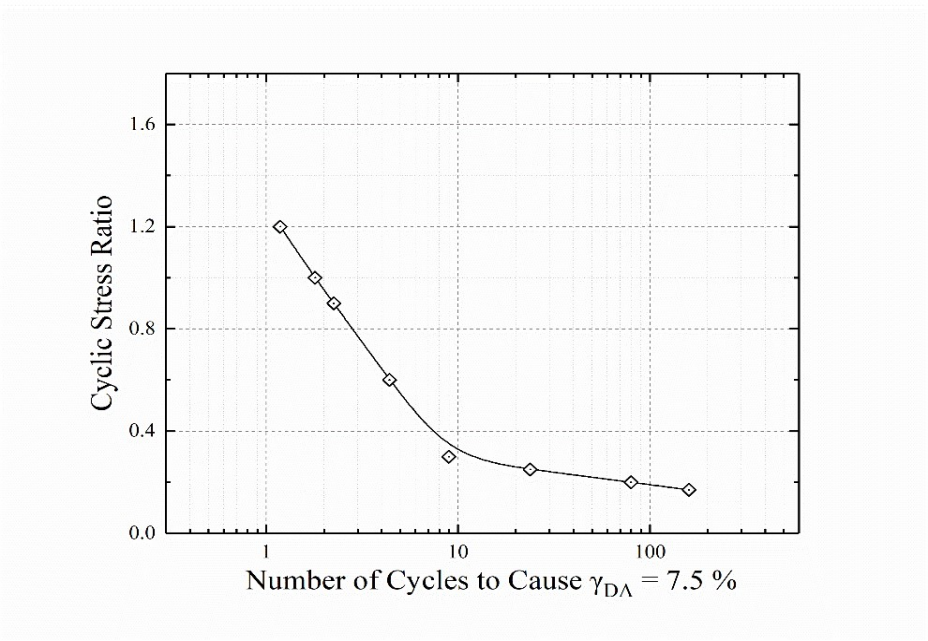

Figure 6-1 Typical liquefaction resistance curve

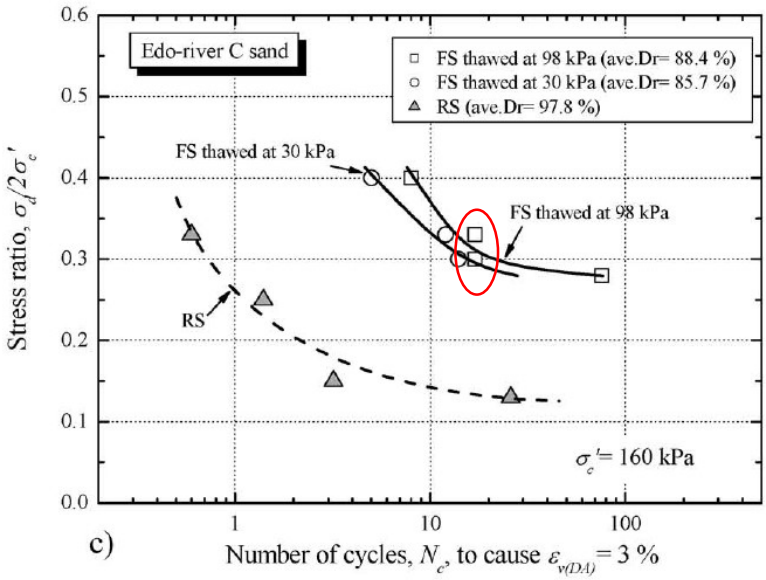

Figure 6-2 Liquefaction resistance curve of different samples (Kiyota et al., 2009)

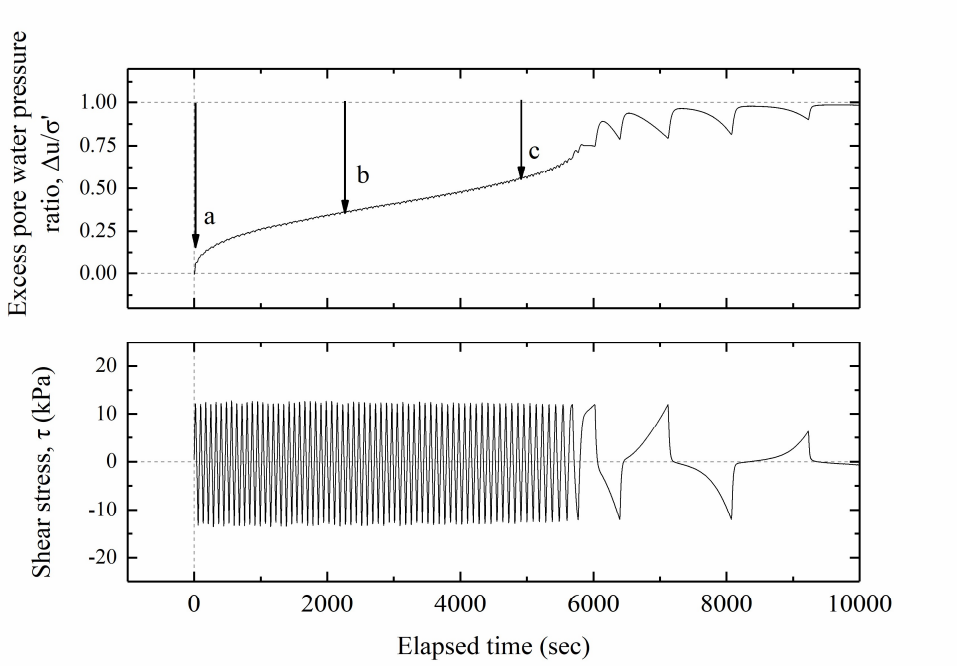

Figure 6-3 Liquefaction test result

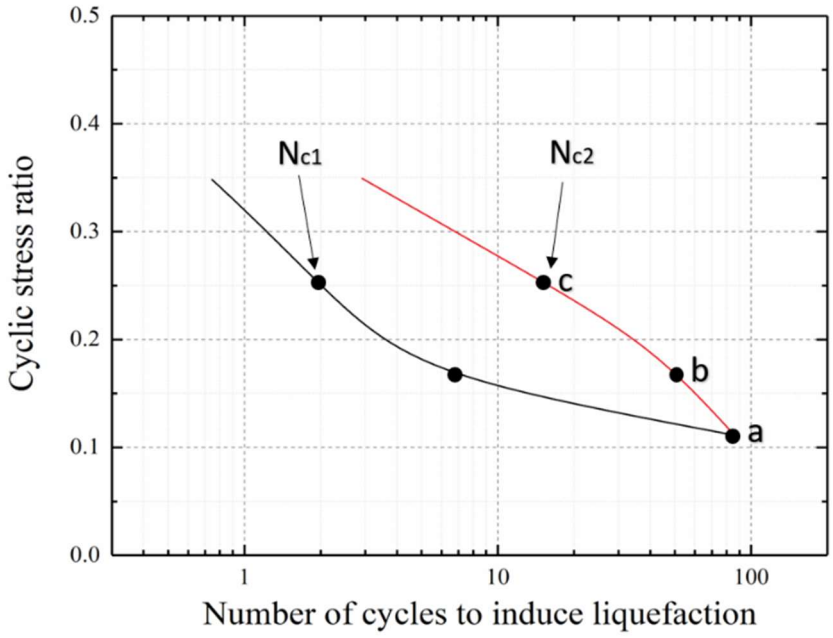

Figure 6-4 Liquefaction resistance curve obtained by a series of tests (N_{c1}) and a single test (N_{c2})

6.3 Trials for quantify the relationship between $N_{cr} = N_{c2}/N_{c1}$ and normalized dissipated energy

Based on the test results of several cases in test series A, attempts were made to find the common relationship between the correction parameter N_{cr} and the normalized dissipated energy. In addition, as introduced in the 5th chapter, "positive impact" is much more dominant in dense sand cases. Therefore in this part, the normalized positive impact will be used instead of the normalized dissipated energy.

Figure 6-5 shows the liquefaction resistance curves obtained by the single case A-7 (CSR = 0.20), single case A-8 (CSR = 0.17) and all the typical liquefaction resistance curve obtained by all cases in test series A. In order to calculate the correction parameter N_{cr}, it is necessary to estimate the formula of the typical liquefaction resistance curve and use it to calculate the corresponding N_{c1}. In these cases, the trend line of liquefaction resistance curve is calculated as follows.

$$N_{c1} = 1.552 \times CSR^{-2.24} \qquad (6\text{-}1)$$

Then the relationships between N_{cr} and "normalized positive impact" are calculated and shown in Figure 6-6.

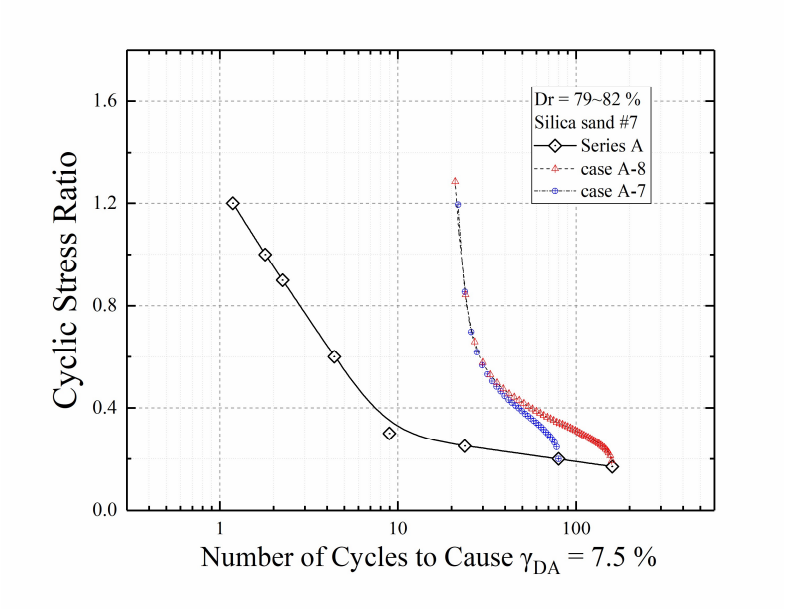

Figure 6-5 Liquefaction resistance curve obtained with different cases

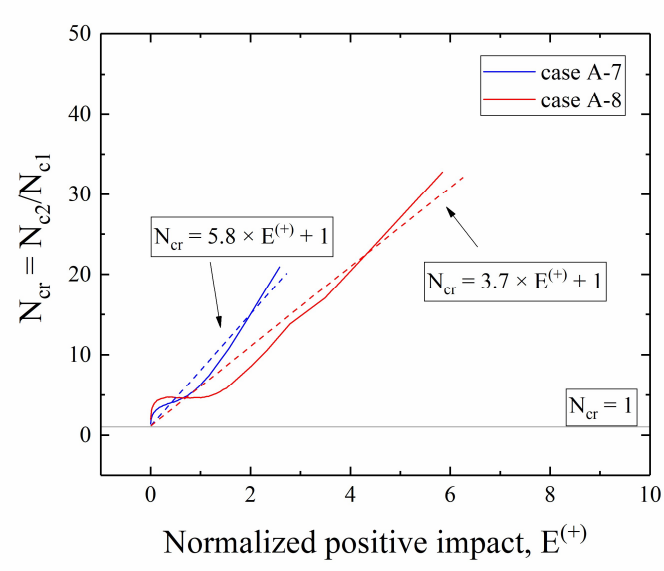

Figure 6-6 Relationship between N_{cr} and normalized positive impact

As shown in the figure, the relationships can be fitted into a linear function as:

$$N_{cr} = a \times E^{(+)} + 1 \qquad (6\text{-}2)$$

where a is the parameter that differs in different cases.

With the parameter N_{cr} described by the trend line, liquefaction resistance curve that is obtained by single test can be modified. The modified curves (N_{c1}') in cases A-7 and A-8 are shown in Figure 6-7.

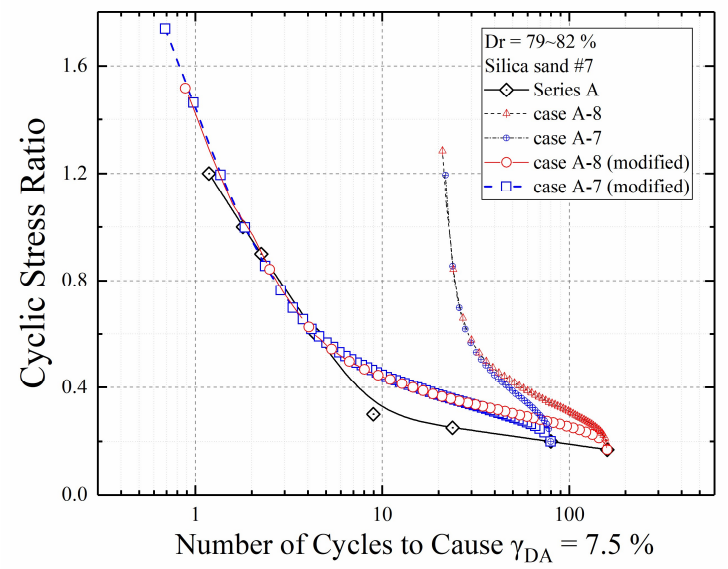

Figure 6-7 Liquefaction resistance curve before and after modification

It can be observed that the liquefaction resistance curve obtained by single test becomes much closer to the real liquefaction resistance curve after the modification. This suggests that if the parameter "*a*" can be determined in a test, then it is possible to estimate the liquefaction resistance curve with this method.

It can be observed that the parameter "*a*" seemed to be inversely related with the normalized positive impact. By simply suggesting a linear relationship, the parameter "*a*" in other cases can be calculated by the total amount of normalized positive impact.

In order to check the applicability of this method, the liquefaction resistance curve drawn by single test case D-5 (with undrained pre-shear histories) and its modified curve are calculated and shown in Figure 6-8. It can be observed that even the liquefaction resistance curve became closer to the real one, the part with lower CSR was still not good enough. In fact, as can be observed in Figure 6-6, the whole trend of

the N_{cr}-$E^{(+)}$ relationship was linear but the initial part was not. It means that if the N_{cr}-$E^{(+)}$ relationship can be described more accurately, the accuracy of modification can be improved.

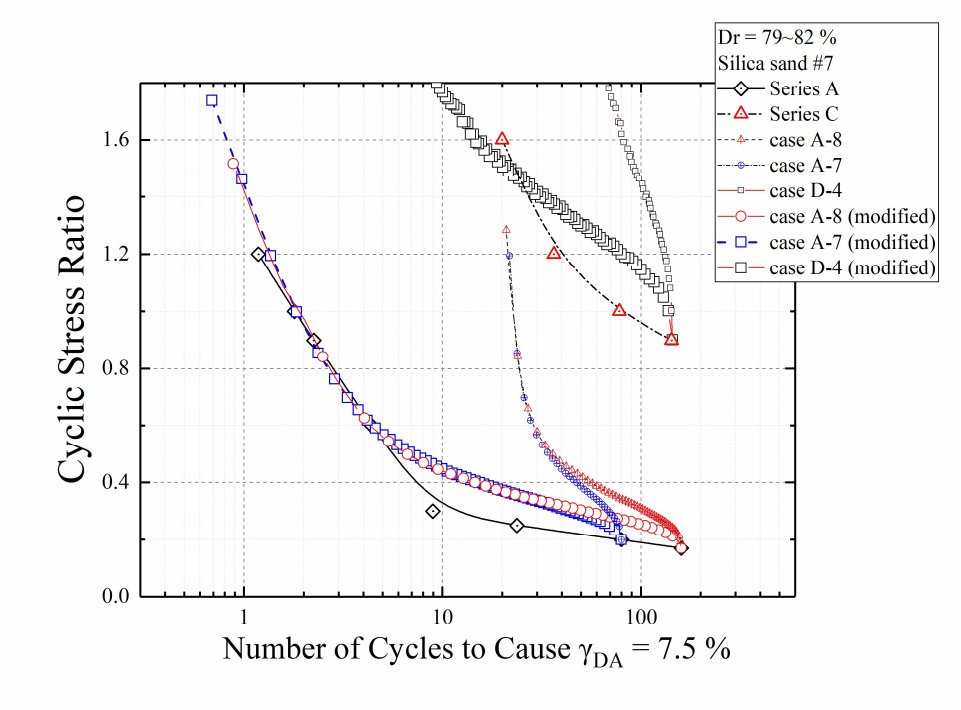

Figure 6-8 Liquefaction resistance curve before and after modification

Further attempts were carried out on medium dense sand cases. With a series of liquefaction tests on medium dense sand (labeled as series E), a typical liquefaction resistance curve was obtained. With the method introduced above, two tests in the series with low CSR were chosen to estimate the liquefaction resistance curve independently. The liquefaction resistance curves before and after modification are shown in Figure 6-9.

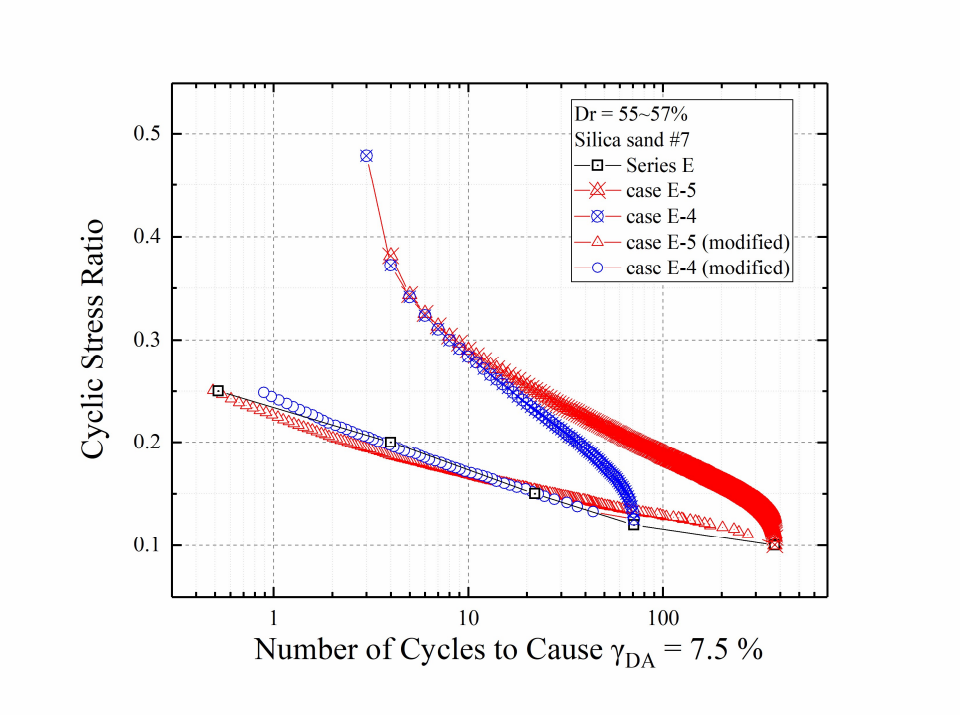

Figure 6-9 Liquefaction resistance curve of medium dense sand cases

It can be observed that the liquefaction resistance curve obtained by single test became very close to the real liquefaction resistance curve after modification. From Figure 6-10, it can be observed that the N_{cr}-$E^{(+)}$ relationships of these medium dense cases were much closer to be linear than in the dense sand cases. Therefore the modification worked better.

The analysis result using the net impact are shown in Figures 6-11 and 6-12. There is no obvious change can be observed.

This result also suggests that the property and behavior of dense sand and medium dense sand are quite different. In future studies, with more testing cases on dense sand, better description and modeling of the N_{cr}-$E^{(+)}$ relationship can be expected and then the liquefaction resistance curve can be estimated more accurately by a single test.

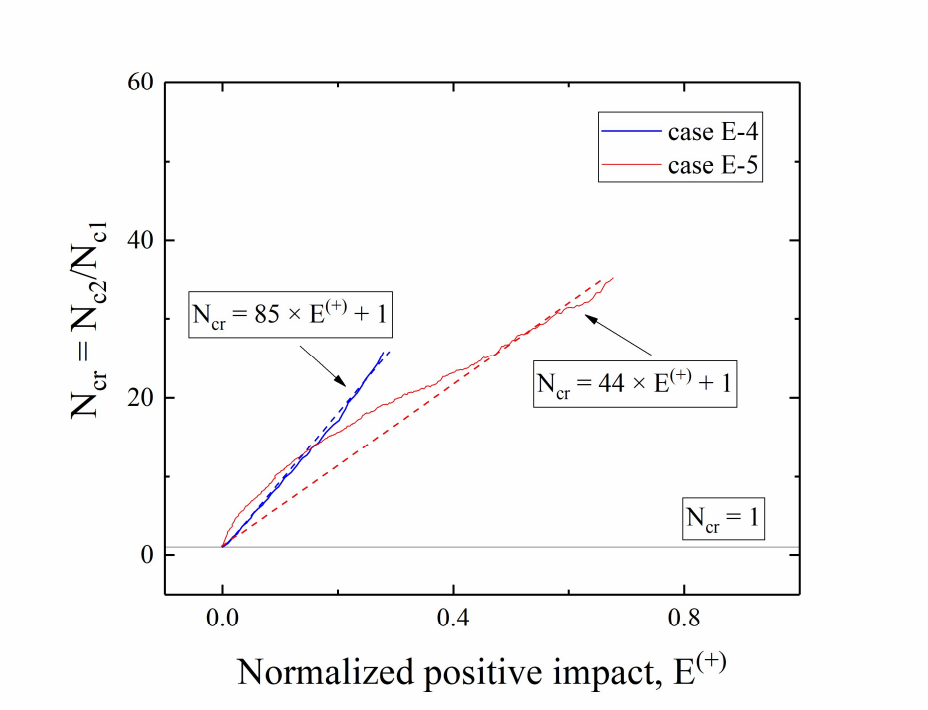

Figure 6-10 Relationship between N_{cr} and normalized positive impact

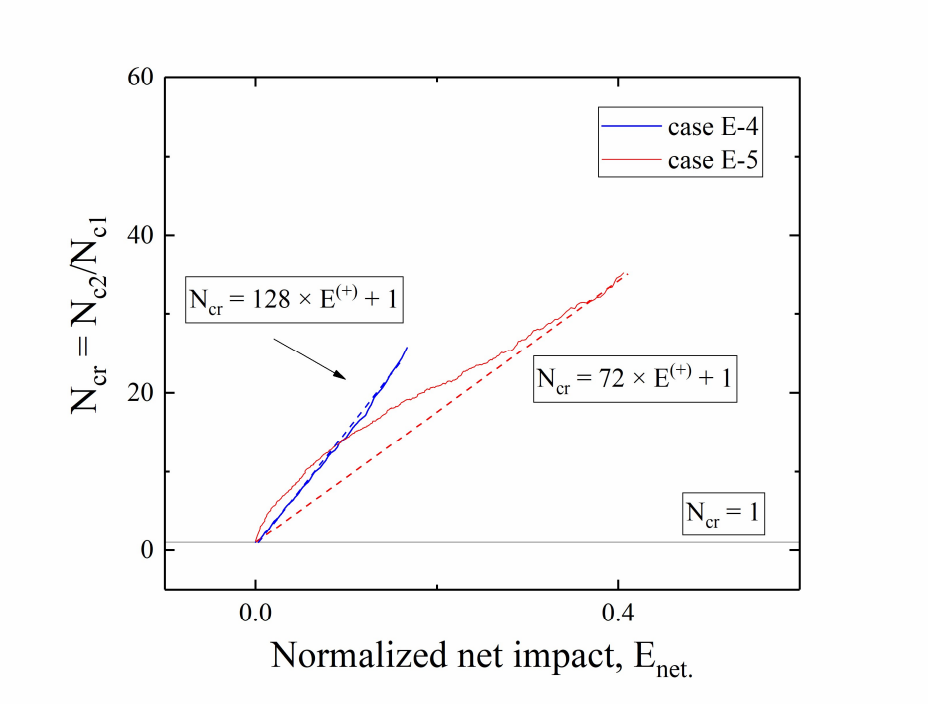

Figure 6-11 Relationship between N_{cr} and normalized net impact

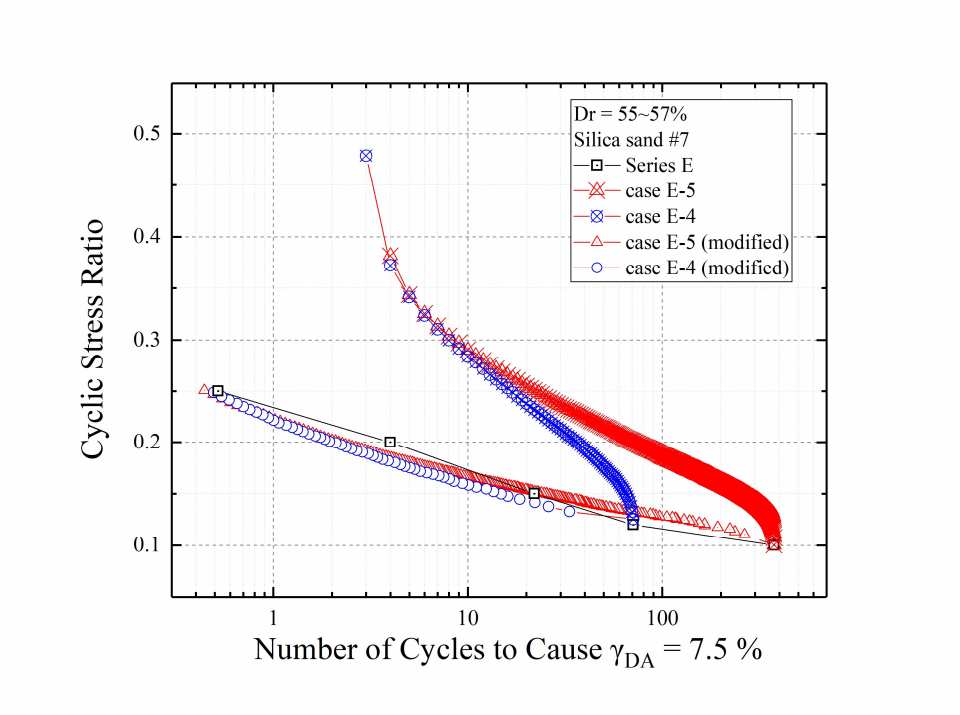

Figure 6-12 Liquefaction resistance curve of medium dense sand cases

6.4 Summary

With the analysis and trials on both dense sand and medium dense sand cases, the applicability of the method to estimate the liquefaction resistance curve by single test was discussed. Based on the results, some conclusions can be made as follows.

1. With modification, the liquefaction resistance curve estimated by a single test became better and partly consistent with the typical liquefaction resistance curve obtained by a series of tests. The part that was still not consistent after modification was considered because of the inaccuracy during describing the N_{cr}-$E^{(+)}$ relationship.

2. Since the N_{cr}-$E^{(+)}$ relationships in medium dense sand cases were much closer to a linear relation, the results of modification were much better than in the dense sand cases. This result indicated that it is possible to modify the liquefaction resistance curve obtained by a single test more accurately if the N_{cr}-$E^{(+)}$ relationship can be modeled with more tests data.

6.5 References

KIYOTA, T., KOSEKI, J., SATO, T., TSUTSUMI, Y., 2009. Effects of sample disturbance on small strain characteristics and liquefaction properties of Holocene and Pleistocene sandy soils. *Soils and Foundations*, Vol. 49(4), pp. 509-523.

KOSEKI, J., ZHAO, C., LIU, W., AOYAGI, Y., MATSUI, Y., 2019. Proposal of a method to estimate the liquefaction resistance curve from a single test using normalized dissipated energy. *Symposium on energy-based liquefaction prediction methods*, *Japanese Geotechnical* Society, 2019(3) pp. 301-304 (in Japanese).

Chapter 7 Conclusions and Recommendations for Future Works

7.1 Conclusions

Based on the three main objectives introduced in the first chapter, four series of liquefaction tests were carried out on torsional shear apparatus and the results were analyzed using the energy concept. Corresponding to the three main objectives, some conclusions are made as follows.

7.1.1 Liquefaction behavior of dense sands without/with different kinds of pre-shear histories

1. The liquefaction resistance in repeated liquefaction tests increased with liquefaction stages.

In the repeated liquefaction tests without pre-shear history, the specimen showed increasing liquefaction resistance during repeated liquefaction. This behavior is different from what was reported on medium dense sand by pioneer researchers.

2. Pre-shear history under drained conditions affected the liquefaction resistance of dense sand specimen differently with various loading programs.

In test series C, by conducting liquefaction tests with different drained pre-shears, it was found that both the amplitude of shear strain and the number of loading cycles affected the liquefaction resistance in the following liquefaction test. However, it was noticed that the pre-shear seemed to only affect the liquefaction stage immediately after, since the liquefaction resistance from the second stage reduced to the same level as the one with no pre-shear.

3. Pre-shear history under undrained conditions was found to affect the liquefaction resistance as well.

Tests with pre-shear history under undrained conditions were applied with a "partial liquefaction" history by inducing excess pore water pressure ratio to 0.5. It was found that this kind of pre-shear can be accumulated in different pre-shear stages. After 18 stages of pre-shear loadings, the sand specimen became extremely strong to liquefaction even though it had similar relative density as the virgin sample in cases with no pre-shear. It was noticed that the complex pre-shear history could not be fully eliminated after the first liquefaction stage as in the drained pre-shear cases.

4. A simple comparison was made between pre-shear histories in different drainage conditions and no significant difference was found.

No significant difference was found by conducting tests with the same stress history but in different drainage conditions. It seemed that the accumulation of excess pore water pressure during the undrained condition did not affect the liquefaction resistance very much. However, due to the limited test numbers, it cannot be concluded that the drainage condition has no effect during the pre-shear stage. Further investigations based on more testing cases are still necessary to provide more evidence.

7.1.2 Analysis of liquefaction behavior (pre-shear effects) of dense sands using the energy concept

1. Different accumulation progress was found on dense sand compared with medium dense ones.

With the increase of repeated liquefaction stages, the total dissipated energy and normalized dissipated energy increased. However, the accumulated shear strain and dissipated energy or normalized dissipated energy did not show the similar tri-linear or bi-linear relationship as reported in medium dense sand cases.

Due to the large cyclic stress ratio applied in the liquefaction tests on dense sand, the phase transformed in very early loading cycles. This kind of history was considered as the "negative impact" which could reduce the repeated liquefaction resistance based on the tests results of

medium dense sand. However, the increase in repeated liquefaction resistance of dense sand indicated that the liquefaction properties were different between dense sands and medium dense or loose ones.

2. Increase of liquefaction resistance was found to be related with the energy/normalized energy dissipated during its pre-shear stage.

In the liquefaction tests with drained pre-shear histories, it was found that with more energy dissipated during the pre-shear, the liquefaction resistance tended to be stronger in the liquefaction stage after pre-shear.

Liquefaction tests with undrained pre-shear history showed similar results as the drained one. With more pre-shear stage, the total dissipated energy and normalized dissipated energy increased while the liquefaction resistance increased as well.

3. The energy/normalized energy was considered to be consist of both "positive impact" and "negative impact".

Analysis of the two cases with same pre-shear program but in different drainage conditions showed that due to the difference of excess pore water pressure, the normalized dissipated energy differed a lot. However, the similar liquefaction resistance in the two cases indicated that the "effect part" of dissipated energy or normalized dissipated energy was similar. Therefore, new method is necessary to distinguish the different "impact".

By plotting the dissipated energy or normalized dissipated energy in all cases together, it was found that relationships between dissipated energy or normalized dissipated energy and liquefaction resistance were not consistent in different kinds of pre-shear histories. It might be because of the different proportion of "positive impact" and "negative impact" in the dissipated energy of different cases.

4. New method to distinguish the "positive impact" and "negative impact" was proposed.

In order to compute the "positive impact" and "negative impact" of dissipated energy and normalized dissipated energy, a new method was proposed. With the boundary determined by the line of phase transformation, every cyclic loading cycle was divided into three parts. The parts with a shear stress or normalized shear stress beyond the boundary were considered as the "negative impact" due to the positive dilatancy. The rest parts showing negative dilatancy were considered as the "positive impact".

After calculating the "positive impact" and "negative impact" using the new method, it was found that the relationship between the liquefaction resistance and "normalized positive impact" became more consistent. However, the relationship between the liquefaction resistance and "positive dissipated energy" was still scattered.

5. The "negative impact" was found to have different influence on liquefaction resistance in different density ranges.

In order to verify the applicability of the new method, re-analysis of the liquefaction tests on medium dense sand by Aoyagi was conducted. However, although cases with same shear histories showed the correlation between liquefaction resistance and the "positive impact", the relationships were not consistent in cases with different shear history. Then the "net impact" was introduced by considering the "negative impact" on medium dense sand. It was found that with consideration of the negative impact, the relationships between the "normalized net impact" and the liquefaction resistance became more consistent in cases with different histories. However, the non-normalized ones become even worse.

7.1.3 Application of the energy concept in predicting the liquefaction resistance curve through a single test

1. With modification, the liquefaction resistance curve estimated by a single test became better and partly consistent with the typical liquefaction resistance curve obtained by a series of tests.

The part that was still not consistent after modification was considered because of the inaccuracy during describing the N_{cr}-$E^{(+)}$ relationship.

2. Since the N_{cr}-$E^{(+)}$ relationships in medium dense sand cases were much closer to a linear relationship, the results of modification were much better than in the dense sand cases. This result indicated that it is possible to modify the liquefaction resistance curve obtained by a single test more accurately if the N_{cr}-$E^{(+)}$ relationship can be modeled with more tests data.

7.2 Recommendations for future works

According to the objectives and their corresponding conclusions, recommendations for future work can be summarized as follows.

7.2.1 Liquefaction behavior of dense sands without/with different kinds of pre-shear histories

1. Liquefaction behavior of dense sands under different cyclic stress ratios.

In this study, the effect of pre-shear on liquefaction behavior of dense sands was mainly discussed based on the test with CSR = 1.00. In future works, it is recommended to investigate the effect of different kinds of pre-shear with different CSR (i.e. 0.60 or 0.30) in liquefaction stage.

2. Further investigation about the influence of drainage condition in pre-shear stage.

In this study, simple comparison of pre-shear under different drainage conditions was conducted with only 2 cases. In future works, it is recommended to study the influence of drainage condition with more cases.

7.2.2 Analysis of liquefaction behavior (pre-shear effects) of dense sands using the energy concept

1. More detailed investigation about full liquefaction history with energy approach.

liquefaction tests were considered as a kind of liquefaction test with full liquefaction history. However, due to the increase of relative density during repeated liquefaction stages, it is difficult to distinguish the influence of dissipated energy (pre-shear effect) and the increase of relative density. Therefore in future works, it is necessary to study the influence of these two factors separately.

2. Different judging methods are recommended.

In this study, the liquefaction resistance in the next liquefaction stage was chosen to describe the pre-shear effect using the energy concept. In future works, it is recommended to establish a relationship between the pre-shear effects (dissipated energy) and the increment of liquefaction resistance or the ratio of increase in liquefaction resistance.

3. Further study on different density ranges.

It was found that the "negative impact" had different influence on liquefaction resistance in cases with different relative densities. Therefore in the future, with more testing cases, it is expected to quantitively determine the influence of "negative impact" among different density ranges.

7.2.3 Application of the energy concept in predicting the liquefaction resistance curve through a single test

With more tests in the future, the relationship between Nc2/Nc1 and the positive impact (or net impact) can be modeled more accurately. Then it is expected to predict the liquefaction resistance curve more accurately with single test.